ASTROGEOLOGIC STUDIES

ANNUAL PROGRESS REPORT

July 1, 1964 to

July 1, 1965

PART A: LUNAR AND PLANETARY INVESTIGATIONS

November 1965

This preliminary report is distributed
without editorial and technical review
for conformity with official standards
and nomenclature.   It should not be
        quoted without permission.

This report concerns work done on behalf of the
National Aeronautics and Space Administration.

DEPARTMENT OF THE INTERIOR
UNITED STATES GEOLOGICAL SURVEY

CONTENTS

PART A--LUNAR AND PLANETARY INVESTIGATIONS

CONTENTS--Continued

CONTENTS--Continued

INTRODUCTION

This Annual Report is the sixth of a series describing the results of research conducted by the U.S. Geological Survey on behalf of the National Aeronautics and Space Administration. The report is in three volumes corresponding to three main areas of research: Part A, Lunar and Planetary Investigations; Part B, Crater Investigations; and Part C, Cosmic Chemistry and Petrology; and a map supplement. An additional volume presents abstracts of the papers in Parts A, B, and C.

The major long-range objectives of the astrogeologic studies program are to determine and map the stratigraphy and structure of the Moon's crust, to work out from these the sequence of events that led to the present condition of the Moon's surface, and to determine the processes by which these events took place. Work that leads toward these objectives includes a program of lunar geologic mapping; studies on the discrimination of geologic materials on the lunar surface by their photometric, polarimetric, and infrared properties; field studies of structures of impact, explosive, and volcanic origin; laboratory studies on the behavior of rocks and minerals subjected to shock; and study of the chemical, petrographic and physical properties of materials of possible lunar origin and the development of special techniques for their analysis.

Members of the Astrogeologic Studies section of the Branch of Astrogeology have used photographs from the three successful Ranger missions, VII, VIII, and IX, to study the geology and surface properties of the Moon at scales larger than the 1:1,000,000 scale used for reconnaissance geologic mapping. The results of these investigations are described in a series of Technical Reports published by the Jet Propulsion Laboratory for the National Aeronautics and Space Administration and are briefly summarized in the Summary volume of this report.

Part A, Lunar and Planetary Investigations (with map supplement), contains the preliminary results of detailed geologic mapping of 15 new quadrangles on a scale of 1:1,000,000. The equatorial belt of the Moon (32°N-32°S, 70°E-70°W) has now been completely mapped in this preliminary fashion. Results of new mapping and of detailed studies of previously defined stratigraphic units are included. Photometric and polarimetric studies to supplement the mapping program are also reported on.

PRELIMINARY REPORT ON THE GEOLOGY

OF THE BYRGIUS QUADRANGLE OF THE MOON

by N. J. Trask

Introduction

The Byrgius quadrangle lies at the southwest corner of the equa-
torial belt between latitudes 16°S and 32°S, and longitudes 50°W and
70°W. Upland material with complex stratigraphy and structure occupies
most of the quadrangle. Parts of ejecta blankets from two mare basins,
Mare Orientale and Mare Humorum, are present. Many of the structures in
the quadrangle are related to the Mare Orientale basin, a large and rela-
tively young feature centered 500 km directly to the west described by
McCauley (1964). The deposits and structures of the Mare Orientale and
Mare Humorum basins will eventually provide important facts bearing on
the early history of the Moon.

Stratigraphy

Humorum rim material

Hummocky regional material extending outward from the margin of the
Mare Humorum basin has been classed as Humorum rim material by Titley
(1964). A lobe of this material extends from the eastern boundary of the
Byrgius quadrangle near the crater Mersenius northwestward to the vicin-
ity of the crater Fontana. The material consists largely of hummocks
1 to 4 km in diameter that crest in a relatively sharp point (fig. 1).
The hummocks are essentially equidimensional and occur in clumps. Ma-
terial between the hummocks is smooth or studded with a few irregular
pits and depressions. Through-cutting, closely spaced lineaments along
which slight movement may have taken place are relatively abundant. Some
of the protuberances in the Humorum rim material may be fault blocks up-
lifted between intersecting fractures; many of the hummocks are unrelated
to the fracture system, however, and are probably clots of ejects from

the Mare Humorum basin. The topographic form of the Humorum rim material closely resembles that of the hummocky facies of the Fra Mauro Formation in the Apennine Mountains (Hackman, 1963). The hummocky facies of the Fra Mauro Formation grades outward from Mare Imbrium to a smooth facies characterized by linear, gently rounded, braided ridges (Wilhelms, 1964). The two facies have been interpreted as analogous to the hummocky rims and radial ridges of typical impact craters such as Copernicus. In the Byrgius quadrangle, the outer part of the Humorum rim material is buried by younger deposits so that similar outward facies changes cannot be detected. On the geologic map of the Byrgius quadrangle accompanying this report, the Humorum rim material is provisionally assigned to the pre-Imbrian because of the large number of lineaments cutting it.

Level, mare-like material with medium albedo at and near the margins of the Mare Humorum basin has been mapped as Humorum bench material by Titley (1964). This unit also extends westward into the Byrgius quadrangle. The Humorum bench material has a high density of rilles, small craters and irregular depressions; locally it appears smooth. The material forms level terrain on a large scale (5 km) and clearly overlaps and surrounds the more rugged topography of the Humorum rim material in many places. The geologic relations indicate that the Humorum bench material spans the time interval from the deposition of the Humorum rim material to the deposition of the Procellarum Group and is therefore of pre-Imbrian to Imbrian age.

Cordillera group

A blanket of regional material surrounding the Mare Orientale basin has been designated the Cordillera Group by McCauley (1964). He informally recognized two subunits, a hummocky ejecta blanket and smooth, bench-forming material, together analogous to the Humorum rim and Humorum bench units. The hummocky material is best exposed in the Cordillera Mountains, 250 km west of the Byrgius quadrangle; the bench material is confined to the area between the Cordillera Mountains and the Mare Orientale basin itself. The hummocky material extends eastward
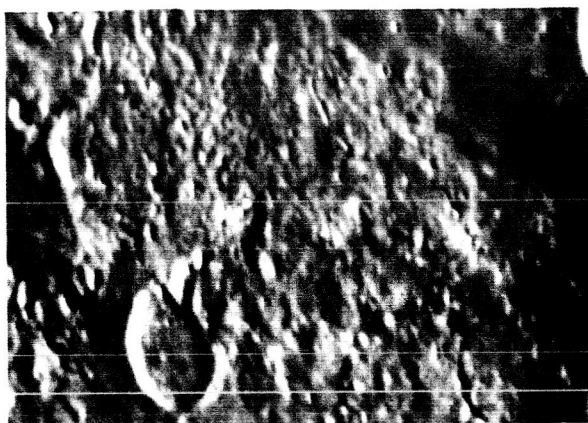
Fig. 1.--Typical Humorum rim material showing equidimensional hummocks north and east of large crater Fontana; north (top)-south distance approximately 115 km.

Fig. 2.--Typical pitted material and plains-forming material. Large craters are Prosper Henry on left and Paul Henry on right. Pitted material is northwest and northeast of Prosper Henry; plains-forming material is west of Prosper Henry and fills floor of Paul Henry. Note broad dome with summit crater 50 km north of Prosper Henry; north (top)-south distance approximately 115 km.

into the Byrgius quadrangle to the approximate longitude of Crüger and Byrgius. It partially fills and overlaps the older crater Darwin at the northwestern corner. The hummocks are up to 4 km in diameter; their exact nature will be determined by further telescopic observations at favorable librations. McCauley (1964) provisionally assigned an Archimedian age to the Cordillera Group.

Regional pitted material

Upland material in which negative relief features are the principal topographic elements is common in the middle two-thirds of the Byrgius quadrangle. This material occupies relatively high ground and is surrounded, embayed and, in places, covered by younger material. The negative relief features consist of shallow, round to irregularly shaped depressions from several hundred meters to 5 km across. Some of the depressions have distinct raised rims, but most have no rims or very subdued rims. The pits are superimposed on a broadly undulating topography that is cut in places by numerous lineaments. Good examples of this material are found due south of Fontana and northwest of Prosper Henry (fig. 2). A few isolated hummocks are present within areas mapped as the pitted material; and a few smooth, rounded hills with summit craters resemble terrestrial volcanoes. An example of the latter is located 50 km north of Prosper Henry (fig. 2). The pitted material may represent a field of secondary impact craters formed by fragments ejected from the Mare Orientale and Mare Humorum basins. Alternatively, it may represent lava flows with numerous volcanic collapse features.

Plains-forming material

A widespread unit in the Byrgius quadrangle is flat, level plains-forming material. It fills almost all the depressions and extensive low areas in the central part of the quadrangle. It has a moderate albedo, higher than that of typical mare material, and in places has a density of small craters an order of magnitude greater than that on the maria. Plains-forming material surrounds and embays all older units and locally forms a thin covering over them. The lineaments, so prominent

in the older units, are absent in the plains-forming material; domes
and ridges are also missing. The material seems identical to the
plains-forming material mapped by Milton (1964) in the Theophilus
quadrangle and by Morris and Wilhelms (1965) in the Julius Caesar
quadrangle. Material of this sort is apparently widespread over
the entire lunar terrae. Whether all of it is the same age is un-
certain at present. The Humorum bench material is very similar and
occupies a similar stratigraphic position but has a slightly lower
albedo. It may be partially equivalent to the plains-forming material.

Gassendi and Crüger Groups

Craters superposed on Humorum rim material and embayed by mare
material belong to the Gassendi Group (Titley, 1964); craters super-
posed on materials of the Cordillera Group and embayed and filled by
mare material have been mapped as the Crüger Group (McCauley, 1964).
In the Byrgius quadrangle, mare material is rare, and only a few
craters can be definitely assigned to these groups.

Structure

Many ridges, rilles, scarps, and lineaments are present in the
complex uplands in the quadrangle. The lineaments appear to be orien-
ted predominantly northwest-southeast. In the southern part of the
quadrangle, this direction coincides with the direction radial to the
Mare Orientale basin; and some of the northwest-southeast lineaments
there are probably part of a system of structural elements that was
formed at the time of the formation of the basin. A few east-northeast-
trending lineaments near Darwin and Fontana may also be parts of such
a system. The main development of lineaments radial to the Mare
Orientale basin is west of the Byrgius quadrangle (Hartmann, 1965).

Structures concentric with the Mare Orientale basin are also pre-
sent. Two prominent scarps, one running along the east side of Darwin
and Lamarck and a second extending southwest from a point 35 km east
of Byrgius, have been pointed out by Hartmann and Kuiper (1962). The
scarps follow the east sides of old craters and have scalloped out-
lines. Another concentric feature, still farther removed from Mare

Orientale, a broad, shallow valley, 35 km wide, filled with plains-forming material, runs from a point just west of Fontana south to Vieta.

References

Hackman, R. J., 1963, Stratigraphy and structure of the Apennine region of the Moon, in Astrogeologic Studies Ann. Prog. Rept., Aug. 25, 1961 - Aug. 24, 1962, pt. A: U.S. Geol. Survey open-file report, p. 2-10.

Hartmann, W. K., 1965, Radial structures surrounding lunar basins, II-Orientale and other systems, Conclusions: Arizona Univ. Lunar and Planetary Lab. Comm., v. 2, no. 36, p. 175-192.

Hartmann, W. K., and Kuiper, G. P., 1962, Concentric structures surrounding lunar basins: Arizona Univ. Lunar and Planetary Lab. Comm., v. 1, no. 12, p. 51-72.

McCauley, J. F., 1964, The stratigraphy of the Mare Orientale region of the Moon, in Astrogeologic Studies Ann. Prog. Rept., Aug. 25, 1962-July 1, 1963, pt. A: U.S. Geol. Survey open-file report, p. 86-98.

Milton, D. J., 1964, Stratigraphy of the terra part of the Theophilus quadrangle, in Astrogeologic Studies Ann. Prog. Rept., July 1, 1963-July 1, 1964, pt. A: U.S. Geol. Survey open-file report, p. 17-27.

Morris, E. C., and Wilhelms, D. E., 1965, Preliminary geologic map of the Julius Caesar quadrangle: map supplement, this report.

Titley, S. R., 1964, A summary of the geology of the Mare Humorum quadrangle of the Moon, in Astrogeologic Studies Ann. Prog. Rept., Aug. 25, 1962 - July 1, 1963, pt. A: U.S. Geol. Survey open-file report, p. 64-72.

Wilhelms, D. E., 1964, Major structural features of the Mare Vaporum quadrangle: Astrogeologic Studies Ann. Prog. Rept., July 1, 1963-July 1, 1964, pt. A: U.S. Geol. Survey open-file report, p. 1-15.

THE SERENITATIS BENCH AND THE BOND FORMATION

By H. A. Pohn

The northeast margin of the Mare Serenitatis basin is closely
similar to the southeast margin of the Mare Imbrium basin as brought
out by recent geologic mapping in the Macrobius quadrangle of the Moon.
This report summarizes the similarities and differences between these
two areas. The Macrobius quadrangle has been mapped geologically as
part of the geologic study of the equatorial belt of the Moon; the
mapping was carried out largely by telescopic viewing at the 29-inch
reflector of the U.S. Geological Survey in Flagstaff, Arizona.

The northeast margin of the Serenitatis basin is bordered by a
concentric band of relatively low-lying terrain approximately 100 km
wide (ACIC chart, LAC 43). This marginal trough is recognized as a
distinct topographic feature for the first time in this report and is
termed the Serenitatis bench; it resembles the Apennine bench, a low-
lying area southeast of the inner margin of the Imbrium basin (Hackman,
1963). A deposit of material with a flat, heavily cratered surface
fills large segments of the low area marginal to the Serenitatis basin.
It is named the Bond Formation and is analogous to the Apennine Bench
Formation of the Imbrium basin.

Serenitatis bench

The Serenitatis bench is bounded on the west by a series of craters
that form the east margin of the Serenitatis basin and on the east by
low cliffs roughly concentric with the basin. The cliffs belong in part
to the Montes Taurus. The bench is cut by rilles concentric to the
basin. Similar rilles are present on the Apennine bench of the Imbrium
basin. Both benches have the same general form, but the bounding cliffs
of the Apennine bench, the front of the Montes Apenninus, are much high-
er and more sharply defined than the cliffs bordering the Serenitatis
bench on the east. This difference may result from the greater age of

the Serenitatis basin, which has allowed more time for isostatic adjust-
ment of concentric cliffs that were originally much higher. A second
explanation is that the height of the cliffs surrounding the benches is
a measure of the size of the impact events that presumably produced the
two basins. The Serenitatis basin would have been produced by an event
of smaller magnitude than the Imbrium basin.

Many of the craters on the Serenitatis bench are believed to pre-
date the Serenitatis basin. These craters have polygonal shapes tend-
ing toward squares (e.g., G. Bond, LeMonnier V), and many of the straight
segments are approximately radial to the center of the Mare Serenitatis
basin. The straight walls of the craters probably resulted from the
faulting of originally circular craters at the time of the formation of
the Serenitatis basin. The system of faults radial to the center of
the Mare Serenitatis basin is analogous to the system radial to the
center of Mare Imbrium (Hartmann, 1963) but is much less well developed.
Many of the craters with polygonal outlines also have markedly subdued
profiles due possibly to mantling by ejecta from the Mare Serenitatis
basin. The Serenitatis bench has a greater number of such subdued,
older-appearing craters than the Apennine bench; nearly all evidence of
prebasin craters has been eliminated on the Apennine bench, probably by
the strong impact-associated tectonics of the Mare Imbrium basin.

Bond Formation

The Bond Formation is the most extensive single deposit on the
Serenitatis bench. The type locality is in the crater G. Bond B near
the northwest corner of the Macrobius quadrangle. The surface of the
formation is flat overall but is rough in detail; it is cut by many
rilles and chain craters and in addition has a high density of small,
single craters. The albedo is moderately high. The Bond Formation
occupies intercrater lows and overlaps the lower parts of the rim
deposits of craters such as LeMonnier. It also covers the floors of
the older-appearing craters, such as G. Bond C, that have polygonal
outlines and subdued rims and walls. The formation is sufficiently
thick to obscure all details that may have originally been present on

the floor of these craters. It does not cover the higher parts of crater walls or rims. A conservative estimate of the thickness of the formation is 500 to 1,000 meters.

The Bond Formation resembles the mare material of the Procellarum Group in its flatness, apparent thickness and restriction to low-lying areas; it differs in its higher albedo, greater density of small craters and greater dissection by rilles. The Bond appears to be an early generation of mare-like material. The less cratered Procellarum Group is in contact with the Bond Formation around the craters LeMonnier and G. Bond B. Numerous secondary craters from the crater Posidonius occur on the surface of the Bond Formation but not on the Procellarum. The Bond therefore predates the Procellarum Group and the crater Posidonius. The formation postdates the old subdued craters with polygonal outlines on the Serenitatis bench and is thus younger than the formation of the Serenitatis basin. The lower limit on the age of the formation is sometime within pre-Imbrian time; the upper limit is within the Imbrian Period. The formation is therefore designated Imbrian-pre-Imbrian. The Apennine Bench Formation similarly postdates the formation of the Imbrium basin and predates the formation of large craters such as Archimedes and the deposition of the Procellarum Group. The geologic history of both the Imbrium and Serenitatis basins can be summarized as follows: (1) prebasin cratering; (2) formation of the basins by impact with concurrent obliteration or modification of old, prebasin craters; (3) formation of mare-like bench material (Apennine Bench Formation in the Imbrium basin, Bond Formation in the Serenitatis basin); (4) additional cratering (Archimedes in the Imbrium basin, Posidonius in the Serenitatis basin); (5) formation of the mare material of the Procellarum Group.

References

Hackman, R. J., 1963, Stratigraphy and structure of the Apennine region of the Moon, in Astrogeologic Studies Ann. Prog. Rept., Aug. 25, 1961 to Aug. 24, 1962, pt. A: U.S. Geol. Survey open-file report, p. 2.

Hartmann, W. K., 1963, Radial structures surrounding lunar basins, I--The Imbrium System, Arizona Univ. and Planetary Lab. Commun., v. 2, no. 24, p. 1-15, pl. 1-30.

FRA MAURO AND CAYLEY FORMATIONS IN THE
MARE VAPORUM AND JULIUS CAESAR QUADRANGLES

by D. E. Wilhelms

Introduction

Two of the most extensive rock-stratigraphic units of the Mare
Vaporum and Julius Caesar quadrangles[1] are the Fra Mauro and Cayley
Formations. The Fra Mauro Formation covers a large part of the terra
of the lunar earthside hemisphere, and careful mapping of its distri-
bution is prerequisite to its interpretation and to an understanding of
lunar geologic history.

Materials similar to those in the Cayley Formation are also wide-
spread in the terra. In this paper the physical properties of several
facies of the Fra Mauro Formation in the Mare Vaporum and Julius Caesar
quadrangles are described and compared with those of the type area west
of these quadrangles. The most critical and difficult problem is the
location of the outer contact, farthest from the Imbrium basin, because
the characteristic hummocky morphology of the Fra Mauro disappears grad-
ually outward from the basin. Previous workers, noting the steady out-
ward decrease in relief, included in the Fra Mauro certain completely
level and smooth materials beyond exposures with the morphology of the
type area. However, much of the lunar terra is covered by such level
and smooth materials. Accordingly, such materials in the Mare Vaporum
and Julius Caesar quadrangles are withdrawn from the Fra Mauro, and the
definition of the so-called smooth facies of the Fra Mauro is clarified
to embrace only those materials with morphologic affinity to the Fra
Mauro at its type area.

---

[1]Preliminary geologic maps at a scale of 1:1,000,000 of the Mare
Vaporum (Wilhelms, map supplement to Astrogeologic Studies Annual Progress
Report, July 1, 1963 to July 1, 1964) and Julius Caesar quadrangles
(Morris and Wilhelms, map supplement to this report).

The level, smooth materials in the Mare Vaporum and Julius Caesar quadrangles are designated the Cayley Formation. Because of the abundance of Cayley and Cayley-like materials, their interpretation and placement in the stratigraphic column is important in understanding lunar geologic history and processes. They are here interpreted as mare-like materials older than the Procellarum Group. Interpretation of the Fra Mauro Formation as the impact ejecta from the Mare Imbrium basin is supported by studies of the distribution of the facies of the Fra Mauro and their similarity to the facies of crater rim material.

Previous work

Early in the lunar geologic studies of the Geological Survey, Shoemaker and Hackman (1962, p. 293-294) recognized that the terra surrounding Mare Imbrium appears to consist of an old surface buried by a blanket of material whose topography near the basin is everywhere similar. Land forms such as scarps, troughs, and craters, including quite large ones, are muted. The blanket of material was first called simply regional material of the Imbrian System and later designated the Apenninian Series (Shoemaker and others, 1962, p. 114). Eggleton and Marshall (1962, p. 132-134), pointed out that the topographic characteristics of the Apenninian vary systematically with respect to distance from the Imbrium basin, being hummocky close to the basin and smoother farther out, and mapped the approximate limits of the hummocky and smooth facies on much of the earthside hemisphere. Eggleton (1963; 1964, p. 55-56) attempted to calculate the thickness of the Apenninian. Eggleton (1964, p. 50) redesignated the blanketing material as the Fra Mauro Formation in accord with terrestrial practice of designating units which are laterally continuous and either homogeneous or uniformly variable as rock-stratigraphic units. Eggleton designated type areas for the hummocky and smooth facies in and near the crater Fra Mauro in the Montes Riphaeus quadrangle. A unit which lies close to the Imbrium basin and whose surface is much smoother than that of the Fra Mauro was designated the Apennine Bench Formation (Hackman, 1964, p. 3-4; Eggleton, 1964, p. 56), but similar smooth materials farther from the Imbrium basin,

including some adjacent to the type smooth Fra Mauro and some in the Mare
Vaporum and Julius Caesar quadrangles (here called Cayley Formation),
were not explicitly excluded from the smooth Fra Mauro. In an earlier
paper on the Mare Vaporum quadrangle, Wilhelms (1964) briefly discussed
the Fra Mauro Formation and described two variants of its hummocky facies.
The present paper is an extension of this earlier paper. Descriptions
of the hummocky facies are reviewed and expanded and particular attention
is given to the "smooth" facies and to smooth, level materials (Cayley)
mentioned only briefly in previous work.

Fra Mauro Formation

Description

The morphology of the Fra Mauro Formation is generally the same in
belts concentric with the Imbrium basin but changes with increasing dis-
tance from the basin. Several facies can be discriminated on the basis
of this variation: the hummocky facies, with "random" and "lineated"
variants; the smooth facies, which as here defined is not completely
smooth but is smooth relative to the hummocky facies; and the pitted
facies, described here for the first time.

Hummocky facies (Ifh).--The Mare Vaporum and Julius Caesar quadran-
gles are separated from the type areas of the hummocky and smooth facies
of the Fra Mauro Formation by an expanse of mare material, so correlation
of units must be based on comparison of physical properties. Eggleton
(1964, p. 52) provided a clear definition of the hummocky facies: "In
its type area the hummocky facies of the Fra Mauro Formation is charac-
terized by a range of moderate values of normal albedo and by abundant
close-spaced, low, rounded subequidimensional hills and intervening
depressions generally 2 to 4 kilometers across." (The type area is
north of the crater Fra Mauro.) A detailed contour map of this terrain
would show an array of closed positive contours with rounded but irregu-
lar form. The prevalent characteristic of the terrain is disorder or
irregularity; such terrain is aptly described as "hummocky." Approxi-
mately half the terra surface of the Mare Vaporum quadrangle and a

small part of the Julius Caesar quadrangle matches this description[2], and there is little doubt that the hummocky Fra Mauro is present there. The exposures in these quadrangles and in the type area are no doubt continuous beneath the overlying mare material.

Two gradational variants of the hummocky facies are recognized in the Mare Vaporum and Julius Caesar quadrangles. In one, positive and negative relief elements have little preferred orientation; the topography appears completely disordered. This variant, here called "random Ifh," occurs in a belt close to the Imbrium basin, notably on the southeast slope of Montes Apenninus where its hummocky character is well developed (fig. 2). The other variant is also largely disordered and hummocky, but has less relief; positive and negative elements are vaguely sinuous and braidlike and are elongated subradial to the Imbrium basin with length-to-width ratios of from 2:1 to 8:1 (Wilhelms, 1964, p. 3-4). This variant, here called "lineated Ifh," occurs in a belt farther from the Imbrium basin than random Ifh and is well seen south and east of Sinus Aestuum (fig. 3). It is more like the type hummocky Fra Mauro than is the random Ifh, but the difference between lineated and random variants is so slight that there is no doubt that they are gradational variants of the same rock-stratigraphic unit and that the random Ifh is also Fra Mauro Formation.

Smooth facies.--Another facies of the Fra Mauro Formation is the so-called smooth facies (Ifs), which lies still farther from the Imbrium basin than the lineated Ifh. The type area is in the southwest part of the crater Fra Mauro (Eggleton, 1964, p. 51-52). The identification of Ifs as Fra Mauro is based on three properties: it mantles subjacent terrain, is laterally continuous with Ifh, and displays vague, braidlike

---

[2] Some of the Fra Mauro of the Mare Vaporum quadrangle has a very low albedo and thereby differs from the type. The difference in albedo may be due to a cover of younger materials (Carr, following article). On the 1:1,000,000 and 1:5,000,000 geologic maps in the map supplement to this report, Ifh is divided into dark (Ifhd) and light (Ifhl) facies rather than into the "random" and "lineated" facies discussed in this report and shown in figure 1.

EXPLANATION

lpm

Craters

lfhr

lfhl

lfs

lfp

lcy

Fig. 1.

17

ridges with orientation and shape similar to the braidlike complexes of lineated Ifh (figs. 2 and 4). Ifs is distinguished from Ifh by the much more subdued relief of its braidlike ridges and by the lack of hillocks resolvable on very high resolution photographs (Lick L-24). The difference in "smoothness" between Ifs and Ifh is one of degree, because the gentle surface of Ifs is also hummocky, in the sense of being mostly disordered. Completely flat and smooth materials, some previously mapped as Ifs, are assigned in the interest of stratigraphic objectivity to other units such as the Apennine Bench Formation (Hackman, 1964, p. 3-4; and Eggleton, 1964, p. 56) and the Cayley Formation, defined and described in a later section.

Since the presence of subelongate ridges is one of the criteria for mapping both Ifs and lineated Ifh, care must be taken to distinguish ridges intrinsic to the Fra Mauro Formation from structural ridges of the Imbrian sculpture system[3], which are largely coextensive with the Fra Mauro. The distinction is not always possible, because Imbrian sculpture is mantled by Fra Mauro and expressed in subdued form; but for the most part sculpture elements are straighter than Fra Mauro ridges. In the Mare Vaporum and Julius Caesar quadrangles the outer contact of Ifs is drawn where observable low sinuous ridges give way to straight ridges; of course, this contact is gradational and its placement subject to considerable uncertainity. Telescopic observations or very high resolution photographs are necessary to distinguish the kinds of ridges. The many very small, straight lineaments beyond the Ifs contact drawn in this way are taken as an indication that Ifs is either absent or very thin, and the terrain containing them is presently mapped as pre-Imbrian undifferentiated. Milton (1964, p. 20-21) mapped such terrain as questionable Fra Mauro, to show that at least no post-Fra Mauro units were present. Materials of the Fra Mauro may, of course, be present but undetectable.

---

[3]Imbrian sculpture is a convenient collective term for the prominent system of scarps, ridges, and troughs closely radial to the center of the Mare Imbrium basin. For a review see Hartmann (1963).
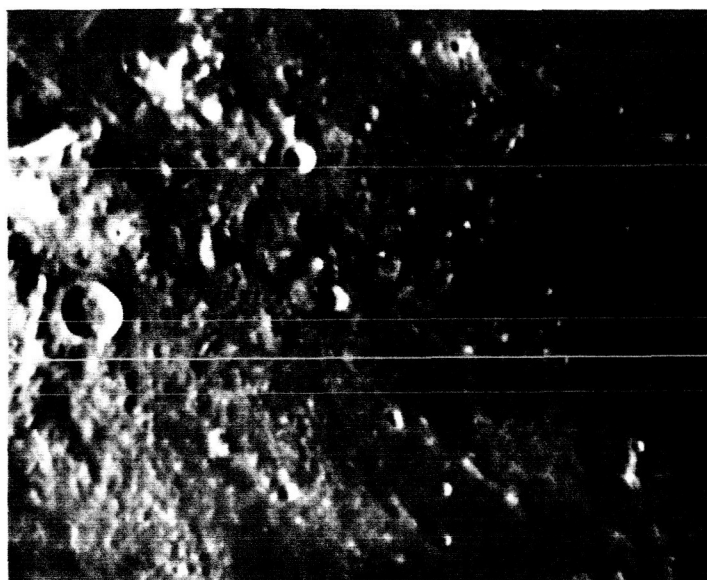
Fig. 2.--Northwest front of Montes Apenninus at left, part of Montes Haemus at lower right; large crater is Conon, 22 km in diameter. Shows typical "random" hummocky facies of the Fra Mauro Formation on the flank of Montes Apenninus, near the Mare Imbrium basin, and the smooth facies of the Fra Mauro in Montes Haemus, farther from the basin. Large, bright-appearing blocks in Montes Apenninus are probably pre-Fra Mauro bedrock.

Fig. 3.--"Lineated" hummocky facies of the Fra Mauro Formation east of Sinus Aestuum, showing braidlike lineation radial to Mare Imbrium.
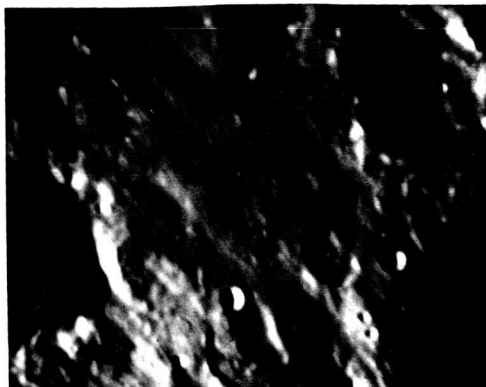
Fig. 4.--Smooth facies of the Fra Mauro Formation in center. Irregular crater at left is Boscovich; smooth floor is 34 km north to south.

Fig. 5.--Cayley Formation and pitted facies of the Fra Mauro Formation. Middle one of three sharp craters at top is Cayley, 14 km in diameter. Large irregular crater is d'Arrest. Most of terra is pitted facies of the Fra Mauro Formation. Smooth material east (right) of Cayley is type locality of Cayley Formation.

Terrain differing from Ifh and Ifs occurs in the southwest corner of the Julius Caesar quadrangle, in the vicinity of the crater d'Arrest (fig. 5), farther from the Imbrium basin than Ifh and Ifs, and may constitute a third facies of the Fra Mauro. An important characteristic of this terrain is the presence of many irregular, equidimensional to elongate shallow depressions, predominantly of the order of 1 km across but ranging up to 3 km wide and 8 km long. This terrain differs from Ifh by having no discrete hillocks, although the topography is hummocky in the sense of being irregular and rolling; a detailed contour map would show the dominance of negative closed contours. Much of the terrain resembles Ifs, but in common with other terrain far from the Imbrium basin, many ridges are present that are straighter and sharper than those of Ifs. Possibly Ifs is present in isolated patches. The small scale of the map (fig. 1) precludes mapping the individual depressions or the small areas of possible Ifs, so the terrain is collectively designated the pitted facies of the Fra Mauro Formation (Ifp). It may not be a true facies, however, because of the possible lack of a primary mantling deposit, a point that is discussed below. An interpretation of the origin of Ifp, which follows from the interpretation of the other Fra Mauro facies, is given below.

Interpretation

Many lunar geologists agree that the Fra Mauro Formation is the ejecta from an impact that excavated the Mare Imbrium basin (bibliography in Shoemaker and Hackman, 1962, p. 293). The close geographic relation of the Fra Mauro to the Imbrium basin implies a genetic relation, and the Fra Mauro characteristically mantles subjacent terrain. The best evidence for the impact-ejecta hypothesis lies in the morphologic similarity of the facies of the Fra Mauro to the facies of crater rim material. The purpose of this section is to examine this similarity, and in a general way to account for the morphologic characteristics of the Fra Mauro in terms of an impact model.

Large, fresh lunar craters, confidently interpreted to be of impact origin (for example, Copernicus and Aristoteles; see Shoemaker, 1962,

p. 307-344), characteristically are surrounded by rim material with pro-
nounced positive relief near the rim crest that grades outward to a field
of secondary impact craters where negative relief dominates (fig. 6).
Rim material forms a continuous blanket out to about one crater diameter
beyond the rim crest. This blanket consists of two main facies whose
transition is marked by a break in slope: an inner, thick facies with
a surface topography of randomly oriented hills and ridges, that is,
coarsely hummocky topography (fig. 6, facies a), and an outer, thinner
facies characterized by elongate ridges and depressions with an orienta-
tion approximately radial to the crater (fig. 6, facies b). The ridges
become subdued outward, and the continuous blanket passes into a region
where discontinuous deposits of low relief and secondary craters occur
together (fig. 6, facies c). Finally, there is an outer region where
only secondary craters occur, along with ray material which has no dis-
cernible positive relief and is probably mostly ejecta from the second-
aries (fig. 6, facies d).

The morphologic characteristics of the Fra Mauro Formation change
outward from the Imbrium basin in a similar fashion. The hummocky Fra
Mauro has both a thick inner facies of disoriented surface topography
("random Ifh") and an outer facies of lesser relief and elongate ridges
subradial to its presumed source, the Imbrium basin ("lineated Ifh");
and the transition between these facies occurs at a break in slope, the
southeast base of Montes Apenninus. The smooth facies (Ifs), which is
smooth only relative to Ifh, probably corresponds to the outer, subdued
part of the continuous blanket of crater rim material.

The pitted "facies" (Ifp) also has a parallel in crater deposits,
the region in which shallow secondaries and thin, discontinuous primary
deposits occur together. By analogy with crater deposits, deposits of
ejecta from Ifp "secondary craters" would be expected, as well as thin
deposits of primary ejecta (the patches of possible Ifs). The probable
presence of these deposits partially justifies designation of Ifp as a
facies of the Fra Mauro Formation, but the designation is largely for
convenience.

22
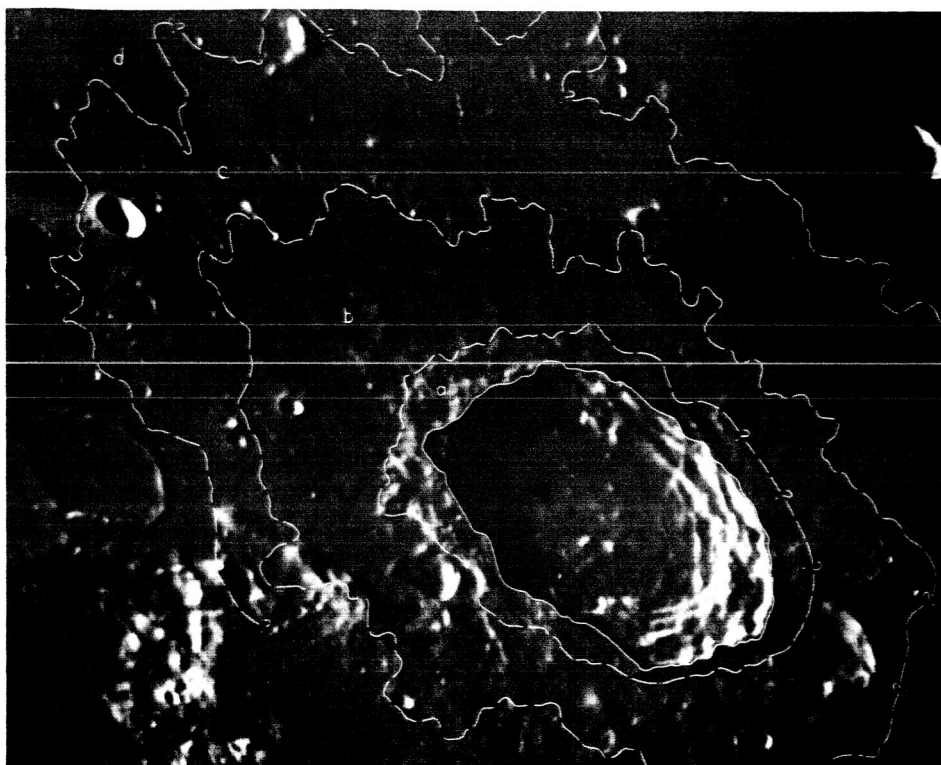
Fig. 6.--Crater Aristoteles, 90 km in diameter, showing facies of
its rim material (all contacts are gradational): (a) very thick rough
hummocky material; (b) subdued ridges subradial to crater; (c) second-
ary craters and discontinuous primary deposits with slight relief; (d)
secondary craters with no primary deposits with detectable relief.

Fig. 7.--Rolling terrain with possible Imbrian secondary craters
(right). Crater in upper right (NE) corner is Moltke, 7 km in diameter.

Since the facies of the Fra Mauro Formation seem to resemble those of the material around impact craters, the problem arises of locating the main field of deep Imbrian secondaries. Broad, smooth-surfaced, rolling terrain, with many pits, occurs in the area just southeast of Ifp in the Julius Caesar quadrangle (fig. 7). The pits are strongly suggestive of secondary craters from the Imbrium primary crater.

Scaling relations between the very large Imbrium crater and smaller craters are of course uncertain because of the many variables involved, but I believe one can explain the outward changes of typical impact-crater rim materials and the Fra Mauro Formation qualitatively as a function of the amount of material available for dispersal over a given area. The amount of material decreases outward, while the amount of energy in each clot of ejecta increases, resulting in an increasing dominance outward of cratering over deposition. In the continuous blanket, shallow craters are formed by clots with low specific energies but are immediately swamped by more material which forms more craters and covers the rims of the earlier craters; disoriented hummocky topography is the result. The lineated facies may result from a combination of effects: ejecta has a tendency to travel in stringers because of anisotropic breakup of target rocks (Shoemaker, 1962, p. 335-340); it would also be expected to streak out upon impact because of low trajectories of ejection [Shoemaker (1962, p. 335) calculates that the continuous blanket of Copernicus is formed by material ejected below about 14°]. The discontinuous blanket and the regime of deep secondaries are the products of impact of much less material with much greater specific energy.

Cayley Formation

Definition

The outer contact of the Fra Mauro Formation is difficult to locate because the formation thins and its surface relief decreases outward from the Imbrium basin. Noting this steady decrease in relief and assuming that the relief would decrease to complete flatness, some workers have mapped materials which form smooth, flat plains, including some

immediately adjacent to the type area of the smooth Fra Mauro, as "smooth Apenninian" (Eggleton and Marshall, 1962, p. 132-134) and smooth Fra Mauro Formation (Eggleton, 1964, p. 51-54). However, definition and mapping of the Fra Mauro Formation, like that of all rock-stratigraphic units, lunar and terrestrial, must be based on a set of observable physical properties by which the unit can be recognized uniquely. Extension of the definition of the Fra Mauro to include flat and smooth materials makes this unique recognition impossible, because smooth plains-forming materials occur over much of the lunar surface, and not all can be Fra Mauro. Even if some of these materials should be correlative with the Fra Mauro, there is no way to distinguish them from other similar materials. Some plains-forming materials mantle subjacent terrain, but the property of mantling is not sufficient for identification of Fra Mauro because many lunar materials, including mare material, mantle objects of considerable size.

Accordingly, smooth plains-forming materials of the lunar terrae without the low, undulating, braidlike ridges and depressions characteristic of Ifs are here withdrawn from the Fra Mauro Formation. Such materials may fall into several rock-stratigraphic units, but only one, the Cayley Formation, is defined here, with its type area east of the crater Cayley in the Julius Caesar quadrangle (fig. 5)[4]. The Cayley resembles the Apennine Bench Formation (Hackman, 1964, p. 3-4; Eggleton, 1964, p. 56), but the two formations are too far apart to be correlated and separate names are desirable.

Description

Two large and several small areas in the Mare Vaporum and Julius Caesar quadrangles are mapped as Cayley Formation, all in topographic depressions. Parts of two large, broad troughs concentric with the Mare Imbrium basin lie in the two quadrangles (Wilhelms, 1964, p. 5-6); one

---

[4]Cayley is a later superimposed crater and has no genetic connection with the formation.

includes Sinus Medii, and another farther out from the basin is the site
of the crater Cayley. The Cayley Formation occupies a large area of the
first trough northeast of Sinus Medii, and fills most of the second. All
the Cayley in these troughs is smooth, except for superimposed craters,
and most is flat. Its flatness is interrupted locally by the muted forms
of craters, scarps, and ridges. Contacts with hummocky and pitted Fra
Mauro are sharp, but some contacts with smooth Fra Mauro are not sharp.

The contrast between the topography of the Cayley Formation and that
of the Fra Mauro and other surrounding materials is especially clear in
the small areas of Cayley. These local deposits are mostly in steep-
sided depressions, and their contacts with surrounding terrain are sharp.

The stratigraphic position of the Cayley is well established. Trun-
cation of Imbrian sculpture and sharp contacts of patches isolated with-
in the Fra Mauro Formation establish that its lower limit lies within
the Imbrian System. Embayment by mare material of the Procellarum Group
and much greater density of superimposed craters than that of the Pro-
cellarum Group establish its upper limit as also within the Imbrian.
Although all the Cayley is therefore Imbrian, ages of materials on the
surface of individual patches may differ locally.

All Cayley has approximately the same albedo (.100-.115) and polar-
ization (7%). The albedo is higher and the polarization lower than those
of the Procellarum Group.

Interpretation

The patches of Cayley Formation in the small depressions provide the
best evidence that the modes of deposition of the Cayley and Fra Mauro
Formations are different. The sharp contacts with surrounding rugged
terrain and abrupt termination of structures show that a considerable
thickness of material is sharply localized. It is unlikely that ejecta
would pool in this way, even though it may tend to shed from highs.

An interpretation that accounts well for the smoothness, flatness,
and localization of the Cayley is that it consists of volcanic flows.
The alternative of "air"-fall tuff seems excluded by the same character-
istic that excludes ejecta, localization. Another alternative, that

the Cayley is the product of erosion from adjacent terrain, might be reasonable for the small deposits but not for those of the broad troughs. In general, the Cayley behaves like mare material; it forms extensive, smooth, flat surfaces and preferentially fills depressions. It may therefore be the product of an early generation of material like that of the Procellarum Group.

The property of mantling which is imputed to the Cayley by the mapping of it over muted forms of craters and other features can also be accounted for by volcanic genesis. Terrestrial ash-flow tuff is capable of compaction after emplacement of up to 50% of its volume (R. L. Smith, personal communication), and differential compaction that leaves subjacent relief visible in muted form is known in areas of thick ash-flow deposits (Valley of 10,000 Smokes). Thus the Cayley Formation, as well as much of the Procellarum Group, may be ash-flow tuff.

Conclusions

The Fra Mauro Formation is identified in the Mare Vaporum and Julius Caesar quadrangles on the basis of lithologic similarity to the formation in its type locality. The previous interpretation of the Fra Mauro Formation as impact ejecta from the Mare Imbrium basin is supported by comparison of the distribution and gradational morphology of its facies with the facies of crater rim material. Smooth, flat materials previously considered as Fra Mauro are withdrawn from the formation and designated the Cayley Formation. The Cayley is Imbrian in age and is interpreted as pre-Procellarum mare-like material, possibly ash-flow tuff.

References

Eggleton, R. E., 1963, Thickness of the Apenninian Series in the Lansberg region of the Moon, in Astrogeologic Studies Annual Prog. Rept., August 25, 1961 - August 24, 1962, Pt. A: U.S. Geol. Survey open-file report, p. 19-31.

References--Continued

Eggleton, R. E., 1964, Preliminary geology of the Riphaeus quadrangle
    of the Moon and definition of the Fra Mauro Formation, in Astrogeo-
    logic Studies Annual Prog. Rept., August 25, 1962 - July 1, 1963,
    Pt. A: U.S. Geol. Survey open-file report, p. 46-63.

Eggleton, R. E., and Marshall, C. H., 1962, Notes on the Apenninian
    Series and pre-Imbrian stratigraphy in the vicinity of Mare Humorum
    and Mare Nubium, in Astrogeologic Studies Semiannual Prog. Rept.,
    February 26, 1961 - August 24, 1961: U.S. Geol. Survey open-file
    report, p. 132-137.

Hackman, R. J., 1964, Stratigraphy and structure of the Montes Apenninus
    quadrangle of the Moon, in Astrogeologic Studies Annual Prog. Rept.,
    August 25, 1962 - July 1, 1963, Pt. A: U.S. Geol. Survey open-file
    report, p. 1-8.

Hartmann, W. K., 1963, Radial structures surrounding lunar basins, I:
    The Imbrium System: Univ. Arizona Lunar and Planetary Lab. Commun.,
    v. 2, no. 24, p. 1-15.

Milton, D. J., 1964, Stratigraphy of the terra part of the Theophilus
    quadrangle, in Astrogeologic Studies Annual Prog. Rept., July 1,
    1963 - July 1, 1964, Pt. A: U.S. Geol. Survey open-file report,
    p. 17-27.

Shoemaker, E. M., 1962, Interpretation of lunar craters, in Kopal, Zdenek,
    ed., Physics and Astronomy of the Moon: New York and London, Academic
    Press, p. 283-359.

Shoemaker, E. M., and Hackman, R. J., 1962, Stratigraphic basis for a
    lunar time scale, in Kopal, Zdenek, and Mikhailov, Z. K., eds.,
    The Moon-Symposium no. 14 of the International Astronomical Union:
    London, Academic Press, p. 289-300.

Shoemaker, E. M., Hackman, R. J., Eggleton, R. E., and Marshall, C. H.,
    1962, Lunar stratigraphic nomenclature, in Astrogeologic Studies
    Semiannual Prog. Rept., February 26, 1961 - August 24, 1961: U.S.
    Geol. Survey open-file report, p. 114-116.

Wilhelms, D. E., 1964, Major structural features of the Mare Vaporum quad-
    rangle, in Astrogeologic Studies Annual Prog. Rept., July 1, 1963 -
    July 1, 1964, Pt. A: U.S. Geol. Survey open-file report, p. 1-16.

COMPILATION OF GEOLOGY IN THE LUNAR EQUATORIAL BELT

by D. E. Wilhelms and N. J. Trask

Included in the map supplement to this report is a compilation of
the geology of the lunar equatorial belt, 70°W-70°E, 32°N-32°S, at a
scale of 1:5,000,000. This map was constructed from existing maps at
a scale of 1:1,000,000 made by members of the Branch of Astrogeology
and from reconnaissance maps made by the authors in some incompletely
mapped areas. This preliminary effort shows the status of lunar stra-
tigraphy at the time of the compilation, and it has already been in
part superseded by new work. Revised editions will be issued from time
to time as mapping progresses and stratigtaphic concepts evolve.

The conventions employed on the compiled map are as follows. Each
geologic unit or formation is designated by a symbol composed of two
parts--an abbreviation of its age (capital) and of its name (lower case).
Table 1 gives the meanings of these abbreviations. The order of the
geologic units has been determined by application of the principles of
superposition and intersection; the assigned ages follow the lunar time
scale of Shoemaker and Hackman (1962).

The development of each mare basin provides a series of convenient
time markers. Materials older than, contemporaneous with, and younger
than, the formation of each basin have been recognized. The local
stratigraphic columns for the basins are correlated in figure 1, which
provides a composite stratigraphic section for the entire equatorial
belt. Materials older than the formation of each basin are identified
simply as pre-Imbrian crater materials (pIc) and pre-Imbrian materials,
undifferentiated (pIu). Materials identified as contemporaneous with
the origin of the mare basins occur on the raised rims of some basins
and extend outward for varying distances around them. Most distinctive
of these are hummocky materials around the Imbrium basin (If), Orientale
basin (Ico), Humorum basin (pIhr), and Fecunditatis basin (pIse). These
materials are believed to be impact ejecta. Around the Crisium, Nectaris,

ROCK - STRATIGRAPHIC UNITS

Fig. 1.

and Serenitatis basins, materials of the raised rims surrounding the basins are mapped simply as rim materials (e.g., pIkr, Crisium rim material) and are only tentatively identified as basin-contemporaneous deposits. In addition, near the Nectaris basin, certain hummocky materials (pIh) are mapped separately, as they are thought to be contemporaneous with that basin. Certain other terrains are shown in the stratigraphic section as possibly contemporaneous with some nearby basins; these terrains (IpIt) are highly pitted by craters that resemble secondary impact craters and may in fact be secondaries from the nearby basins. The age sequence of basin rim materials shown in figure 1 is tentative and is based on the amount of subsequent modification of the materials and associated structures, intersection relations among associated structures, and density of superimposed craters.

Materials younger than the basins are of two main kinds: regional materials and crater materials. The best-known regional material is the plains-forming mare material (Procellarum Group, Ipm), much of which is of about the same age in every basin. In addition, near each basin are other plains-forming materials that are older than the Procellarum Group but younger than the basin; these are given various formal and informal names (Apennine Bench Formation, Iab; plains-forming material, Ip, etc.). They are shown on the right side of the stratigraphic column for each basin (fig. 1). Crater materials that are younger than the basin but older than the Procellarum Group are shown in a parallel space on the left side of each column. Crater materials of this type in each basin are assigned to a rock-stratigraphic group (table 1) named for a typical crater in each basin (Gassendi Group, IpIg, for the Humorum basin; Fracastorius Group, IpIf, for the Nectaris basin, etc.). The crater materials of this type first recognized are those like Archimedes, which are younger than the Imbrium basin but older than the Procellarum Group.

The youngest materials, those that are younger than the Procellarum Group, are given the same designations in each area--for example, Ec for materials associated with rayless craters, Cc for materials associated with rayed craters, and Cs for young, bright slope material. Finally, certain special units of local extent are shown in the column of the

nearest basin, although they may have no direct relation to the basin (Cre, Ch, etc.).

Table 1. Explanation of abbreviations used in compilation of geology
in the lunar equatorial belt

Time-stratigraphic units of the lunar time scale

      C = Copernican System
      E = Eratosthenian System
      I = Imbrian System
     pI = pre-Imbrian rocks

Pre-basin units

      pIc   crater materials
      pIu   undifferentiated materials

Units contemporaneous with formation of basins

      Ico Cordillera Group
      If   Fra Mauro Fm
        Ifu   undifferentiated
        Ifhl hummocky light facies
        Ifhd hummocky dark facies
        Ifs   smooth facies
      pIkr   Crisium rim material
      pIhr   Humorum rim material
      pInr   Nectaris rim material
      pIsr   Serenitatis rim material
      pIse   Secchi Fm
      IpIt   pitted material
      pIh   hummocky material

Post-basin, pre-mare plains-forming materials

Ip	plains-forming material, undifferentiated
Icy	Cayley Fm
Iab	Apennine Bench Fm
Inb	Nectaris Bench Fm
Iso	Somni Fm
IpIhb	Humorum Bench Fm
pIb	Bond Fm

Post-basin, pre-mare craters

Ik	Crüger Group
Ic	Archimedes Group (and other Archimedian Series craters)
IpIy	Yerkes Group
IpIg	Gassendi Group
IpIf	Fracastorius Group
IpIp	Posidonius Group

Mare materials-Procellarum Group

Ipm	plains-forming mare material
Ipd	mare domes
Iph	hummocky mare materials

Post-mare crater units

Cs	bright slope material
Cd	dark halo craters
Cc	material of rayed craters
Ec	material of rayless craters

Miscellaneous post-mare units

    CEmd   dark mare material (near several basins)

    Cre   Reiner Gamma Fm (very bright patches with no visible relief)

    Ct   Theophilus Fm (very smooth plains-forming materials)

    Ch   Cobra Head Fm (large steep hill at end of Vallis Schröteri)

    CEv   Vallis Schröteri Fm (smooth, very dark materials)

    Em   Marius Fm (domes and undulating mare-like materials)

    EIh   Harbinger Fm (dark mare-like materials with craters and rilles)

    ch   chain crater

    sr   sinous rille

Note: materials of large craters of all groups are subdivided as
     follows:

    r   rim material

    w   wall material

    f   floor material

    p   peak material

      examples: Ccr, rim material of Copernican crater
                IpIgp, central peak of Gassendi Group crater
                EIcw, wall material of crater of either E or I age.

Reference

Shoemaker, E. M., and Hackman, R. J., 1962, Stratigraphic basis for a
    lunar time scale, in Kopal, Zdenek, and Mikhailov, Z. K., eds.,
    The Moon--Symposium no. 14 of the International Astronomical Union:
    New York, Academic Press, p. 289-300.

DARK VOLCANIC MATERIALS AND RILLE COMPLEXES IN THE

NORTH-CENTRAL REGION OF THE MOON

by M. H. Carr

Introduction

Along the southern margin of Mare Serenitatis and around Sinus Aestuum and Mare Vaporum are several areas with very low albedos both in the maria and the uplands. The dark upland areas and dark mare areas appear to be related in origin. Both are near the mare-upland boundary and both are commonly associated with rilles. The dark areas are here interpreted as volcanic materials. These dark volcanics, where they occur in the uplands, appear to be pyroclastic and in some places are younger than the adjacent mare material and in other places older. The very dark volcanics in the mare are probably in large part flows, and represent the final stages in the filling of the maria. They are considered younger than the Procellarum Group. The dark upland areas have previously been interpreted as indicating a dark facies of the Fra Mauro Formation (Shoemaker and Hackman, 1962), but new photographic evidence and detailed geologic mapping has shown that this interpretation is unlikely.

Within Mare Serenitatis, the surface of the Procellarum Group itself has different albedos in different regions. The darkest material of the group is probably its youngest member; the material with the highest albedo is probably the oldest exposed member in Mare Serenitatis.

Description of selected areas with very low albedo

Within Mare Serenitatis, at its southern edge, is a set of rilles in an area of low albedo, the Menelaus rille system (Mt. Wilson photographs W-108 and W-111, Lick Observatory photograph L-32, the map of Mare Serenitatis in the Supplement to this report). Most of the rilles are parallel to the edge of the mare, but a few are at an angle to the edge and intersect the other rilles. The rilles are in general linear and grabenlike. Along them are many small craters, some with and some without bright

halos, and between them are numerous low hills 1 to 2 km across whose albedos are higher than that of the mare. Most of the material between and immediately adjacent to the rilles has a very low albedo, lower than that of the adjacent mare material. This dark material is here named the Tacquet Formation, dark member, after the crater Tacquet. Surrounding the dark member at the western end of the rille system is a lighter material, the topography of which is characterized by very low, broad ridges and depressions. This brighter material is here named the light member of the Tacquet Formation.

The distinguishing properties of the dark member are its very low albedo and its association with rilles; the unit occurs everywhere within 10 km of a rille. At the western end of the rille system the unit forms smooth, rounded, low domelike hills 5 to 8 km across and elongate in a direction parallel to the length of Rima Menelaus I. This rille cuts through the center of the elongate domes so that the dark member appears to form raised smooth rims on the rille. Farther east, between Rima Menelaus III and the crater Tacquet, the surface of the dark member is marked by irregular low hills 1 to 2 km across and shallow depressions. Since many of the areas of higher elevation are at the edges of rilles, the rims of the rilles commonly have a higher elevation than the immediately adjacent terrain. A low scarp marks the edge of the dark member, with the dark facies on the upper side.

At the western end of the Menelaus rille system, partly surrounding the dark facies, is a lighter unit forming a scarplike contact with the Procellarum Group. This unit is the light facies of the Tacquet Formation. The albedo of the unit is approximately the same as that of the surrounding mare, but the unit is distinguished from the mare by its surface texture; some very low ridges 3 to 5 km across are barely discernible even under optimum illumination. To the west the ridges are roughly radial to the center of Menelaus γ, and farther east they are at right angles to the length of Rima Menelaus II. The unit is partly covered with ejecta from the crater Menelaus.

The age of the Tacquet Formation is indicated by its relation to the rilles and ray craters. The Menelaus rilles cut the mare, and therefore

appear to be younger than the mare. The close association between the
Tacquet Formation and the rilles suggests that they are related in origin
and possibly approximately equivalent in age. This would date the Tacquet
Formation as post-Imbrian. Ray material and ejecta from the Copernican
craters Menelaus and Tacquet partly cover the Tacquet Formation, indica-
ting that the formation is pre- or early Copernican. The unit is, there-
fore, probably Eratosthenian or early Copernican in age.

Also within Mare Serenitatis but at the eastern edge, is another
network of rilles that is associated with materials with very low albedos.
This is the Littrow rille system (Mt. Wilson photograph W-90, Lick Observ-
atory photograph L-32 and map of Mare Serenitatis in the Supplement to
this report). These rilles cut both the mare and the uplands, but the
dark region is restricted to the mare. In contrast to the Tacquet Forma-
tion, the dark material between and around the Littrow rilles is smooth
and level and resembles the Procellarum Group in every respect except
that it has an unusually low albedo. To the north of Littrow BA, the
contact with the Procellarum Group is marked by a low scarp; south of
Littrow BA, the contact is indicated only by an albedo change. The dark
material terminates abruptly against the uplands to the east. Around
Littrow BA are several small craters and irregular depressions up to 3 km
in diameter. This cluster of craters is surrounded by raylike material
with a high albedo and no discernible relief.

At the western edge of Mare Serenitatis, near the Haemus Mountains,
is yet another system of rilles surrounded by material with a very low
albedo (Mt. Wilson photograph W-108, Lick Observatory photograph ECD-82
and fig. 1). These are the Sulpicius Gallus rilles, and they resemble the
Littrow rilles in that they cut both upland and mare units. The rilles
are grabenlike linear depressions along which are several craters. The
edges of the rilles are scalloped so that they in part resemble crater
chains. The associated dark materials, in contrast to those around the
Littrow and Menelaus rilles, occur both on the upland and on the mare.
The boundary of the dark units cuts across the contacts between the Pro-
cellarum Group and the Fra Mauro Formation; the dark material is, there-
fore, younger than both of these units. The contact between the dark unit
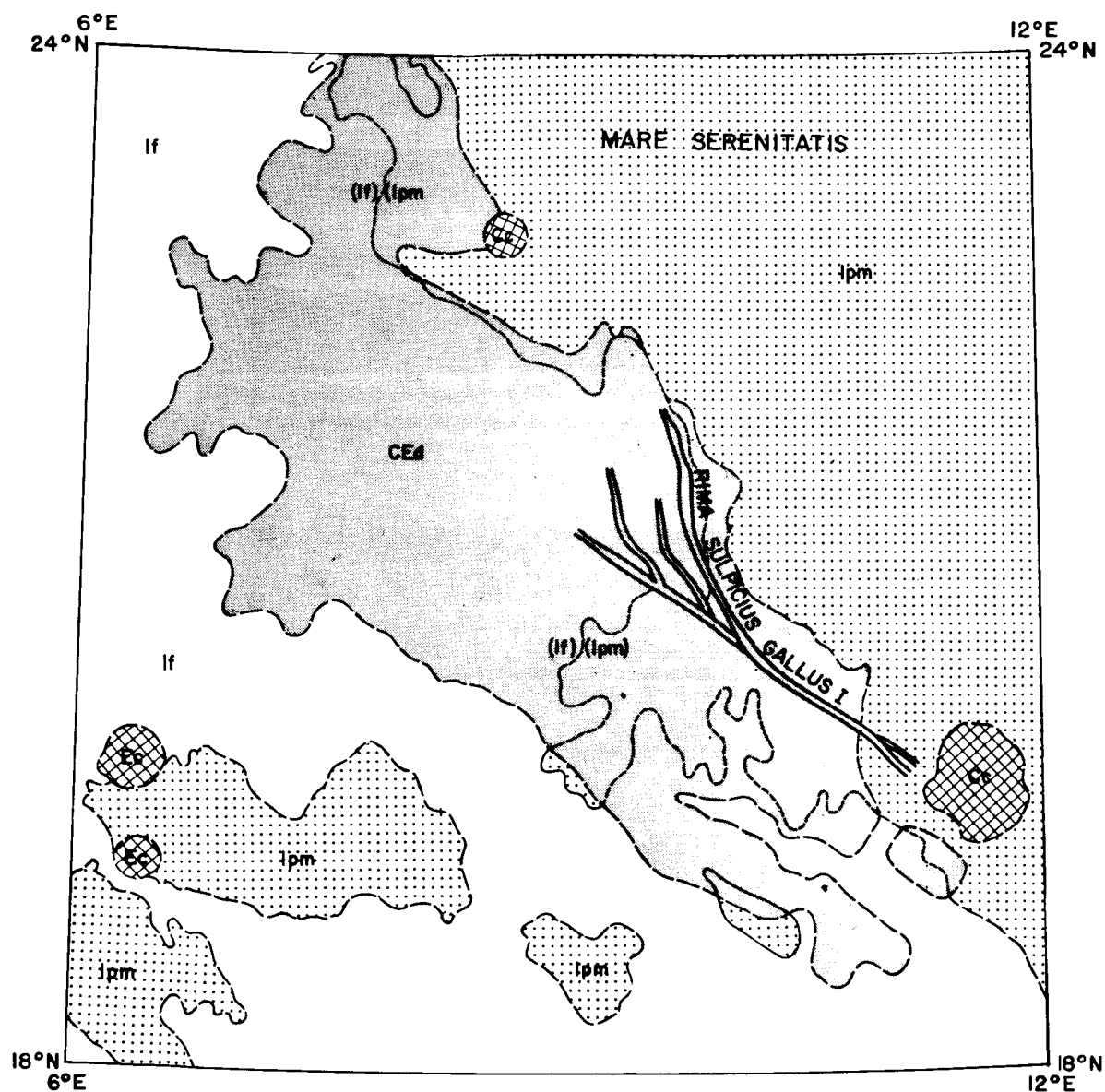and the Procellarum Group is indicated by a sharp albedo change. However,

Fig. 1.--Geologic map of an area on the southwest edge of Mare Serenitatis showing the dark volcanics (CEd) cutting across the contacts between the Fra Mauro Formation (If) and the Procellarum Group (Ipm). For meaning of other abbreviations see the table on page 31.
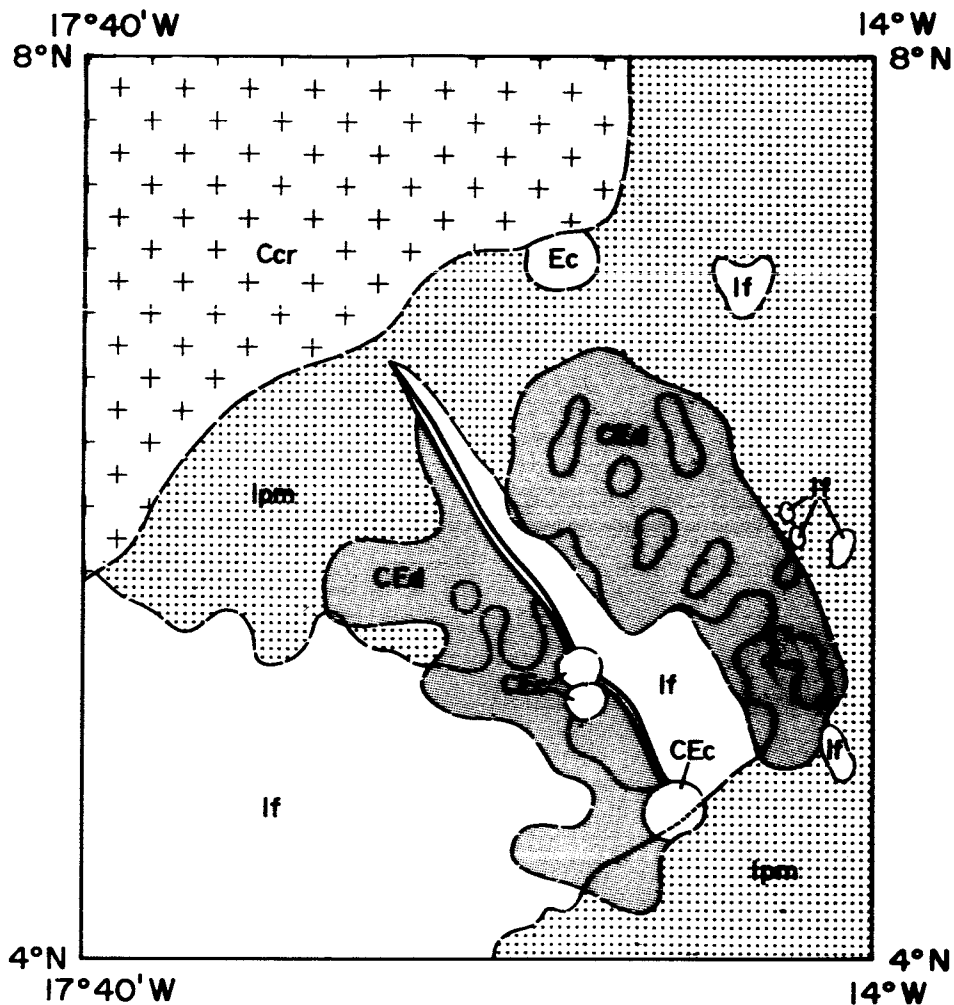
Fig. 2.--Geologic map of an area 150 km southeast of Copernicus
showing the dark volcanics (CEd) cutting across the contacts between
the Fra Mauro Formation (If) and the Procellarum Group (Ipm). For
meaning of other abbreviations see the table on page 31.

because many hills and steep slopes within the dark area have moderate albedo, the contact between the dark unit and the Fra Mauro Formation is a transitional albedo change. Nowhere has the contact any topographic expression. The dark material has observable relief only close to the rilles, where it appears to form raised rims. Within the dark area are some irregular elliptical craters with dark halos and a narrow rille terminating in a crater. The dark material overlies the Procellarum Group and has Copernican craters on it; therefore, like the Tacquet Formation, it is probably Eratosthenian or early Copernican in age.

Dark upland areas are not restricted to the Mare Serenitatis region. Southeast of Copernicus is a small dark area (Mt. Wilson photograph W-124 and Lick Observatory photograph ECD-54 and fig. 2) that resembles the dark area around the Sulpicius Gallus rilles. The dark area includes both the flat and level terrain of the mare and the characteristically hilly terrain of the upland; the boundaries of the dark area cut across the contacts between the Fra Mauro Formation and the Procellarum Group, showing that the dark material is younger than both these units. Furthermore, within the dark area is a rille in which are several craters. The rille has rounded walls and is very shallow, but is still clearly visible under good illumination. The dark material has no observable relief, and no scarp marks its contact with the Procellarum Group. The dark unit here, therefore, resembles that near the Sulpicius Gallus rilles in every respect, and probably is similar in origin.

Other dark upland areas occur around Sinus Aestuum and Mare Vaporum. These areas will not be discussed in detail. They all occur close to the upland-mare boundary, and the rille Rima Conon is in one of the dark areas. They resemble the dark upland area around the Sulpicius Gallus rilles, except that the areas of low albedo abruptly terminate against the mare. If the dark areas indicate a mantling of the Fra Mauro by a dark material, then this dark material is older than the present surface of the Procellarum Group in these areas. Parenthetically, it may be noted that in Mare Vaporum, as in the Mare Serenitatis, the Procellarum Group close to the mare-upland contact has a lower albedo than that in the center of the mare.

Interpretation

The dark mare units near the edge of Mare Serenitatis must be locally derived and related in origin to the rilles; the association of dark mare units with rilles is too recurrent to be fortuitous. This implies that the dark units are the product of some form of volcanism that is operative only in the immediate vicinity of rilles. Localization of volcanism in the vicinity of terrestrial rifts, possible analogs of lunar rilles, is not uncommon; well known examples are the Rhine and East African rifts. Further evidence that the rilles might be a source of volcanic materials is the fact that many craters are found along all the rilles (they are especially abundant along the Menelaus rilles). Where fully formed craters are absent, the rille walls are commonly scalloped so that the rille appears to be formed of a line of overlapping craters. A possible terrestrial analog of such a rille is Eldgja in Iceland, which has been the source of voluminous volcanic material.

On the earth, surface volcanic materials are the product of either pyroclastic or flow volcanism. The dark lunar materials being considered here are also probably either pyroclasts or flows. In the case of the Littrow and Menelaus rilles, a low scarp marks the edge of the dark material, which terminates abruptly against the upland. This dark material is probably composed largely of flows, although some pyroclastic material may be present, especially near the rilles. It is unlikely that a pyroclastic deposit could form the smooth and level surface around the Littrow rilles or the smooth broad dome, Menelaus γ, and also form a scarplike contact with the rest of the mare.

On the other hand, the dark material surrounding the Sulpicius Gallus rilles and in the dark region to the southeast of Copernicus appears to blanket the underlying terrain. The unit has no observable relief, except close to the rilles, and its contact with other geologic units has no observable topographic expression. These characteristics suggest that the dark units are here not composed of flows but are pyroclastic in origin. Some local extrusion of lava may have taken place near the rilles where the dark material has some intrinsic relief.

The origin of the dark upland region to the east of Sinus Aestuum

and that to the southeast of Mare Vaporum is in doubt. These areas re-
semble the region around the Sulpicius Gallus rilles except that only one
small rille, Rima Conon, is found in the Sinus Aestuum and Mare Vaporum
dark areas; if more rilles were originally present, they have been des-
troyed by erosion or, more probably, by burial under the Procellarum Group.
The resemblance between the dark upland areas on the shores of Mare Va-
porum and Sinus Aestuum and the area around the Sulpicius Gallus rilles
is so strong that a similar origin for the dark materials in all these
regions is suggested. The only difference between the dark materials
around the Sulpicius Gallus rilles and the dark materials in the other two
areas is their age. The Sulpicius Gallus materials are younger than the
present surface of the Procellarum Group in that area, whereas the Mare
Vaporum and Sinus Aestuum dark materials are older than the present sur-
face of the Procellarum Group in these areas. Several mare units have
been described that are younger than the Procellarum Group.

Within Mare Serenitatis, the Procellarum Group itself has been sub-
divided on the basis of difference in albedo (map of Mare Serenitatis in
the Supplement to this report). Several of the boundaries mapped solely
on albedo coincide with scarplike features on the mare surface; an es-
pecially prominent scarp that coincides with an albedo boundary parallels
the southern shore of the mare. By analogy with the dark materials around
the Menelaus and Littrow rilles, the different albedo units are interpreted
as volcanic flows of different ages, the darkest being the youngest and
the lightest the oldest. Although no systematic crater counts have yet
been made for the different mare units, the dark units appear to have fewer
craters on their surface than the lighter units, especially for craters
with diameters less than 3 km. The assignment of a younger age to the
darker units is largely based on the assumption that the extremely dark
mare units around the Menelaus and Littrow rilles are the youngest mare
units exposed within Mare Serenitatis. If this is true, then it is not
unreasonable that successively younger units have successively higher
albedos.

Conclusions

1. Dark pyroclastic volcanics, younger than the Procellarum Group, blanket parts of both the mare and the uplands to the southeast of Copernicus and around the Sulpicius Gallus rille.

2. Dark pyroclastic volcanics, older than the present surface of the Procellarum Group, lie on top of the Fra Mauro Formation around Mare Vaporum and Sinus Aestuum and account for the low albedo of these areas.

3. Volcanic flows, younger than the Procellarum Group, occur within Mare Serenitatis in the region of the Menelaus and Littrow rilles.

4. The Procellarum Group consists largely of volcanic flows that have successively higher albedos with increasing age.

Reference

Shoemaker, E. M., and Hackman, R. J., 1962, Stratigraphic basis for a
     lunar time scale, in Kopal, Zdenek, and Mikhailov, Z. K., eds.,
     The Moon--Symposium no. 14 of the International Astronomical Union:
     London, Academic Press, p. 289-300.

PRELIMINARY GEOLOGIC MAPPING OF THE EASTERNMOST PART
OF THE LUNAR EQUATORIAL BELT

by D. E. Wilhelms, Harold Masursky, A. B. Binder[1], and J. D. Ryan[2]

Introduction

The area described in this report extends from 50°E to 70°E and
from 32°N to 32°S; it includes the following quadrangles: Cleomedes,
mapped by Binder; Mare Undarum, by Masursky; Langrenus, by Ryan and
Wilhelms; and Petavius, by Wilhelms.

The most significant results of preliminary geologic mapping of
the four quadrangles derive from recognition of the similarity of struc-
tures of the Mare Crisium basin and the crater Petavius. Crisium is the
freshest and presumably the youngest of the small lunar mare basins.
Petavius is the largest fresh crater of the lunar equatorial belt and
bridges the gap in size between features commonly called craters and
small mare basins. It had previously been recognized that mare basins
are surrounded concentrically by depressed rings (Hartmann and Kuiper,
1962; Wilhelms, 1964b), but the rings had not been studied in detail.
Study of the Crisium rings, facilitated by their pronounced relief, has
shown them to be broken into irregular depressions bounded by scarps
which are principally tangential to the basin or of diverse trend, but
rarely radial. The rim material of Petavius is broken by irregular de-
pressions similar to those on the flank of the Crisium basin. These
depressions around Petavius may be the initial stages of a concentric
trough in process of development. Restudy of other mare basins and
large craters discloses similar though less well developed irregular
depressions around their rims. A large graben along the rim crest of
Petavius may be a small-scale analogue of another feature of mare
basins, the broad shelves such as those around the Crisium and Imbrium

---

[1]Lunar and Planetary Laboratory, Tucson, Arizona.
[2]Lehigh University, Bethlehem, Pennsylvania.

basins. These shelves probably originated as grabens rather than as terraces such as observed in craters smaller than Petavius.

Besides Crisium and Petavius, important features of the area are Mare Fecunditatis, which occupies a basin about the size of Crisium but is much less well defined, and Langrenus, the largest known crater of Copernican age.

Mare Crisium

The Mare Crisium basin is a complex feature and is surrounded by several concentric structural units (fig. 1). The basin is partially filled with mare material and comprises an outer shelf (fig. 1, S) with many partially buried craters and other "islands" of terra material, and an inner basin (B) without such islands. The inner basin is therefore presumably deeper than the shelf. The boundary between inner basin and shelf is marked in places by a ridge (r) and in places by an inward-facing scarp (s), both covered with mare material. The shelf is surrounded by a high rim (R1) with a steep inner scarp. In places the rim is cut into steep-sided, irregular blocks surrounded by mare material.

Outside the rim are several well-defined concentric structures. Closest of these to the basin is a depressed zone which comprises a series of jagged, steep-sided depressions (D1, D2). Some depressions are filled with mare material (for example, D1); others (D2) are filled with smooth, plains-forming materials believed to be older than the Procellarum on the basis of their greater crater density (Somni Formation; see Wilhelms, 1964a, p. 27, and Pohn, this report, p. 7) and the overlapping relationship of the mare material. Outside this depressed zone indicated by D1 and D2, is a ring (R2) which is raised relative to D1 and D2 but is lower than R1 and is considerably broken by faults. Finally, beyond R2 is a second depressed zone (D3, D4) consisting of troughs and irregular depressions filled with mare material (D3) and Somni Formation (D4). Most of the mare material of this zone has very low albedo and may be younger than the Procellarum Group (for example, Mare Undarum, D3).
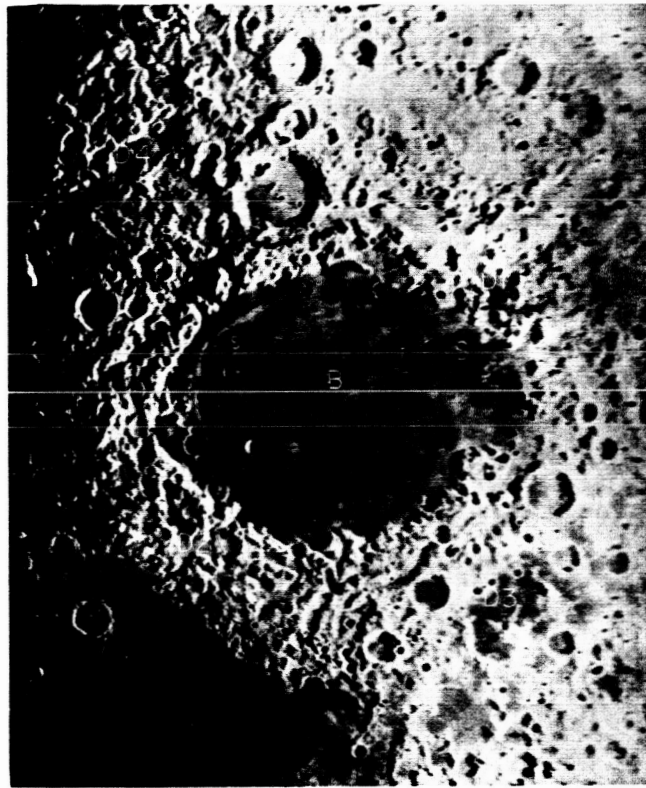
Fig. 1.--Mare Crisium, rectified. North at top; diameter
of mare approximately 400 km north to south. See page 46 for explana-
tion of letters. Photograph from Hartmann and Kuiper (1962), plate 12.52.
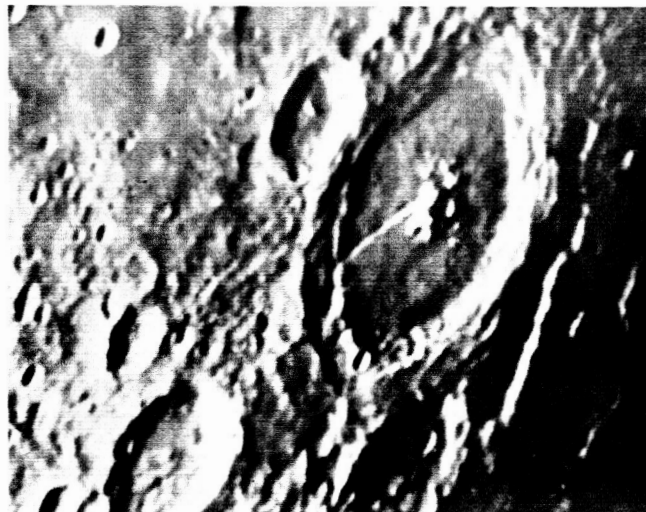

Fig. 2.--Crater Petavius, 160 km rim crest to rim crest.
North at top. Rim crest graben on southwest rim and M-shaped depression
at center bottom are discussed in text. Crater Wrottesley cuts north-
west rim of Petavius. Elongate depression east of Petavius is Palitzsch.
Photograph by Yerkes Observatory, plate A6-b from Photographic Lunar
Atlas, G. P. Kuiper, ed.

The high topographic relief and freshness of the Crisium basin provides an opportunity to study the large concentric structural units and their subordinate structures. The irregular depressions filled with mare material and Somni Formation are prominent features of the region around Crisium. Their bounding scarps are primarily concentric or tangential to the basin or have diverse trends; they are only subordinately parallel to basin radials. Many of the scarps follow the lunar grid. Restudy of other basins, particularly the Humorum basin which is about the size of Crisium but is less rugged and presumably older, discloses similar though less prominent irregular depressions. Basin radials independent of lunar grid are well developed only around the largest mare basins: Imbrium, Orientale, and Nectaris. Even around these basins are many irregular structural blocks like those around Crisium. Concentric troughs formed purely by foldlike deformation are rare (part of Mare Frigoris may be one). It is concluded that subsidence along faults of diverse trend contributes importantly to the formation of depressed zones concentric with mare basins. Contemporaneous extrusion of smooth, plains-forming volcanic materials from depth may provide the room for subsidence.

Petavius

The large, fresh-appearing crater Petavius (fig. 2), 160 to 170 km from rim crest to rim crest, possesses well-developed rim material, easily mappable across 400 km, with a thick, hummocky inner facies and an outer, more subdued facies of subradial ridges and grooves. The crater is surrounded by a rich field of large secondary craters, many with prominent rims. Petavius appears too fresh to be pre-Imbrian but is older than the Imbrian Procellarum Group, so is probably Imbrian (Archimedian Series). Of special interest are scarps in the crater rim material, and a broad graben along part of the rim crest.

Scarps in rim material

In all large young craters, there is a break in slope at one-third to one-fourth of a crater diameter out from the rim crest. The rim

material beyond this break becomes increasingly subdued with increasing age of the crater, and in old craters only a narrow inner doughnut-shaped ring remains. In Petavius, the break is marked in two places by scarps tangential to the high inner rim. One scarp cuts the crater Wrottesley, which is younger than Petavius. Apparently, post-crater subsidence has occurred at least partially along tangential faults.

An irregular, M-shaped depression is also present in the Petavius rim material (fig. 2). An extension of one of the tangential scarps discussed above would bisect the depression. The depression resembles the Crisium depressions in several respects. Both the Petavius and Crisium depressions occur between the high inner rim and the more sub-dued flank. The Petavius depression has steep zigzag bounding scarps like those of Crisium. The trends of the scarps coincide roughly with those of the lunar grid. The material filling the depression has a fairly smooth, flat surface as do the Procellarum and Somni materials in the Crisium depressions. All these characteristics are shared by depressions in the rim materials of the craters Theophilus and Macrobius, although these depressions are less distinct than that of Petavius. (The "crater" Politzsch east of Petavius may be another structural depression.) Regardless of what factor or combination of factors is primarily responsible for the concentric depressions of small mare basins and large craters[3], subsidence appears to be strongly modified by downfaulting along tangential faults and faults of diverse trend.

Rim-crest graben

The rim-crest graben of Petavius occupies about one-third of the circumference of the rim, and passes laterally into rim with a flattened crest; about half the rim is neither faulted nor flattened but has a

---

[3]Daneš, cited by Masursky (1964) showed that isostatic adjustment would theoretically produce a depressed ring around craters. On the other hand, Baldwin (1963, especially p. 106-109) cites terrestrial examples to show that shock waves from crater-forming impacts produce concentric "synclines."

normal single rim crest (fig. 2). The inner scarp of the graben is lower than the outer. Like the tangential scarps in the rim flank, the graben cuts rim material of the crater Wrottesley, which is younger than Petavius, so the graben is younger than Petavius. The slopes of the graben are not bright, although they are steep, so the graben is probably pre-Copernican in age.

The Petavius graben is probably not unique, although it is the freshest example of its class. Possibly the shelves of the Crisium and other mare basins are similar grabens, which have been largely covered by mare material. The shelves are better explained as grabens than as terraces formed by inward slumping. Such terraces are ubiquitous in medium-sized craters but are poorly developed in Petavius. A buried ridge like that which in places forms the inner boundary of the Crisium shelf would result from burial of the inner lip of a graben such as that in Petavius but would not result from burial of a terrace. Another wide shelf that may have originated as a graben is that of the Imbrium basin, where the shelf-inner basin boundary is a discontinuous circle of extremely rugged and steep islands protruding through the mare surface (Pico, Piton, Straight Range, etc.). The great width of the shelf, whose exposed part is the Apennine Bench, 300 km long from Apennine scarp to inner basin, makes its formation by terracing unlikely. Extensive terracing probably does not occur in craters and basins larger than Petavius because these craters are too shallow relative to their diameter to allow development of large inclined faults. Accordingly, the hypothesis is advanced that the rim material of the Crisium, Imbrium and other mare basins formerly came to a crest over the present site of the shelves and then subsided in a graben like that of Petavius. (A possible remnant of the crest of the Imbrium rim material is the rugged, disordered mound southwest of the crater Archimedes.)

Mare Fecunditatis

Mare Fecunditatis probably occupies an old mare basin once similar to Mare Crisium but leveled by isostasy, erosion, and subsequent crater formation. A circular mare ridge in the center of the mare may mark

the inner lip of the shelf[4]. The southern extension of the mare, north-
west of Petavius and southwest of Vendelinus, is probably another small-
er basin (or large crater). The terra surrounding Mare Fecunditatis,
except that on the south flank of the younger Crisium basin, has a
high density of large craters. Islands in the mare material of Mare
Tranquillitatis to the west of the report area form arcs concentric
with the margin of Mare Fecunditatis. Possible continuations in the
terra of the Petavius and Langrenus quadrangles of the troughs bounded
by these arcs of islands are very subdued. They appear to be filled
with plains-forming materials like the Somni Formation.

Langrenus

The crater Langrenus, 130 km in diameter, is a typical Copernican
crater, with rays, well-developed hummocky and radial rim-material
facies, and many prominent secondary craters. Some of its rim material
is dark, as is that of many other Copernican craters. One of the larg-
est dark-halo craters known on the Moon, Langrenus C, 17 km in diameter,
occurs on the rim near a large patch of the dark rim material. The
origin of dark rim material is unknown, and may be either impact ejecta
derived from dark source rock, volcanic ejecta, or a later volcanic
cover. The occurrence of the dark-halo crater with dark Langrenus rim
material, as well as the apparent blotting out of some of the Langrenus
rays by dark material, lends support to the volcanic origin of the
dark materials. Possibly, fractures reactivated by the impact that
produced Langrenus provided feeders for volcanic materials. Depressions
like those in the Petavius rim flank may eventually form along these
fractures but have not done so because Langrenus is at an early stage
of its history.

------

[4]See the 1:5,000,000 compilation and the preliminary geologic maps
of the four quadrangles of this belt in the map supplement to this re-
port for the locations and interrelations of the features discussed
here.

Conclusions

Similar structures are present in and around the Mare Crisium basin, a small fresh mare basin, and Petavius, a very large fresh crater of probable Imbrian age. The Crisium basin and Petavius display on their rims depressed zones which are structurally broken into deep, prominent depressions bounded by scarps of diverse trend. The scarps are probably produced mainly by faulting along concentric and tangential fractures and by faults parallel to the lunar grid. Faulting radial to the basin or crater and independent of the lunar grid is subordinate. The depressions are filled with smooth, level-surfaced materials of different ages. Restudy of other basins shows that peripheral concentric depressed zones around them are also modified by irregularly bounded depressions filled by mare and pre-mare level materials. The broad shelves of Crisium and other mare basins are probably grabens formed along the crest of the basin rim deposits and analogous to the rim-crest graben of Petavius. Both the graben and rim-flank depressions of Petavius formed later than the crater. The resemblance of the Crisium structures to those of Petavius suggest similar histories. Probably the shelves and peripheral depressions of Crisium and other mare basins continue to develop after formation of the basin and result in increasing degradation of the basin area with time. Mare Fecunditatis occupies an old basin formerly like that of Crisium but now with only the remnants of concentric peripheral structures and a possible indication of a buried shelf. Possible volcanic rocks associated with the crater Langrenus may have been extruded along preexisting fractures reactivated by the Langrenus impact.

References

Baldwin, R. B., 1963, The measure of the Moon: Chicago, Univ. Chicago Press, 488 p.

Hartmann, W. K., and Kuiper, G. P., 1962, Concentric structures surrounding lunar basins: Arizona Univ. Lunar and Planetary Lab. Commun., v. 1, no. 12, p. 51-72.

References--Continued

Masursky, Harold, 1964, A preliminary report on the role of isostatic
   rebound in the geologic development of the lunar crater Ptolemaeus,
   in Astrogeologic Studies Ann. Prog. Rept., July 1, 1963 to July 1,
   1964, pt. A: U.S. Geol. Survey open-file report, p. 102-134.

Wilhelms, D. E., 1964a, Progress in mapping the Taruntius quadrangle,
   in Astrogeologic Studies Ann. Prog. Rept., August 25, 1962 to July 1,
   1963, pt. A: U.S. Geol. Survey open-file report, p. 24-30.

_____ 1964b, Major structural features of the Mare Vaporum quadrangle,
   in Astrogeologic Studies Ann. Prog. Rept., July 1, 1963 to July 1,
   1964, pt A: U.S. Geol. Survey open-file report, p. 1-16.

SMALL-SCALE ROUGHNESS FROM LUNAR INFRARED EMISSION

by Kenneth Watson

Introduction

Infrared emission observations of the illuminated Moon have been
interpreted in terms of albedo variations, variations in the photo-
metric function, and crater shadowing (Pettit and Nicholson, 1930;
Shorthill, 1962). Variations in thermal properties (conductivity and
specific heat) produce emission changes which are too small to be
recognized on the illuminated surface and require observations during
eclipses and the dark phase.

Pettit and Nicholson measured the distribution of infrared emitted
energy over the lunar disk at full moon, and observed that the limbs
were brighter than the emission from a sphere which absorbs and emits
as a Lambert surface. They concluded that this effect can be explained
by the roughness of the surface at a scale greater than 1 km. Watson
(1964) discussed their conclusions and pointed out that the observed
mean slope at this scale was much too low to explain the observed limb
darkening. From an examination of the effect of the lunar photometric
function on the infrared emission, it is concluded that the infrared
emission observations can best be explained by the presence of micro-
relief below a 1-meter scale.

This paper presents quantitative data in support of this conclusion
and analyzes the possible utility of infrared emission from the illumi-
nated lunar surface as a means for determining the microrelief (roughness
below 1 meter) of different geologic units within the region to be
covered by manned lunar orbiter missions.

Theoretical model

It shall be assumed that each element of the lunar surface absorbs
energy from the sun and re-emits heat as a Lambert surface. Thus the
absorbed energy is the product of the coalbedo, the cosine of the
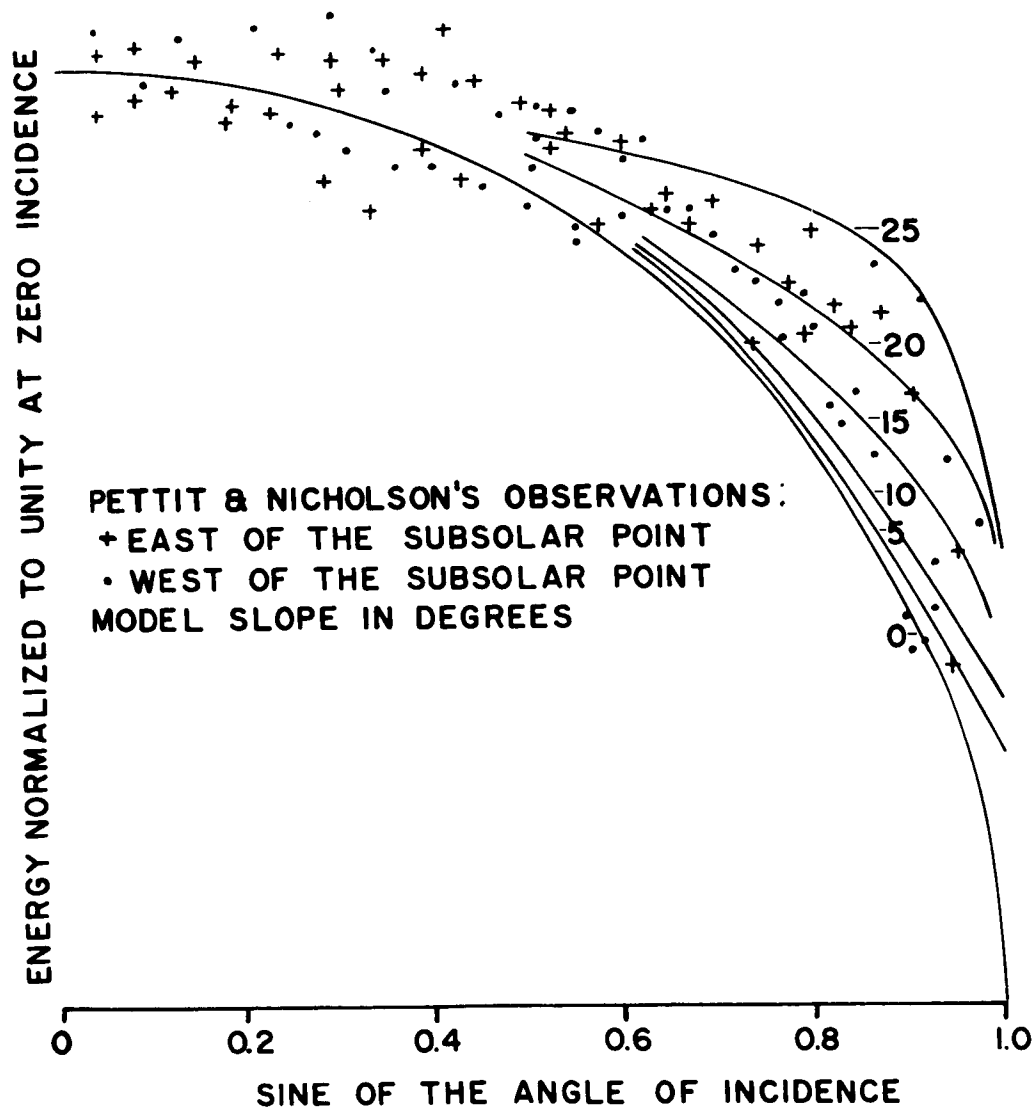
Fig. 1.--Computed absorbed energy as a function of sine of angle of incidence compared with Pettit and Nicholson's infrared observations of emitted energy.

local angle of incidence and the solar flux; the emitted energy is the product of the absorbed energy and the cosine of the local angle of emergence to the Earth. If the incident ray or the emitted ray is obstructed by an adjacent element, then the emitted energy is zero.

A simple surface model is assumed with a single slope angle whose direction reverses at each element. The emitted energy was computed as a function of the incident and emergent angles for a suite of slope angles. The equations used in the computation are given below, and the theoretical models are compared with Pettit and Nicholson's observations in figure 1.

$$E = \frac{\gamma_i \gamma_e \cos (i + \phi) \cos (e + \phi)}{\gamma_e \cos (e + \phi) + \cos (e + \phi)} + \frac{\cos (i - \phi) \cos (e - \phi)}{\gamma_e \cos (e + \phi) + \cos (e - \phi)}$$

$$\gamma_i = 1 \qquad\qquad i + \phi < \frac{\Pi}{2}$$

$$\gamma_i = 0 \qquad\qquad i + \phi \geq \frac{\Pi}{2}$$

$$\gamma_e = 1 \qquad\qquad e + \phi < \frac{\Pi}{2}$$

$$\gamma_e = 0 \qquad\qquad e + \phi \geq \frac{\Pi}{2}$$

where E = emitted energy observed terrestrially (where the product of solar energy and coalbedo is normalized to unity); ϕ = slope angle of element; i = incident angle to a flat surface; e = emergent angle from a flat surface. γ_i and γ_e are introduced to account for shadowing of slope elements from the sun or the observer.

Comparison of theory with observational measurements

A crude fit of the model occurs at a slope of approximately 18°. There is an appreciable data scatter, suggesting significant variations in microrelief across the lunar equatorial belt. Since this paper is only intended to suggest the applicability of infrared emission to study fine textural detail, no attempt was made to correct for albedo variations (which introduce a maximum error of 10 percent in the emitted energy) or to relocate Pettit and Nicholson's observational areas and relate the computed mean slope to the geologic rock units.
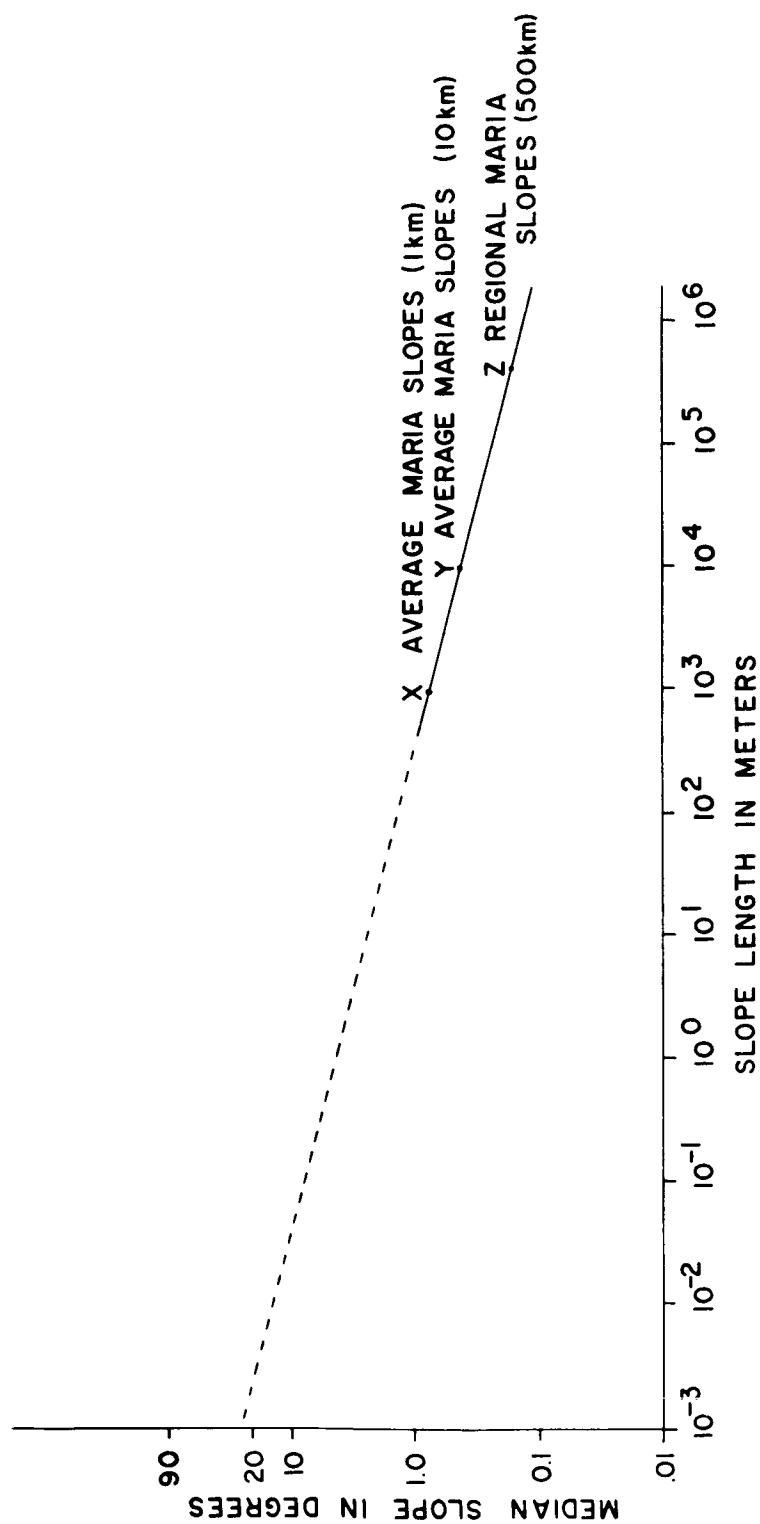
Fig. 2.--Median slopes plotted as a function of slope length for the lunar maria.

McCauley (1964) has presented a plot of the median slope versus slope length for the lunar maria from terrestrial observations. The agreement between the extrapolated slope value at 1 meter with measurements on Ranger VII suggests that there is some basis for extrapolation of this relationship. A median slope of 18° occurs on this plot at a slope length of approximately 1 to 10 cm (fig. 2). It is recognized that this extrapolation is useful only in a very general sense, that the uplands will, in general, have a greater median slope at the higher resolutions, and that entirely different processes may be operating at the submeter scales.

It seems reasonable to propose, however, that infrared emission from the illuminated lunar surface can provide fine textural information about features several orders of magnitude smaller than surface resolution from manned lunar orbiting spacecraft.

References

McCauley, J. F., 1964, Terrain analysis of the lunar equatorial belt--Preliminary report: U.S. Geol. Survey open-file report, 44 p.

Pettit, Edison, and Nicholson, S. B., 1930, Lunar radiation and temperatures: Astrophys. Jour., v. 71, p. 102-135.

Shorthill, R. W., 1962, Measurements of lunar temperature variations during an eclipse and throughout a lunation: Geo-Astrophysics Laboratory, Boeing Scientific Research Laboratories.

Watson, Kenneth, 1964, Infrared emission from the illuminated Moon, in Astrogeologic Studies Ann. Prog. Rept., July 1, 1963 to July 1, 1964, pt. A: U.S. Geol. Survey open-file report, p. 67-78.

THE FEASIBILITY OF MEASURING
THE LUNAR FIGURE BY OPTICAL LASER RADAR

by R. L. Wildey

A detailed feasibility study of the use of optical laser radar to determine the figure of the Moon has been carried out by the author with the assistance of E. M. Shoemaker and K. A. Watson. We have concluded that a lunar laser-radar program could be executed to provide conservatively 50 lunar regions per year where the lunar radius vector would be known to within 50 to 100 meters. The program would make use of reflected photons from ultra-short burst (10^{-8} sec) lasers firing through telescopes. In contrast, it was concluded that lunar photogrammetric techniques of measuring the librational parallax of craterlets could not be guaranteed free of systematic errors smaller than about 2 km in lunar radius vector; this is the average expected error over the lunar surface from the subearth point to within 20° of the limb.

The primary difficulties in determining the shape of the Moon by measuring the light-travel-time to selected spots on the lunar surface are:

1. The maximum beam convergence obtainable by a laser-telescope combination is not greater than 1 to 2 seconds of arc.

2. The most energetic work cycle for a ruby-laser that is permissible without a high probability of damage requires one to employ low counting rate photon statistics.

3. Measurements cannot be made by ranging on recognized features because of high day-side solar background and because of possible systematic errors in positioning by any kind of gestalt process.

4. The Moon varies in libration and orbital range on a scale that is great compared to the ranging accuracy of which laser radar is capable.

In spite of these difficulties, it appears possible to design a system auxiliary to the U.S. Geological Survey 30-inch reflector which would provide data to improve our knowledge of the lunar figure by a factor of approximately 20 over that obtainable by conventional lunar photogrammetry.

A qualitative account of the technique and a treatment of the mathematical astrometry and laser technology are in preparation.

POLARIZATION PROPERTIES OF SOME LUNAR GEOLOGIC UNITS

by D. E. Wilhelms and N. J. Trask

Several previous studies of the polarization of moonlight have demonstrated that the ratio of reflected polarized light to total reflected light is not the same everywhere on the lunar disc (Lyot, 1929; Wright, 1938; Wright and others, 1963; Dzhapiashvili, 1957; Dollfus, 1961, 1962; Gehrels and others, 1964; and Clarke, 1964). Differences in the percentages of polarized light from selected areas are therefore potentially useful for geologic mapping. We have been conducting a program of polarization measurements directed toward discriminating lunar geologic units as they are now recognized by the U.S. Geological Survey. Our systematic measurements to date indicate that polarization can supplement other properties such as normal albedo and morphology as a means of defining these units. Theoretical studies of the physical significance of polarization and comparisons of the polarization of lunar units with terrestrial samples are beyond the present scope of the study; they are being carried out by other workers (e.g., Dollfus, Gehrels, Hapke).

This report presents some of the more significant data obtained to date. Both curves of polarization as a function of phase angle and values of maximum polarization are included. As has been pointed out elsewhere (Hapke, 1964), maximum polarization is inversely related to the albedo of the surface. Thus, most of our readings of maximum polarization may be indirect measures of the albedos of the geologic units involved. We have, however, noted possible departures from an inverse albedo-polarization relation among some mare units.

All observations have been made with a Lyot visual polarimeter mounted on the 12-inch refractor of Lick Observatory, Mount Hamilton, California. Most observations recorded here were made during the lunations of May and June, 1965.

Methods

The Lyot polarimeter and its use have been described elsewhere (Lyot, 1929; Dollfus, 1961). In essence, it is a device for the compensation of incoming polarized light by means of an isotropic celluloid plate. Under the Fresnel reflection principle, the more the plate is tilted, the more the component of light vibrating parallel to the axis of tilt is reflected. When compensation is achieved, the light transmitted by the celluloid plate is natural: the components normal and parallel to the axis of tilt are equal. When the components are not equal, the polarized nature of the transmitted light is indicated by an analyzing device, the Savart-Lyot polariscope. The polariscope produces a bundle of straight interference fringes when the light transmitted by it is polarized. In practice, one superimposes three or more fringes on the area to be measured and reads the angular value of the tilt of the celluloid plate that causes them to disappear. This angular value is converted to the percentage of light polarized by means of a table derived from formulae of Fresnel (Lyot, 1929, p. 21).

With the Lyot polarimeter and the 12-inch refractor, measurements on spots 15 km in diameter are possible under average seeing conditions; the polarization on spots as small as 10 km across can be measured under good seeing and lighting conditions. It has been suggested by some workers (Gehrels and others, 1964, p. 850) that both percentage polarization and brightness levels may change from month to month because of periodic luminescence of lunar surface materials. This effect may be responsible for some of the scatter in our data. A future program of simultaneous photometry and polarimetry will be designed to evaluate this possibility.

Possible sources of error include drift of the telescope off of the point being measured (because of lack of declination drive), admixture of light from the surroundings of small areas, and the difficulty of observing the fringes on dark or rough surfaces within 15° of the terminator. Our best measurements are probably accurate to within 0.1 percent. The polarimeter has not yet been calibrated against other instruments nor the telescope checked for possible depolarization.

Results

The curves of percentage polarization as a function of phase angle in figures 1-12 (p. 71-76) show that there are significant differences in values of maximum polarization of geologic units although the forms of the curves are similar. Each data point in figures 1 through 12 is an average of three or more readings taken consecutively. The curves are an approximate fit to the points. The locations of the regions studied and brief descriptions of the geologic units involved are given in table 1.

On the curves, points above the horizontal line are those measured when the dominant component of polarization vibrates in a plane normal to the plane of vision (the plane containing the sun, observed lunar area, and observer). Such points are termed "positive" by convention; those below the horizontal line, measured when the plane of vibrations is parallel to the plane of vision, are "negative."

All curves have three points of zero polarization, but these have not yet been accurately located for the various geologic units. Other authors (Dollfus, 1962, p. 133; Markov, 1962[1]; Wright, 1938) have determined them to be a full moon and at approximately 23° before and after full moon for the integrated lunar surface.

The phase at which maximum polarization occurs increases with the value of the maximum, as is readily apparent when curves of widely differing units are compared (figs. 13 and 14). For units of low polarization, maximum polarization occurs near 90° phase (first and third quarter); the greater the value at maximum the more the occurrence of the maximum is displaced toward higher phase angles. Curves for units near the central meridian show no maxima because the areas are in shadow or unsuitably close to the terminator when maximum occurs.

---

[1]Markov and other Soviet astronomers report observations of gradual rotation of the plane of polarization before and after the zero points, whereas Lyot and Dollfus believe rotation of exactly 90° occurs within a few hours. We have not made enough measurements to resolve this question.

Table 1. Location, description, and maximum polarization of some geologic units*

Region	ACIC Chart	Center of Region	Geologic Unit	Maximum Polarization (percent)
39-1	Aristarchus	λ, -47°20' β, +23°40'	Floor material within crater Aristarchus	3.7
39-2	Aristarchus	λ, -43°30' β, +27°00'	Harbinger Formation, smooth material with low albedo in Harbinger Mountains	8.4
43-1	Macrobius	λ, +45°30' β, +16°35'	Ray material from crater Proclus	3.9
57-1	Kepler	λ, -36°45' β, +7°30'	Ray material from crater Kepler	5.8
59-3	Mare Vaporum	λ, -0°25' β, +1°10'	Procellarum Group, mare material	10.0†
59-4	Mare Vaporum	λ, +5°30' β, +5°20'	Ray material from crater Manilius covering Cayley Formation	5.5
59-7	Mare Vaporum	λ, -3°35' β, +11°40'	Fra Mauro Formation, dark, hummocky facies; very low albedo, probably ejecta from Mare Imbrium basin	12.8†
60-4	Julius Caesar	λ, +14°45' β, +9°50'	Procellarum Group; mare material within crater Julius Caesar, very low albedo	10.9†
60-5	Julius Caesar	λ, +15°10' β, +8°20'	Fra Mauro Formation; hummocky to gently rolling topography, medium albedo	6.3
60-7	Julius Caesar	λ, +14°50' β, +9°30'	Material transitional between 60-4 and 60-5; either Fra Mauro Formation with a thin covering of mare material, or Cayley Formation	8.5†

ID	Name	Coordinates	Description	Albedo*
60-8	Julius Caesar	λ, +15°50' β, +4°10'	Cayley Formation, level mare-like material with medium albedo	6.9
60-9	Julius Caesar	λ, +10°15' β, +8°00'	Fra Mauro Formation, smooth facies; smooth ridges, moderately low albedo	7.5
61-2	Taruntius	λ, +44°20' β, +10°40'	Procellarum Group, mare material possibly with very low albedo	10.8
61-4	Taruntius	λ, +41°40' β, +4°30'	Secchi Formation; gently rolling to hummocky topography, moderately low albedo, may be ejecta from Mare Fecunditatis basin	9.8
61-5	Taruntius	λ, +44°50' β, +14°40'	Somni Formation, level mare-like material with medium albedo	5.7
61-6	Taruntius	λ, +36°30' β, +15°10'	Procellarum Group, mare material	10.7
61-7	Taruntius	λ, +38°50' β, +11°00'	Procellarum Group, mare material	12.6
74-1	Grimaldi	λ, -68°00' β, -6°30'	Dark mare material within crater Grimaldi; very low albedo	11.0
76-1	Montes Riphaeus	λ, -20°40' β, -10°40'	Procellarum Group, mare material with weakly developed ray from crater Tycho (Ranger VII impact region)	11.0†
77-1	Ptolemaeus	λ, -1°00' β, -9°10'	Cayley Formation within crater Ptolemaeus	5.4

*Albedos estimated visually from full-moon photographs.

†Value of maximum polarization obtained by extrapolating curves from low phase angles to phase angles near quarter moon when maximum polarization occurs.

The positive branches of all curves hold their relative positions throughout all phases. This fact has been used in the construction of table 1, in which some values of maximum polarization have been estimated by extrapolating partial curves obtained at phase angles less than 90°. The partial curves have been continued to phase angles near the maximum by maintaining their relationship to curves for which the maxima are well established.

There are slight differences in the extreme values on the negative branches of the curves among units with wide differences in maxima on the positive branches, e.g., Proclus rays and maria (fig. 13).

Curves of like units are compared in figures 15 through 17--several mare units in figure 15, several smooth terra units in figure 16, etc. It is evident that a high degree of discrimination among similar units can be attained.

In general, polarization and albedo are inversely related. The floor of Aristarchus, one of the brightest spots on the Moon, has the lowest polarization we have measured. Geologic units on the maria have the highest polarization (fig. 13). Whether the inverse relation between polarization and albedo holds in detail can be determined only with a combination of systematic photometry and polarimetry. There is evidence that the polarization of some of the mare units is not a function of albedo only. Regions 61-2 and 74-1 both appear darker to the eye than 61-7 and 76-1 but have polarizations that are the same or slightly lower (table 1, fig. 15). Other patches of very dark-appearing mare material appear to polarize light to a slightly lesser extent than nearby patches with apparently higher albedo. These other dark-appearing patches have been observed in reconnaissance fashion only and are not included in the table and figures of this report. They will be closely studied in the future.

Before concluding that some lunar geologic units display anomalous polarization, it will be necessary to carefully evaluate the uncertainties involved. All of the very dark-appearing patches observed to date are small and many are surrounded by brighter material. It is possible that the surrounding material lowered the measured value of the polarization, although we have tried to avoid this. In addition, visual estimates of

the albedos of small patches are subject to psychological errors. Full-
moon photographs also involve uncertainties; for example, some show 61-2
as darker than 61-7 while others show the two as similar. Future work
will attempt to resolve these questions. Possible departures from an
inverse albedo-polarization relation pose interesting problems in the
study of lunar surface materials. The composition or degree of compaction
of a geologic unit as well as its albedo may control the degree to which
it polarizes incident light.

Conclusions and future work

The value of maximum polarization is found to differ considerably
among lunar geologic units and to be a useful figure for their discrim-
ination. Polarization and albedo may be directly related, and accurate
systematic photometric measurements of albedo may supersede polarization
measurements. Polarization will be useful at least until albedo measure-
ments are available; it can be measured with existing equipment at rela-
tively low cost. Moreover, the polarization of some units may depart from
a direct relation to albedo. If this proves true, the polarization measure-
ments will be of added value in the discrimination of geologic units.

Future effort will be mainly directed toward additional measurements
of maximum polarization. Careful studies with combined photometry and
polarimetry will be made of curves and maxima of units that appear to
depart from the inverse albedo-polarization relation. Upon installation
of a combination photometer-polarimeter on the 29-inch reflector of the
U.S. Geological Survey Observatory in Flagstaff, acquisition of polari-
metric data will be facilitated. The instrument will make measurements
in several wavelengths, making possible refined interpretations.

Figs. 1-12 (p. 71-76).--Polarization-phase angle curves for
12 geologic units. Curves dashed where uncertain. Dots, data
points; open circles, questionable data points. See table 1 for
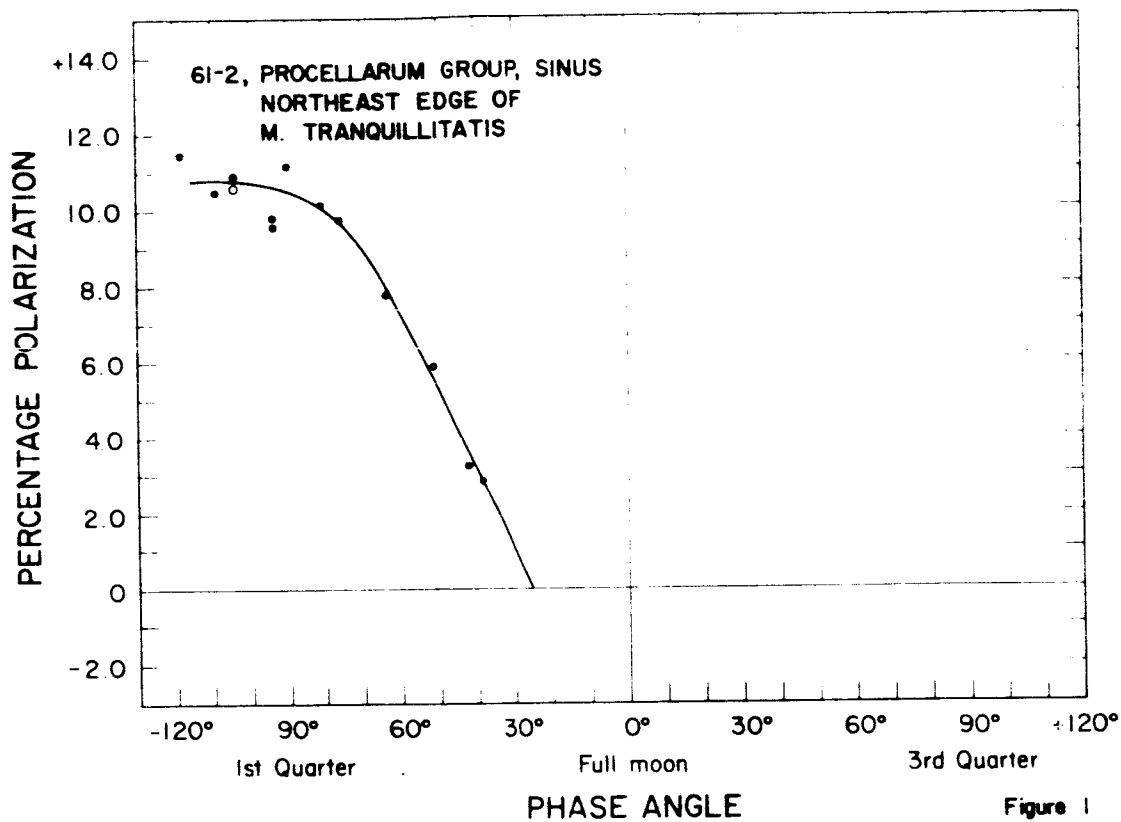location and description of units.

61-2, PROCELLARUM GROUP, SINUS
NORTHEAST EDGE OF
M. TRANQUILLITATIS

PERCENTAGE POLARIZATION

PHASE ANGLE

Figure I

1st Quarter　　　　Full moon　　　　3rd Quarter

61-6, PROCELLARUM GROUP
NORTHERN M. TRANQUILLITATIS

PERCENTAGE POLARIZATION

PHASE ANGLE

Figure 2

1st Quarter　　　　Full moon　　　　3rd Quarter

61-7, PROCELLARUM GROUP
NORTHEAST M. TRANQUILLITATIS

PERCENTAGE POLARIZATION

PHASE ANGLE

1st Quarter Full moon 3rd Quarter

Figure 3

60-9, FRA MAURO FORMATION
SMOOTH FACIES

PERCENTAGE POLARIZATION

PHASE ANGLE

1st Quarter Full moon 3rd Quarter

Figure 4

43-1, PROCLUS RAY MATERIAL

Figure 5

74-1, DARK MARE MATERIAL
FLOOR OF GRIMALDI

Figure 6

60-5, FRA MAURO FORMATION

Figure 7

61-4, SECCHI FORMATION

Figure 8

**59-7, FRA MAURO FORMATION
HUMMOCKY, DARK FACIES**

PERCENTAGE POLARIZATION

PHASE ANGLE

1st Quarter   Full moon   3rd Quarter

Figure 9

60-8, CAYLEY FORMATION

PERCENTAGE POLARIZATION

PHASE ANGLE

1st Quarter   Full moon   3rd Quarter

Figure 10

75

Figure 11

Figure 12

Fig. 13.--Comparison of polarization-phase angle curves of three widely different units: Proclus ray material (43-1), Cayley Formation (60-8), and a subunit of the Procellarum Group (61-6).
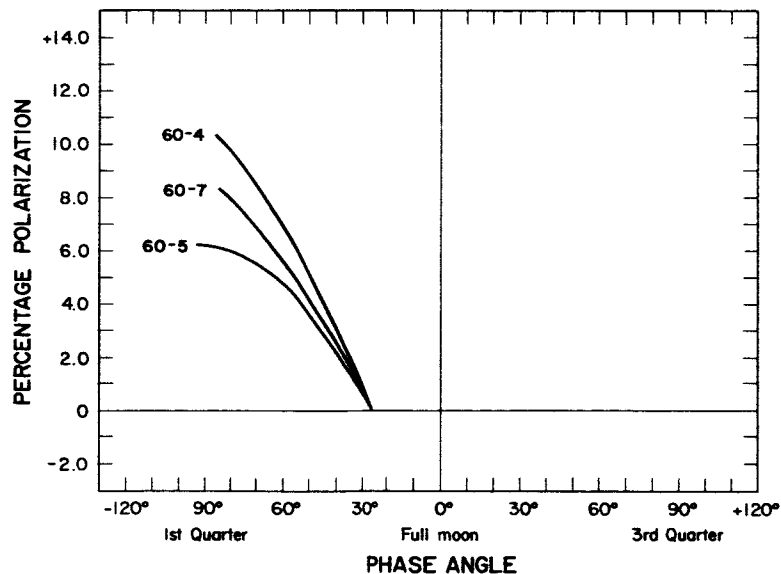
Fig. 14.--Comparison of polarization-phase angle curves for three geologic units on the floor of the crater Julius Caesar; Procellarum Group (60-4), Fra Mauro Formation (60-5), and material transitional between the two (60-7).
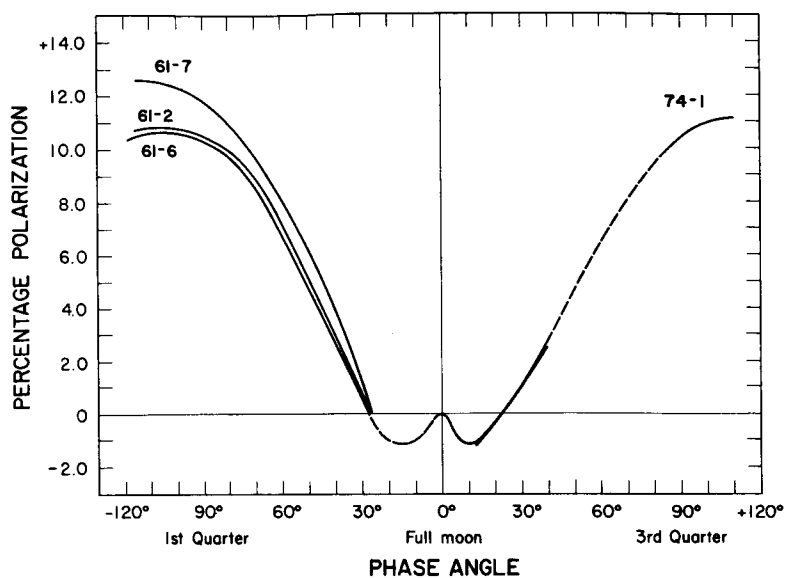
Fig. 15.--Comparison of polarization-phase angle curves of four geologic subunits within the maria: northeast Mare Tranquillitatis (61-7), sinus on northeast edge of Mare Tranquillitatis (61-2), northern margin, Mare Tranquillitatis (61-6), floor of Grimaldi (74-1).

Fig. 16.--Comparison of polarization-phase angle curves of three level terra units: Somni Formation (61-5), Cayley Formation (60-8) and ray-covered Cayley Formation (59-4).

Fig. 17.--Comparison of polarization-phase angle curves of four geologic units in the terra: Fra Mauro Formation, dark hummocky facies (59-7); Fra Mauro Formation, smooth facies (60-9); Fra Mauro Formation, undifferentiated (60-5); Secchi Formation (61-4).

References

Clarke, David, 1964, Observations of the frequency dependence of polari-
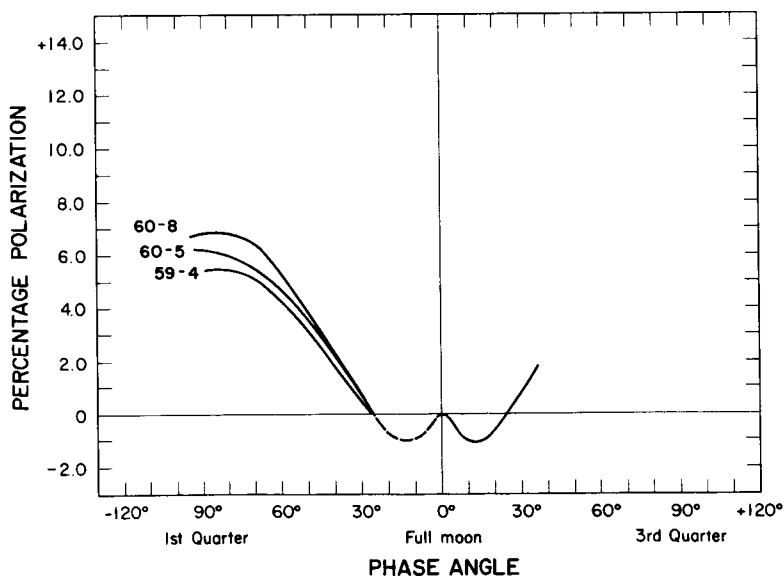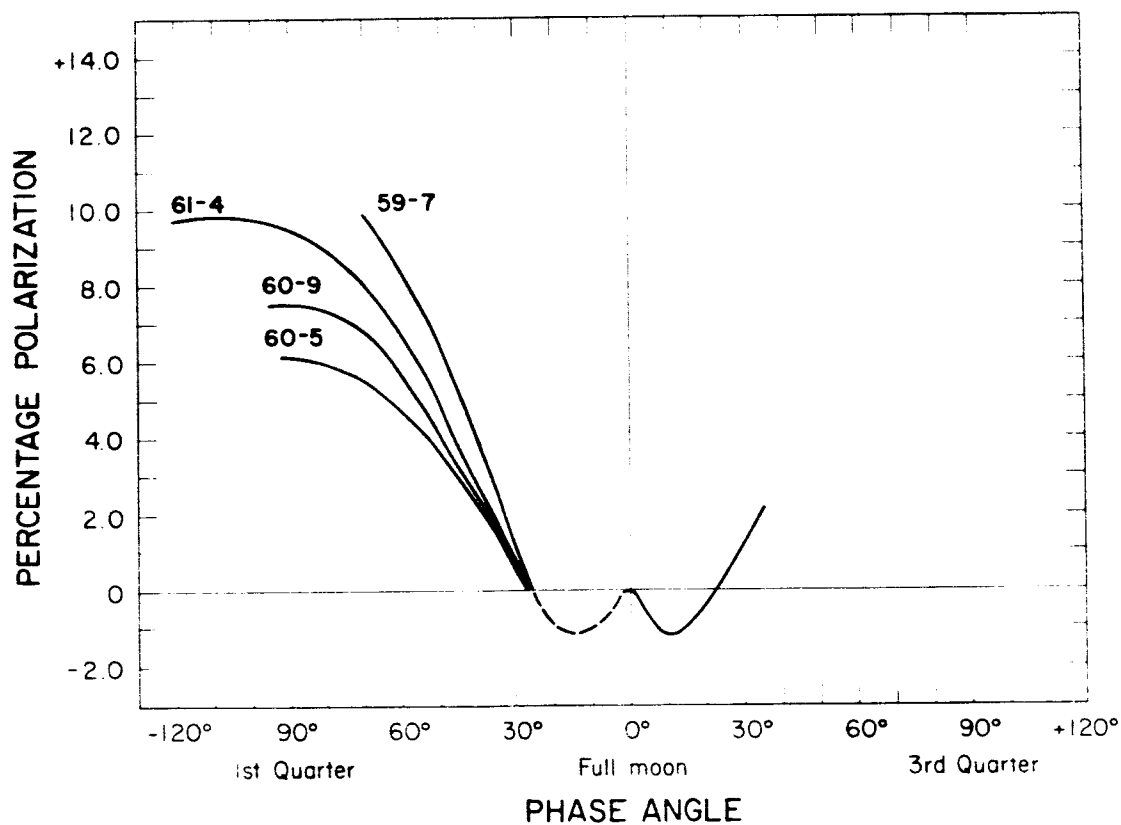   zation of the light of the Moon and of Mars: Manchester Univ.
    Astron. Contr., ser. III, no. 107, 43 p.

Dollfus, Audouin, 1961, Polarization studies of planets, in Kuiper, G. P.,
    and Middlehurst, B. M., eds., Planets and satellites--The solar
    system, vol. 3: Chicago, Univ. of Chicago Press, p. 343-399.

_____ 1962, The polarization of moonlight, in Kopal, Zdenek, ed., Physics
    and astronomy of the Moon: New York, Academic Press, p. 131-159.

Dzhapiashvili, V. P.. 1957, An investigation of the polarizing properties
    of lunar surface formations as derived from electrophotometric
    measurements: Abastumani Astrophys. Observ. Byull., no. 21, p. 3-165
    [in Russian].

Gehrels, Thomas, Coffeen, T., and Owings, D., 1964, Wavelength dependence
    of polarization, III--The lunar surface: Astron. Jour., v. 69, no. 10
    p. 826-852.

Hapke, Bruce, 1964, Photometric and other laboratory studies relating to
    the lunar surface, in Salisbury, J. W., and Glaser, P. E., eds.,
    The lunar surface layer--Materials and characteristics: New York,
    Academic Press, p. 323-344.

Lyot, B., 1929, Recherches sur la polarisation de la lumière des planètes
    et de quelques substances terrestres [Research on the polarization of
    light from planets and from some terrestrial substances]: Paris
    Meudon Observatory Ann., v. 8, pt. 1, 161 p.

Markov, A. V., 1962, Polarization properties of the lunar surface, in
    Markov, A. V., ed., The Moon, a Russian view, translated from the
    Russian by Royer and Royer, Inc.: Chicago, Univ. of Chicago Press,
    p. 156-173.

Wright, F. E., 1938, The surface of the moon--Observations by the
    Committee on the surface features of the moon: Carnegie Inst.
    Washington Pub. no. 501, p. 59-74.

Wright, F. E., Wright, F. H., and Wright, Helen, 1963, The lunar surface--
    Introduction, in Middlehurst, B. M., and Kuiper, G. P., eds., The
    Moon, meteorites and comets--The solar system, vol. 4: Chicago,
    Univ. of Chicago Press, p. 1-56.

REBOUND PROCESSES IN LARGE CRATERS

by Z. F. Daneš

Introduction

Both lunar and terrestrial craters exhibit a wide diversity of
shape (Kopal, 1962; Baldwin, 1949, 1963; Masursky, 1964), even when
their horizontal dimensions are comparable. From the sharply defined
craters with high, complete rims like Copernicus or Bullialdus, there
is a gradual transition to more and more subdued craters, such as
Taruntius and Posidonius, all the way to the nameless, barely recog-
nizable circular features on the mare floors. Some crater floors are
concave, others flat or even convex (Petavius). Many craters have a
pronounced central peak. In at least one (Gassendi), the floor is far
above the surrounding plain (600 m). Some craters show a concentric
high ring inside the main crater (Hesiodus A) (Wright and others, 1963).
And then, of course, there is the anomalous Wargentin; no attempt will
be made to interpret it in this study.

Although modified by erosion, sedimentation, and flooding, terres-
trial craters exhibit similar diversity (Beals and others, 1963; Dietz,
1963).

These differences in shape may be due to one or more of the following:

1. differences in the crater-producing mechanism (mass and/or velocity
of impacting meteorite; volcanism; collapse) resulting in differences of
original shape of crater;

2. differences in the properties of the impacted material (density,
porosity, viscosity, compressibility, hardness, layering, crystallization,
jointing, etc.);

3. changes in shape subsequent to crater formation (Baldwin, 1962a,
1962b, 1963).

To some extent, probably all three factors are responsible, but to
what degree is not known. The writer's intention is to analyze one of
these mechanisms -- a slow creep of rocks under differential load -- and

81

present the results of the theoretical investigation for comparison with observational evidence.

Original theories of this kind of a mechanism, for which Dutton (1889) coined the work "isostasy," assumed rigid crustal blocks standing on (Pratt, 1855), or floating in (Airy, 1855), a deformable substratum. No time factor was involved in these early considerations.

Although the hydrodynamics for the analysis had been developed as early as the middle of the last century, the first geophysical application seems to have been Haskell's (1935, 1936, 1937) study of the Fennoscandian uplift. His results indicated a rock viscosity of the order of 10^{22} poise. Crittenden (1963a, 1963b) used similar reasoning in his analysis of the Lake Bonneville uplift in Utah, but his viscosity value is an order of magnitude lower, i.e. 10^{21} poise. Some laboratory data on rock viscosities have been derived, notably by Griggs (1939, 1940), but the duration of the experiment is by necessity too short compared with the duration of geologic processes, and the results are thus of questionable applicability in the present context. A theoretical derivation of rock viscosity has been given by Ree and Eyring (1958) and by Cook (1963). Interesting as Cook's results are, they call for such a decrease in viscosity with depth (at least ten orders of magnitude within the continental crust) that regional isostatic gravity anomalies would have to come to an equilibrium in a matter of hours, otherwise they would have to be supported by dynamic stresses requiring convection velocities of the order of 1 cm/sec! A fairly recent review of the evidence for a viscous layer beneath the Earth's crust was given by Anderson (1962).

If the uncertainty of viscosities of terrestrial rocks is serious, that of lunar material is even more so. Prior to the observation of Kozyrev (1962) and calculations by Kopal (1963), Levin (1962) and Runcorn (1963), the Moon was thought to be cold, brittle, and unchanged for the past 10^9 years or so. Now it is believed by some to be active, hot and possibly still warming up (Runcorn, 1963).

Mathematical model

All rocks probably behave as a visco-elastic medium (Biot, 1954, 1956). Unfortunately, theoretical treatments of such media encounter a twofold obstacle. First, not enough is known about the parameters involved (Biot and others, 1961). Second, the resulting equations are of such complexity (Ree and Eyring, 1958; Coleman and Noll, 1961) that only the simplest geometries can be analyzed (Biot, 1961).

Yet the work of Crittenden (1963a, 1963b), Cook (1963), Masursky (1964), and Takeuchi and Hasegawa (1964) indicate that a simplified viscous model may be justified. Their results encouraged this writer to continue in his previous work (Daneš, 1962).

The assumptions on which the following analysis is based are listed below and are referred to in the text by the Roman numerals.

I. The body (Earth, Moon, Mars, etc.) is stratified, each stratum being horizontal, homogeneous and isotropic in its physical parameters.

II. The density and viscosity of each stratum is constant.

III. When shearing stresses are applied, the rate of deformation of the medium is directly proportional to the stress.

IV. Vertical dimensions of the perturbation (crater) are small compared with the horizontal ones.

V. Horizontal dimensions of the perturbations are small compared with the radius of curvature of the body being impacted.

VI. The process of deformation is slow, so that inertia terms in the equations of motion can be neglected.

VII. The only driving mechanism in the process of deformation is the perturbation of the upper surface of the top layer; all deeper layers are originally horizontal.

VIII. The perturbation (crater) is of circular symmetry and isolated from other perturbations.

Symbols used

The following symbols are used in the development:

A = coefficient of e^{kz}, e^{mz} in expansion of ϕ and $\vec{\psi}$, respectively

B = coefficient of e^{-kz}, e^{-mz} in expansion of ϕ and $\vec{\psi}$, respectively

C = coefficient in expansion of ζ

D = determinant of matrix of coefficients of ϕ and $\vec{\psi}$

g = gravity acceleration

h = mean z - coordinate of interface

i = subscript pertaining to a particular layer

j = subscript of a particular harmonic component

J = Bessel function

k = coefficient of r and z in scalar potential, ϕ

m = coefficient of z in vector potential, $\vec{\psi}$

n = coefficient of φ ; order of Bessel function

N = number of interfaces, including free surface

p = pressure; stress component

r = radial component, positive sense outward

R = radius of lip crest of crater

t = time

T = characteristic, e-folding time

$\vec{v}$ = velocity of creep of medium

z = vertical coordinate, positive sense upward

ζ = free surface of medium

μ = viscosity

ρ = density

φ = angular coordinate

ϕ = scalar velocity potential

$\vec{\psi}$ = vector velocity potential

Symbols have the same meaning when used as subscripts.

Theory

Assumptions I, II, III and V lead to the equation of motion, for a particular layer (Chandrasekhar, 1955)

$$\frac{\partial \vec{v}}{\partial t} + (\vec{v} \cdot \vec{\nabla}) \vec{v} = -\frac{1}{\rho} \vec{\nabla} p + \vec{g} + \frac{\mu}{\rho} \nabla^2 \vec{v} \tag{1}$$

and equation of continuity

$$\vec{\nabla} \cdot \vec{v} = 0 \tag{2}$$

Due to assumption VI then

$$(\vec{v} \cdot \vec{\nabla}) \vec{v} \approx 0 \tag{3}$$

Deriving the velocity vector from a scalar potential, ϕ, and a vector potential, $\vec{\psi}$,

$$\vec{v} = -\vec{\nabla}\phi + \vec{\nabla} \times \vec{\psi} \tag{4}$$

yields the uncoupled system

$$\nabla^2 \phi = 0 \tag{5}$$

$$\nabla^2 \vec{\psi} = \frac{\rho}{\mu} \frac{\partial \vec{\psi}}{\partial t} \tag{6}$$

$$\frac{\partial \phi}{\partial t} = \frac{p}{\rho} + gz \tag{7}$$

which then gives a set of integrals

$$\phi = \sum_j \sum_n (A_{\phi jn} e^{k_{jn} z} + B_{\phi jn} e^{-k_{jn} z}) \cos n\varphi \, J_n(k_{jn} r) e^{-\frac{t}{T_{jn}}} \tag{8}$$

$$\psi_r = \sum_j \sum_n (A_{rjn} e^{m_{jn} z} + B_{rjn} e^{-m_{jn} z}) \sin n\varphi \, J_{n+1}(k_{jn} r) e^{-\frac{t}{T_{jn}}} \tag{9}$$

$$\psi_\varphi = \sum_j \sum_n (A_{\varphi jn} e^{m_{jn} z} + B_{\varphi jn} e^{-m_{jn} z}) \cos n\varphi \, J_{n+1}(k_{jn} r) e^{-\frac{t}{T_{jn}}} \tag{10}$$

$$\psi_z = \sum_j \sum_n (A_{zjn} e^{m_{jn} z} + B_{zjn} e^{-m_{jn} z}) \sin n\varphi \, J_n(k_{jn} r) e^{-\frac{t}{T_{jn}}} \tag{11}$$

Assumption VIII makes n = 0, thus (9) and (11) become meaningless and (8) and (10) simplify to

$$\phi = \sum_j \left(A_{\phi_j} e^{k_j z} + B_{\phi_j} e^{-k_j z} \right) J_0(k_j r) e^{-\frac{t}{T_j}} \qquad (12)$$

$$\vec{\psi} = \hat{\varphi} \sum_j \left(A_{\psi_j} e^{m_j z} + B_{\phi_j} e^{-m_j z} \right) J_1(k_j r) e^{-\frac{t}{T_j}} \qquad (13)$$

From (6) then follows

$$m_j = k_j \sqrt{1 - \rho / k_j^2 \mu T_j} \qquad (14)$$

Postulating continuity of velocity components, v_r and v_z, and stress components, P_{rz} and P_{zz}, results in a set of 4N equations in 4N unknowns, $A_{\phi_1}, B_{\phi_1}, A_{\psi_1}, B_{\psi_1}, \ldots A_{\psi_N}, B_{\psi_N}$. This system is linear and homogeneous, therefore it has a non-trivial solution if and only if the determinant of the matrix of the coefficients, D, is equal to zero. Thus

$$D = 0 \qquad (15)$$

gives the final relation between k_j and T_j. The characteristic time of the deformation is then given as a function of the physical parameters, ρ_i and μ_i, of all the layers; of g; and of the geometrical parameters, k_j. The determinant of a similar problem had been written out in detail by Daneš (1964).

While the approach just described sounds simple, equation (15) is of such a complexity (Bellman and Pennington, 1954) that closed form solutions are hopeless.

Matters are simplified if we write

$$\vec{v} = \vec{\nabla} \times \vec{\psi} \qquad (16)$$

only and determine the consequences. This is justified for an incompressible medium and is in accord with (2). It reduces the number of simultaneous equations from 4N to 2N. Then, from

$$\vec{\psi} = \hat{\varphi} \sum_j \left(A_{\psi_j} e^{m_j z} + B_{\psi_j} e^{-m_j z} \right) J_1(k_j r) e^{-\frac{t}{T_i}} \qquad (17)$$

follows

$$v_r = \sum_j m_j \left(-A_{\psi_j} e^{m_j z} + B_{\psi_j} e^{-m_j z} \right) J_1(k_j r)\, e^{-\frac{t}{T_j}} \qquad (18)$$

$$v_z = \sum_j k_j \left(A_{\psi_j} e^{m_j z} + B_{\psi_j} e^{-m_j z} \right) J_0(k_j r)\, e^{-\frac{t}{T_j}} \qquad (19)$$

$$P_{rz} = -\mu \sum_j \left(m_j^2 + k_j^2 \right) \left(A_{\psi_j} e^{m_j z} + B_{\psi_j} e^{-m_j z} \right) J_1(k_j r)\, e^{-\frac{t}{T_j}} \qquad (20)$$

$$P_{zz} = \rho g z + 2\mu \sum_j k_j m_j \left(A_{\psi_j} e^{m_j z} - B_{\psi_j} e^{-m_j z} \right) J_0(k_j r)\, e^{-\frac{t}{T_j}} \qquad (21)$$

However, an estimate of magnitudes of various parameters shows that $m_j \approx k_j$ to within one part in 10^{12} or better; ≈ 2 g cm^{-3}, $k_j \approx 3 \times 10^{-7}$cm; μ and T are, of course, unknown for the Moon, but even a very moderate estimate of $\mu \approx 10^{18}$ g cm^{-1}sec^{-1} and T ≈ 300 years $\approx 10^{10}$ sec (viscosity of rock salt and historic record of observations) gives $\rho/k_j^2 \mu T_j \approx 2 \times 10^{-13}$. Therefore satisfactory results are obtained with

$$\vec{v} = -\vec{\nabla}\varphi \qquad (22)$$

replacing (4). In other words, the Reynold's number of the system is negligibly small. This reduces the number of simultaneous equations from 4N to 2N. As a penalty for this simplification, we have to forfeit the requirement of continuity of v_r and P_{rz} across boundaries; but again, the error thus introduced is many orders of magnitude smaller than the quantities analyzed.

This simplification yields integrals (summation with respect to j is no longer repeated)

$$v_r = k \left(A e^{kz} + B e^{-kz} \right) J_1(kr)\, e^{-\frac{t}{T}} \qquad (23)$$

$$v_z = k \left(-A e^{kz} + B e^{-kz} \right) J_0(kr)\, e^{-\frac{t}{T}} \qquad (24)$$

$$P_{rz} = 2\mu k^2 \left(A e^{kz} - B e^{-kz} \right) J_1(kr)\, e^{-\frac{t}{T}} \qquad (25)$$

$$P_{zz} = \rho g z - \left(\frac{\rho}{T} + 2\mu k^2 \right) \left(A e^{kz} + B e^{-kz} \right) J_0(kr)\, e^{-\frac{t}{T}} \qquad (26)$$

According to VII, the only driving force comes from the perturbation

$$\xi = \xi(r, t) \tag{27}$$

of the free surface. Expanding (27) as a series of zero order Bessel functions,

$$\xi_k = c_k J_o(kr) e^{-\frac{t}{T}} \tag{28}$$

The free boundary condition then gives

$$\frac{D\xi}{Dt} \equiv \frac{\partial \xi}{\partial t} + \frac{\partial \xi}{\partial r}\frac{dr}{dt} = (v_z)_{z=\xi} \tag{29}$$

Then, by postulate IV, we may neglect the nonlinear term $(\partial \xi / \partial r)(dr/dt)$ and take $(v_z)_{z=0}$ instead of the right hand side of (29), so that

$$\frac{\partial \xi_k}{\partial t} = -\frac{C}{T} J_o(kr) e^{-\frac{t}{T}} = k(-A+B) J_o(kr) e^{-\frac{t}{T}} \tag{30}$$

and therefore

$$\xi_k = kT(A-B) J_o(kr) e^{-\frac{t}{T}} \tag{31}$$

Then (26) becomes

$$P_{zz} = \left[A\left(\rho g kT - \frac{\rho}{T} - 2\mu k^2\right) e^{kz} - B\left(\rho g kT + \right. \right. $$
$$\left. \left. + \frac{\rho}{T} + 2\mu k^2\right) e^{-kz} \right] J_o(kr) e^{-\frac{t}{T}} \tag{32}$$

For a single medium extending to negative infinity,

$$B = 0 \tag{33}$$

and the vanishing stress component P_{zz} at the free boundary requires

$$\rho g kT - \frac{\rho}{T} - 2\mu k^2 = 0 \tag{34}$$

or

$$T = \frac{\mu k}{\rho g}\left(1 \pm \sqrt{1 + \frac{\rho^2 g}{\mu^2 k^3}}\right) \tag{35}$$

Again, the term $(\rho^2 g)/(\mu^2 k^3)$ is very small; k, even for very large craters, is of the order of 10^{-7} cm^{-1}; therefore

$$(\rho^2 g)/(\mu^2 k^3) \leq 10^{-11} \tag{36}$$

and

$$T \approx \frac{2\mu k}{\rho g} \tag{37}$$

88

The relations may be more complicated if Cook's (1963) results are verified. His model will be investigated in detail in the future.

For a multilayer model, the boundary conditions between the i-th and the (i + 1)-th layer become

$$-A_i e^{kh_i} + B_i e^{-kh_i} + A_{i+1} e^{kh_i} - B_{i+1} e^{-kh_i} = 0 \qquad (38)$$

and

$$\left.\begin{aligned}
&A_i\left(-\rho_i g k T + \frac{\rho_i}{T} + 2\mu_i k^2\right)e^{kh_i} + B_i\left(\rho_i g k T + \right.\\
&\left. + \frac{\rho_i}{T} + 2\mu_i k^2\right)e^{-kh_i} - A_{i+1}\left(-\rho_{i+1} g k T + \right.\\
&\left. + \frac{\rho_{i+1}}{T} + 2\mu_{i+1} k^2\right)e^{kh_i} - B_{i+1}\left(\rho_{i+1} g k T + \right.\\
&\left. + \frac{\rho_{i+1}}{T} + 2\mu_{i+1} k^2\right)e^{-kh_i} = 0
\end{aligned}\right\} \qquad (39)$$

Obviously, the condition (15) derived from all the interfaces results in an implicit function

$$F(T, k, g, \rho_1, \rho_2, \cdots \rho_N, \mu_1, \mu_2, \cdots \mu_N) = 0 \qquad (40)$$

which defines the characteristic, e-folding time, T as function of the other parameters. Unfortunately, this dependence is still too complex for an analytic solution. The problem is at present being analyzed numerically by Roger Bowen at the U.S. Geological Survey, Menlo Park, California, and results will be reported in due time. The only case amenable to analytic solution is that of a single medium. Such was previously investigated by Daneš (1962) and, independently, by Scott (1965). Daneš started with a simplified shape of the lunar crater Copernicus and projected it into the distant future. Various stages of the "future Copernicus" then agreed well with present old craters, both lunar and terrestrial (Masursky, 1964; Quaide and others, 1964). The analysis was, nevertheless, too crude; only a small number of harmonic components was used, and the radial expansion was terminated at 1.5R, so that the crater lip appeared "hinged" at that distance. Both shortcomings have been remedied in the present analysis.

Numerical results

If the results of the present analysis are to be meaningful, the
model must start with the appropriate initial crater shape. To find
such a shape is not a simple task inasmuch as the shape depends in part
on the diameter. The theory of crater formation (Nordyke, 1961) is
still in its infancy and experimental data come either from impact
craters too small for the purpose (Moore and others, 1964) or from
craters generated by chemical and/or nuclear detonations (Carlson and
Roberts, 1963; Fulmer and Roberts, 1964; Murphey and Vortman, 1961).
Most terrestrial impact craters are either too small, or they have been
modified subsequently (Beals and others, 1963; Dietz, 1963; Masursky,
1964). The most dependable data probably come from the Meteor Crater
in Arizona (Shoemaker, 1963) but that feature is still small compared
with those for which the above analysis applies.

With the help of H. J. Moore and M. H. Carr, the author was able
to piece together a plausible "idealized initial impact crater," shown
in table 1 and in figure 1 as the t = 0 curve. It was selected to
match the diameter of the modified craters with which we wish to com-
pare the results, i.e., 30 to 100 km. This shape was then expanded as
a series of zero order Bessel functions. The "spectrum" of that ex-
pansion is shown on figure 2. Then each harmonic was evaluated for
t = T, 2T, 5T, 10T, 20T and 50T. The coefficient k used in (37)
corresponds to the first zero of the first Bessel component of the
expansion, which was taken to a distance of 3R to make sure that the
fictitious boundary effects from the termination of the expansion are
negligible. Thus

$$T = 1.603 \frac{\mu}{\rho g R} \tag{41}$$

The results of the analysis are shown in table 1 and in figure 1.
The expansion was truncated at the 14th harmonic. The difference be-
tween the observed ξ/R and the calculated one is in the $\Delta \xi/R$ column
and represents the cumulative contribution of higher harmonics. The
later stages were then calculated in two ways: (1) neglecting the
contribution of the higher terms, and (2) applying them as if they

Table 1. Shape of crater in the course of time

| r/R	ξ/R (observed)	t = 0			t = T		t = 2T		t = 5T		t = 10T		t = 20T		t = 50T	
		r/R·ξ/R (observed)	ξ/R (calc.)	Δξ/R	ξ/R	corr. ξ/R	ξ/R	corr. ξ/R	ξ/R	corr. ξ/R	ξ/R	corr. ξ/R	ξ/R	corr. ξ/R	ξ/R	corr. ξ/R
.05	-.199	-.00995	-.214	+.015	-.121	-.106	-.059	-.044	+.024	+.039	+.043	+.058	+.023	+.038	+.003	+.018
.15	-.269	-.04035	-.261	-.008	-.166	-.172	-.102	-.110	-.013	-.021	+.018	+.010	+.010	+.002	+.001	-.007
.25	-.296	-.07400	-.304	+.008	-.209	-.201	-.145	-.137	-.049	-.041	-.007	+.001	-.001	+.007	-.001	+.007
.35	-.300	-.10500	-.309	+.009	-.218	-.209	-.156	-.147	-.060	-.051	-.013	-.004	-.001	+.008	-.001	+.008
.45	-.300	-.13500	-.290	-.010	-.206	-.216	-.149	-.159	-.059	-.069	-.011	-.021	+.003	-.007	+.001	-.009
.55	-.285	-.15675	-.264	-.021	-.192	-.213	-.142	-.163	-.063	-.084	-.018	-.039	.000	-.021	+.001	-.020
.65	-.245	-.15925	-.253	+.008	-.192	-.184	-.150	-.142	-.082	-.074	-.037	-.029	-.011	-.003	-.001	+.007
.75	-.172	-.12900	-.177	+.005	-.135	-.130	-.107	-.102	-.061	-.056	-.035	-.030	-.014	-.009	-.001	+.004
.85	-.063	-.05355	-.043	-.020	-.023	-.043	-.013	-.033	-.004	-.024	-.004	-.024	-.003	-.023	.000	-.020
.95	+.090	+.08550	+.085	+.005	+.086	+.091	+.080	+.085	+.057	+.062	+.030	+.035	+.010	+.015	+.001	+.006
1.05	+.172	+.18060	+.155	+.017	+.140	+.157	+.124	+.141	+.082	+.099	+.042	+.059	+.014	+.031	+.001	+.018
1.15	+.136	+.15640	+.148	-.012	+.129	+.117	+.122	+.110	+.065	+.053	+.028	+.016	+.006	-.006	.000	-.012
1.25	+.105	+.13125	+.108	-.003	+.088	+.085	+.070	+.067	+.032	+.029	+.007	+.004	-.003	-.006	+.001	-.002
1.35	+.079	+.10665	+.075	+.004	+.057	+.061	+.041	+.045	+.012	+.016	-.003	+.001	-.005	-.001	-.001	+.003
1.45	+.057	+.08265	+.057	.000	+.041	+.041	+.028	+.028	+.006	+.006	-.003	-.003	-.002	-.002	.000	.000
1.55	+.038	+.05890	+.038	.000	+.028	+.028	+.018	+.018	+.002	+.002	-.002	-.002	.000	.000	.000	.000
1.65	+.023	+.03795	+.022	+.001	+.013	+.014	+.014	+.015	-.004	-.003	-.004	-.003	-.001	.000	+.001	+.001
1.75	+.011	+.01925	+.008	+.003	+.001	+.004	+.004	+.007	-.009	-.006	-.006	-.003	-.001	+.002	.000	+.003
1.85	+.002	+.00370	+.002	.000	-.003	-.003	-.006	-.006	-.008	-.008	-.004	-.004	-.001	-.001	.000	.000
1.95	.000	.00000	+.002	-.002	-.002	-.004	-.004	-.006	-.005	-.007	-.002	-.004	.000	-.002	.000	-.002
2.05	.000	.00000	+.001	-.001	-.002	-.003	-.004	-.005	-.004	-.005	-.001	-.002	+.001	.000	.000	-.001
2.15	.000	.00000	-.001	+.001	-.003	-.002	-.004	-.003	-.004	-.003	-.001	.000	.000	+.001	.000	+.001
2.25	.000	.00000	-.001	+.001	-.003	-.002	-.004	-.003	-.003	-.002	-.001	.000	.000	+.001	.000	+.001
2.35	.000	.00000	.000	.000	-.001	-.001	-.002	-.002	-.002	-.002	.000	.000	.000	.000	.000	.000
2.45	.000	.00000	-.001	+.001	.000	+.001	-.001	-.002	.000	-.001	.000	-.001	.000	-.001	.000	-.001
2.55	.000	.00000	+.006	-.006	-.006	.000	-.006	.000	-.004	+.002	-.002	+.004	-.001	+.005	.000	+.006
2.65	.000	.00000	-.001	+.001	-.001	.000	-.002	-.001	-.001	.000	.000	+.001	.000	+.001	.000	+.001
2.75	.000	.00000	-.001	+.001	-.001	.000	-.002	-.001	-.001	.000	.000	+.001	.000	+.001	.000	+.001
2.85	.000	.00000	-.001	+.001	-.001	.000	-.001	.000	-.001	.000	.000	+.001	.000	+.001	.000	+.001
2.95	.000	.00000	.000	.000	.000	.000	.000	.000	.000	.000	.000	.000	.000	.000	.000	.000

Total = .00000
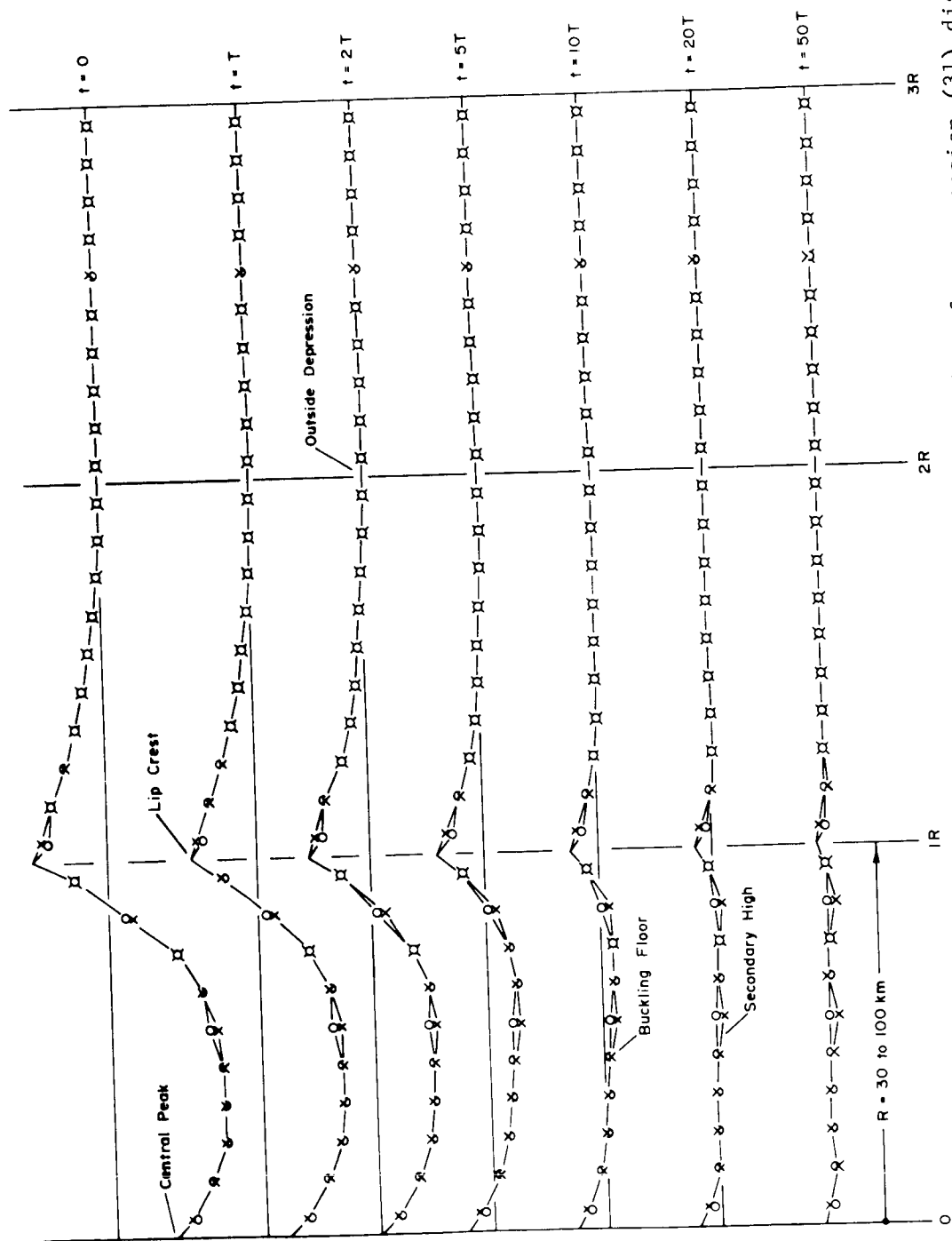
Fig. 1.--Shape of a crater in the course of time. O = values from expansion (31) disregarding harmonics higher than 14. x = values from expansion (31) assuming that harmonics higher than 14 do not decay. Vertical scale arbitrary.
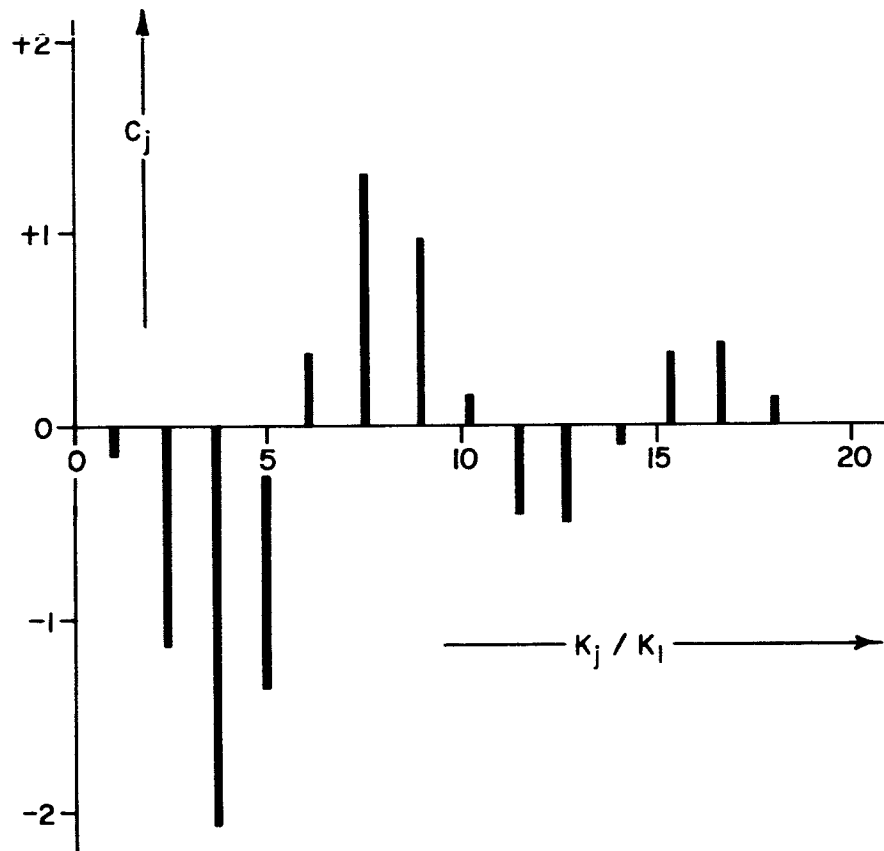
Fig. 2.--Spectrum of initial crater shape. (C_j in arbitrary units of length.)

did not change at all in the course of time. Former values are plotted as small circles; the latter ones, crosses. The true picture is probably close to the crosses during the early stages, but gradually approaches the circles later on. The results reveal the following points:

1. Shortly after the formation of the crater, the lip starts sagging in and the floor starts getting flatter and shallower.

2. The deepest portion of the bottom gradually shifts outward toward the lip.

3. Between 2T and 3T, the central peak reaches the precrater level; subsequently, it stays above that level and in late stages, it may reach a height comparable with that of the lip crest.

4. Around 5T, the floor of the crater, originally concave as seen from above, becomes convex and developes a secondary high ring at about ½R. Later on, around 20T, this secondary ring reaches the precrater level and subsequently exceeds it.

5. Early in the process, a shallow depression developes outside the crater rim; subsequently, this circular trough maintains a more or less constant depth, but both its inner and outer radii are decreasing, so that the trough shrinks and approaches the lip crest.

6. There is some indication -- although not yet conclusive -- that in the course of time, the radius of the lip crest tends to increase slightly; this may result in the development of radial tension cracks in the lip.

Criticism of model and results

Certainly all the assumptions and approximations used in the analysis are sources of errors in the results. Here we may try to estimate the order of magnitude of those errors.

Beals and others (1963) and Urey and others (1959) show that density variation in the vicinity of craters should be anticipated. Probably even more important are the viscosity variations, but of those we know almost nothing. Thus I and II may be considered as temporary working hypotheses, subject to modification as more data become available.

Assumption III seems crude, but for processes of geologic duration, it may not be too bad (Griggs, 1939, 1940; Haskell, 1935, 1936, 1937; Gutenberg, 1958; Cook, 1963; Runcorn, 1963; Takeuchi and Hasegawa, 1964). Laboratory experiments indicate that there is a threshold stress below which no deformation takes place even over long periods; but Crittenden's (1963a, 1963b) results show that in geologic processes such a threshold, if it exists at all, is very small. The next question then is, whether the direct proportionality between stress and deformation rate is justified. While the answer, in general, would be negative, we may accept the proportionality as the first term in the Taylor expansion of the relation of the two quantities; and as long as the stresses are small, III may be reasonably well justified.

Assumption IV may not be justified immediately after the impact; but the originally steep walls of the crater would become more gentle within a short time due to slumping Quaide and others (1964) so that we may take as t = 0 the time when slumping has ceased. The error thus introduced should be quite small.

Assumption V is justified for craters. It would not be adequate for lunar maria. For those, a different model will be worked out.

Assumption VI has been justified above.

If Runcorn's (1963) model of the convective lunar interior is correct, then VIII may be violated; but the effects would probably be noticed only upon features of linear dimensions comparable with those of the convection cells, therefore large compared with craters.

Assumption VIII ignores the possibly interesting effects of crater polygonalism and superposition of adjacent features. Those may be investigated in the future.

As for the results, the correspondence between the theoretical profiles derived here and observed lunar craters seems satisfactory to this writer. Not so satisfactory is the order of magnitude of the time constant, T. For lunar craters, Urey's (1962) results require T of the order of 10^8 years, or 3×10^{15} sec. With R of the order of 100 km = 10^7 cm and density, ρ, of 2 g cm^{-3}, equation (41) gives a viscosity

$$\mu = \frac{1}{1.603} T \rho g R = \frac{1}{1.603} \times 3 \times 10^{15} \sec \times 2 g\, cm^{-3} \times 1.6 \times 10^2\, cm\, sec^{-2} \times 10^7 cm$$

$$\approx 0.6 \times 10^{25}\ poise.$$

This is about two orders of magnitude greater than the highest viscosity values observed in the laboratory; three orders of magnitude greater than the value derived by Haskell (1935, 1936, 1937) from the Fennoscandian uplift, and four orders of magnitude greater than the value found by Crittenden (1963a, 1963b) from the Lake Bonneville analysis.

Conversely, if lunar rock viscosities were comparable with those found by Haskell, large lunar craters would have a time constant, T, of the order of 200,000 years, and would just about disappear in about 10 million years. Crittenden's value would cut both those times by another order of magnitude.

The way out of this dilemma is not clear. Either lunar rocks are much more viscous than terrestrial ones; or the processes studied by Haskell and Crittenden are not of a rebound nature; or lunar features are younger than we believe; or assumptions III and VII are incorrect. This point will be investigated further.

References

Airy, G. B., 1855, On the computation of the effect of the attraction of mountain-masses as disturbing the apparent astronomical latitude of station in geodetic surveys: Trans. Roy. Soc. (London) Ser. B, v. 145, p. 101-104.

Anderson, D. L., 1962, The plastic layer of the earth's mantle: Sci. Amer., v. 207, p. 52-59.

Baldwin, R. B., 1949, The face of the moon: Chicago, Univ. of Chicago Press, 239 p.

_____ 1962a, The nature of the lunar surface and major structural features, in Proceedings of the Conference on lunar exploration: Virginia Polytechnic Inst., Eng. Expt. Stat. Bull. no. 152, pt. A, paper VII, 38 p.

_____ 1962b, Supplementary note, in Proceedings of the Conference on lunar exploration: Virginia Polytechnic Inst., Eng. Expt. Stat. Bull. no. 152, pt. C, appendix, 7 p.

_____ 1963, The measure of the moon: Chicago, Univ. of Chicago Press, 488 p.

Beals, C. S., Innes, M. J. S., and Rottenberg, J. A., 1963, Fossil
meteorite craters, in Middlehurst, B. M., and Kuiper, C. P., eds.,
Moon, meteorites and comets--The solar system, v. 4: Chicago,
Univ. of Chicago Press, p. 235-284.

Bellman, R., and Pennington, R. H., 1954, Effects of surface tension
and viscosity on Taylor instability: Quart. Appl. Math., v. 12,
p. 151-162.

Biot, M. A., 1954, Theory of stress--strain relations in anisotropic
viscoelasticity and relaxation phenomena: J. Appl. Phys., v. 25,
p. 1385-1391.

_____ 1956, Variational and Lagrangean methods in viscoelasticity:
Proc. Internatl. Union of Theor. and Appl. Mech., Colloquium on
deformation and flow in solids, Madrid, 1955; Berlin, Springer
Verlag, p. 251-263.

_____ 1961, Theory of folding of stratified viscoelastic media and
its implication in tectonics and orogenesis: Geol. Soc. America
Bull., v. 72, no. 11, p. 1595-1620.

Biot, M. A., Odé H., and Roever, W. L., 1961, Experimental verification
of the theory of folding of stratified viscoelastic media: Geol.
Soc. America Bull., v. 72, no. 11, p. 1621-1632.

Carlson, R. H., and Roberts, W. A., 1963, Mass distribution and throwout
studies, Project Sedan: U.S. Atomic Commission, PNE-217F, 144 p.

Chandrasekhar, S., 1955, The character of the equilibrium of an incom-
pressible heavy viscous fluid of variable density: Cambridge Philos.
Soc. Proc., v. 51, p. 162-178.

Coleman, Bernard, and Noll, Walter, 1961, Foundations of linear visco-
elasticity: Rev. Modern Physics, v. 33, p. 239-249.

Cook, M. A., 1963, Viscosity-depth profiles according to the Ree-Eyring
viscosity relations: Jour. Geophys. Research, v. 68, p. 3515-3520.

Crittenden, M. D., 1963a, Effective viscosity of the earth derived from
the isostatic loading of Pleistocene Lake Bonneville: Jour.
Geophys. Research, v. 68, p. 5517-5530.

Crittenden, M. D., 1963b, New data on the isostatic deformation of Lake
   Bonneville: U.S. Geol. Survey Prof. Paper 454-E, p. E1-E31.

Daneš, Z. F., 1962, Isostatic compensation of lunar craters: Tacoma,
   Wash., Univ. of Puget Sound Research Inst. Rept., 11 p.

_____ 1964, Mathematical formulation of salt-dome dynamics: Geophysics,
   v. 29, p. 414-424.

Dietz, R. S., 1963, Astroblemes--Ancient meteorite-impact structures
   on the earth, in Middlehurst, B. M., and Kuiper, G. P., eds., The
   Moon, meteorites and comets--The Solar system, vol. 4, Chicago,
   Univ. of Chicago Press, p. 285-300.

Dutton, C. E., 1889, On some of the greater problems of physical geology:
   Philos. Soc. Washington Bull., ser. B, v. 11, p. 51-64.

Fulmer, C. V., and Roberts, W. A., 1964, Rock induration and crater
   shape: Icarus, v. 2, p. 452-456.

Griggs, D. T., 1939, Creep of rock: Jour. Geology, v. 47, p. 225-251.

_____ 1940, Experimental flow of rocks under conditions favoring
   recrystallization: Geol. Soc. America Bull., v. 51, p. 1001-1022.

Gutenberg, Beno, 1958, Theoretical problems of the earth's interior, in
   Eirich, R. R., ed., Rheology, vol 2: New York, Academic Press,
   p. 401-430.

Haskell, N. A., 1935, Motion of viscous fluid under a surface load:
   Physics, v. 6, p. 265-269.

_____ 1936, Motion of viscous fluid under a surface load, part II
   Physics, v. 7, p. 56-61.

_____ 1937, Viscosity of the asthenosphere: Am. Jour. Sci., v. 233,
   p. 22-28.

Kopal, Zdenek, 1962, Topography of the moon, in Kopal, Zdenek, ed.,
   Physics and astronomy of the moon: New York, Academic Press,
   p. 231-282.

_____ 1963, Gravitational heating of the moon: Icarus, v. 1. p. 412-421.

Kozyrev, N. A., 1962, Spectroscopic proof for existence of volcanic
   processes on the moon, in Kopal, Zdenek, and Mikhailov, Z. K., eds.,
   The Moon, New York, Academic Press, p. 263-271.

Levin, B. J., 1962, Thermal history of the moon, in Kopal, Zdenek, and
    Mikhailov, Z. K., eds., The Moon: New York, Academic Press,
    p. 157-167.

Masursky, Harold, 1964: A preliminary report on the role of isostatic
    rebound in the geologic development of the lunar crater Ptolemaeus,
    in Astrogeologic Studies Annual Prog. Rept., July 1, 1963 to
    July 1, 1964, pt. A: U.S. Geol. Survey open-file report, p. 102-134.

Murphey, B. F., and Vortman, L. J., 1961, High explosive craters in
    desert alluvium, tuff and basalt: Jour. Geophys. Research, v. 66,
    p. 3389-3404.

Nordyke, M. D., 1961, Nuclear craters and preliminary theory of the
    mechanics of explosive crater formation: Jour. Geophys. Research,
    v. 66, p. 3439-3459.

Pratt, J. H., 1855, On the attraction of the Himalaya Mountains, and
    of the elevated regions beyond them, upon the plumb-line in India:
    Royal Soc. London Trans., v. 145, pt. 1, p. 53-100.

Quaide, W. L., Gault, D. E., and Schmidt, R. A., 1964, Gravitative
    effects on lunar impact structures: Space Sci. Div., NASA, Ames
    Res. Center, California.

Ree, T., and Eyring, H., 1958, The relaxation theory of transport
    phenomena, in Eirich, R. R., ed., Rheology, vol. 2: New York,
    Academic Press.

Runcorn, S. K., 1963, The interior of the moon: California Inst.
    Technology, Jet Propulsion Lab. Tech. Rept. no. 32-529, 15 p.

Scott, R. F., 1965, Viscous flow of craters: Pasadena, California
    Inst. Technology, 13 p.

Shoemaker, E. M., 1963, Impact mechanics of Meteor Crater, Arizona, in
    Middlehurst, B. M., and Kuiper, G. P., eds., The Moon, meteorites
    and comets--The solar system, vol. 4: New York, Academic Press
    p. 301-336.

Takeuchi, Hitochi, and Hasegawa, Yosaku, 1964, Viscosity distribution
    within the earth: Rept. Geophys. Inst., Faculty of Sci., Univ.
    of Tokyo, Tokyo, Japan.

References--Continued

Urey, H. C., Elsasser, W. M., and Rochester, M. G., 1959, Note on the
internal structure of the moon: Astrophys. Jour., v. 129,
p. 842-848.

_____ 1962, Age of the moon, chemical composition, geological aspects,
stress and cooling history, in Proceedings of the Conference on
lunar exploration: Virginia Polytechnic Inst., Eng. Expt. Stat.
Bull. 152, pt. A, paper III, 31 p.

Wright, F. E., Wright, F. H., and Wright, Helen, 1963, The lunar
surface--Introduction, in Middlehurst, B. M., and Kuiper, G. P.,
eds., The Moon, meteorites and comets--The solar system, vol. 4:
New York, Academic Press, p. 1-56.

A PRELIMINARY ALBEDO MAP OF THE LUNAR EQUATORIAL BELT

by L. C. Rowan and Mareta West

Introduction

Albedo[1] is one of the most critical parameters in lunar investigations, and accurate methods to determine it must be devised. The areal distribution and rate of change of albedo are of particular interest in geologic mapping, topographic mapping, and photometric and photographic preflight programming and calibration of spacecraft imagery systems.

Although albedo has been widely used by lunar geologic mappers in the qualitative description of rock-stratigraphic units, quantitative definition has been generally lacking. Two processes appear to be operative in the development of an equilibrium within the range of lunar albedo: (1) volcanic processes appear to darken the lunar surface, and (2) ray materials produced by impact increase the full-moon reflectivity of the surface. In addition, the brighter ray material apparently darkens as a function of time, possibly because of radiation bombardment. The dark materials of the Marius dome field in Oceanus Procellarum (McCauley, this volume), and the dark border of Mare Serenitatis (see map in supplement to this report) are examples of critical areas where detailed albedo data are important to a better understanding of these processes.

As lunar geologic mapping proceeds at larger scales and in greater detail, the need for information of this type increases. An accurate map which delineates areas of different albedo at the largest possible scale is required. Such information is especially critical to unmanned lunar orbiters, in which the initial images will be on 70-mm film and the possible shutter speeds will be 1/100, 1/50, and 1/25 sec. Rapid, unexpected albedo variations could cause considerable image degradation.

---

[1]Albedo, as used here, is defined by Sytinskaya (1953) as the reflecting power at full moon expressed as a brightness coefficient.

A photographic technique devised by Hawkins and Munsey (1963) has been used in the lunar terrain analysis program to delineate relative albedo levels (McCauley, 1964, p. 4-7). Hackman (1962) and Miesch and Davis (1963) have also investigated the problem. One of the primary goals of the investigations reported here is to relate albedo levels to standard albedo measurements determined by photoelectric telescopic measurements.

Methods

Briefly stated, the photographic technique of discriminating albedo units consists of exposing a full-moon plate or film to a high-contrast film at variable exposure levels. The response of the high contrast film is one of black and clear. Areas of different relative albedo can be mapped, therefore, by tracing the areas from the films at each of the exposure levels. The assignment of albedo ranges to these films requires a relationship between measured albedos of selected points and the optical density of the corresponding points on the full-moon plate.

The full-moon photograph used was a positive film copy of a Lick Observatory negative plate taken at the 36-inch refracting telescope in July 1939. A negative glass plate copy of this positive film constituted the primary source of density data. A series of positive films was prepared from the negative copy on DuPont Ortho Litho S high contrast film. Table 1 lists some of the albedos measured by Sytinskaya (1953) and the optical density of the corresponding points on the negative copy of the Lick 1939 plate. The density measurements were made on a Jarrell-Ash recording microdensitometer. With the exception of three points, the measurements of albedo and plate density can be fitted to a straight line (fig. 1). The deviation of these three points from the fitted line may be due either to inaccuracies in the original albedo measurements, or to positional inaccuracies on the full-moon plate in the microdensitometer.

It is necessary to correlate the response of the Ortho Litho S film at various time exposures with the density levels on the negative full-
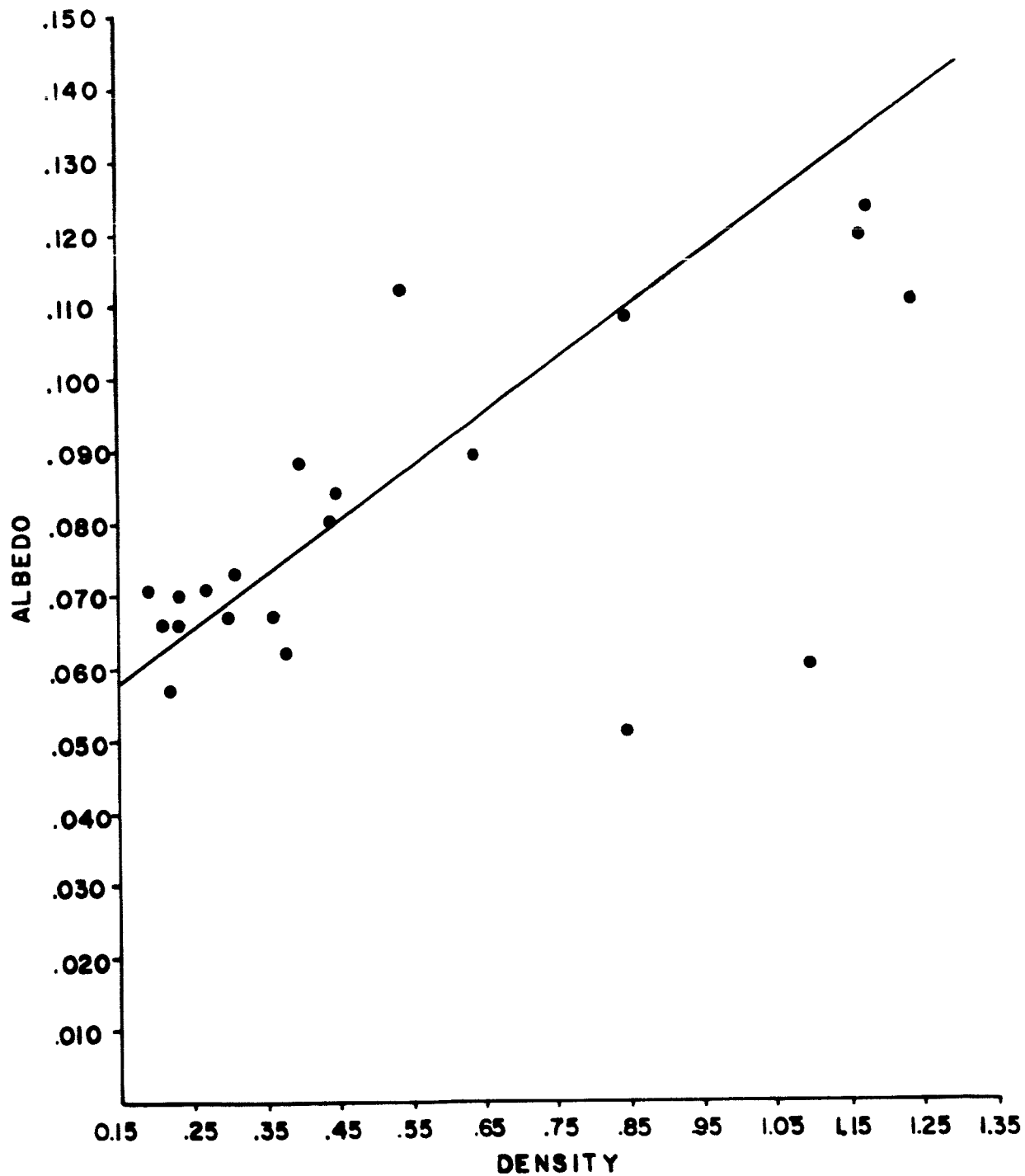
Fig. 1.--Photometrically derived albedo vs. optical density
for the 1939 Lick full-moon negative plate copy. Albedo data from
Sytinskaya (1953).

moon plate. To do this, a 21-step calibrated gray scale was imprinted on the negative plate at the time it was produced from the copy positive. The calibrated step wedge was also imprinted on Ortho Litho S film positives made from the negative at a constant lens setting (f/16) with varying times of exposure. The black and clear separation of adjacent steps of the gray scale on the Ortho Litho S films gives the density values for each time used. In this manner, density can be expressed as a function of time (fig. 3). The H and D curve (fig. 2) defines the character of the density transfer to the negative full-moon plate from the positive plate copy. The H and D curve for Ortho Litho S is nearly horizontal in figure 2 and is shown by a series of horizontal dashed lines.

The linear relation between density and albedo (fig. 1) and the relations between the negative plate copy and the Ortho Litho S positives were used to subdivide the plate density scale at the points shown in figure 2. Five Ortho Litho S positives, therefore, represent these subdivisions, the ranges for which are shown in figure 2.

Map preparation

A 1:5,000,000 scale isopleth map of the equatorial zone was compiled by projecting the Ortho Litho S positives onto a 1:5,000,000 scale 1939 full-moon print and tracing out the contact between the black and white portions. Successive tracings outline areas of known albedo ranges. Selenographic control was obtained from charts made by the Aeronautical Chart and Information Center, and great care was taken to maintain proper registration. The resulting 1:5,000,000 isopleth map, reduced 50 percent to 1:10,000,000 is included in the map supplement of this report.

Technical limitations

The following factors limit the accuracy of the 1:5,000,000 scale map:

1. Photographic inconsistencies such as emulsion heterogeneity, exposure and development times, and temperature variations.
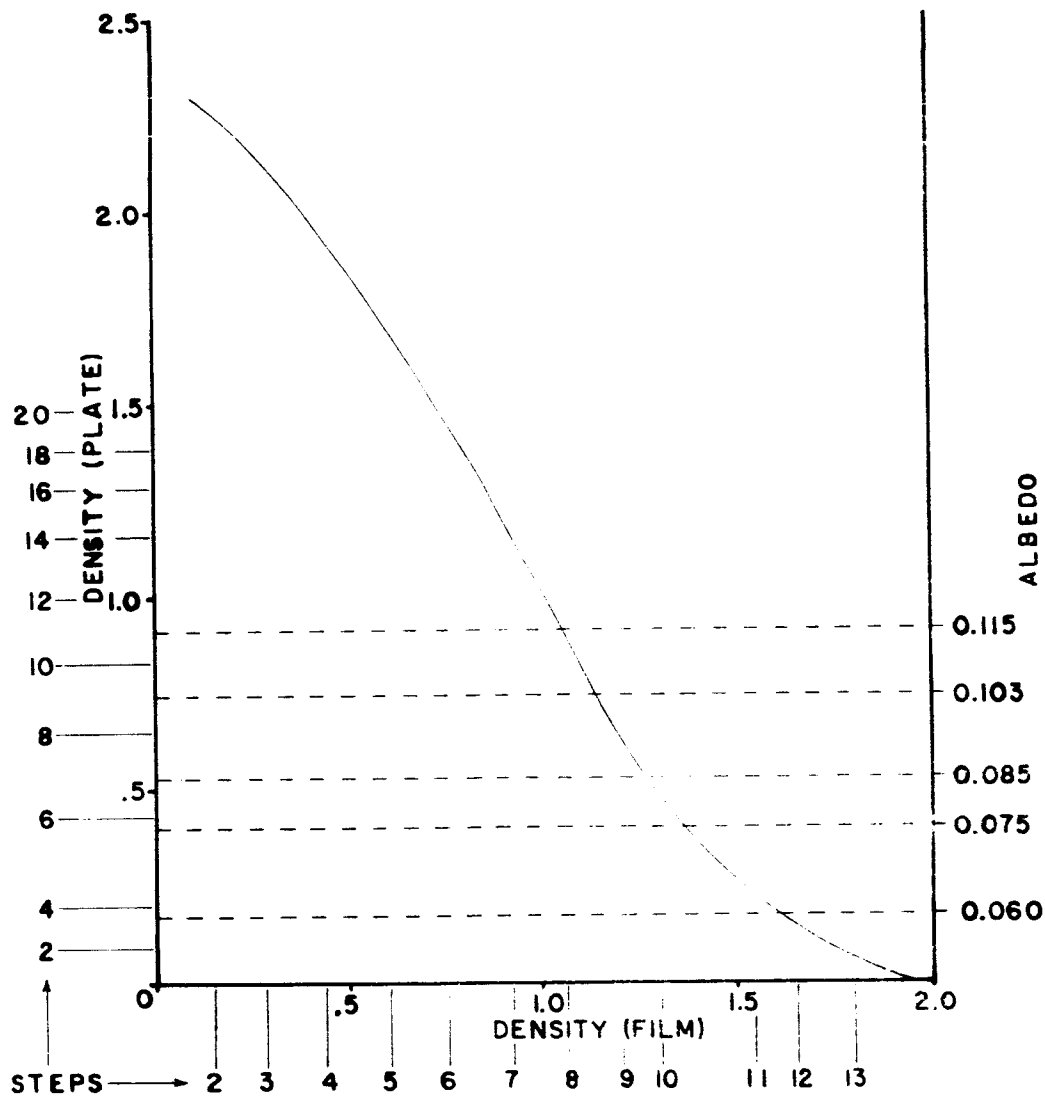
Fig. 2.--H and D curve for the negative plate copy of the 1939 Lick full-moon positive film segmented into six albedo units. Steps of the calibration gray scale are also shown.
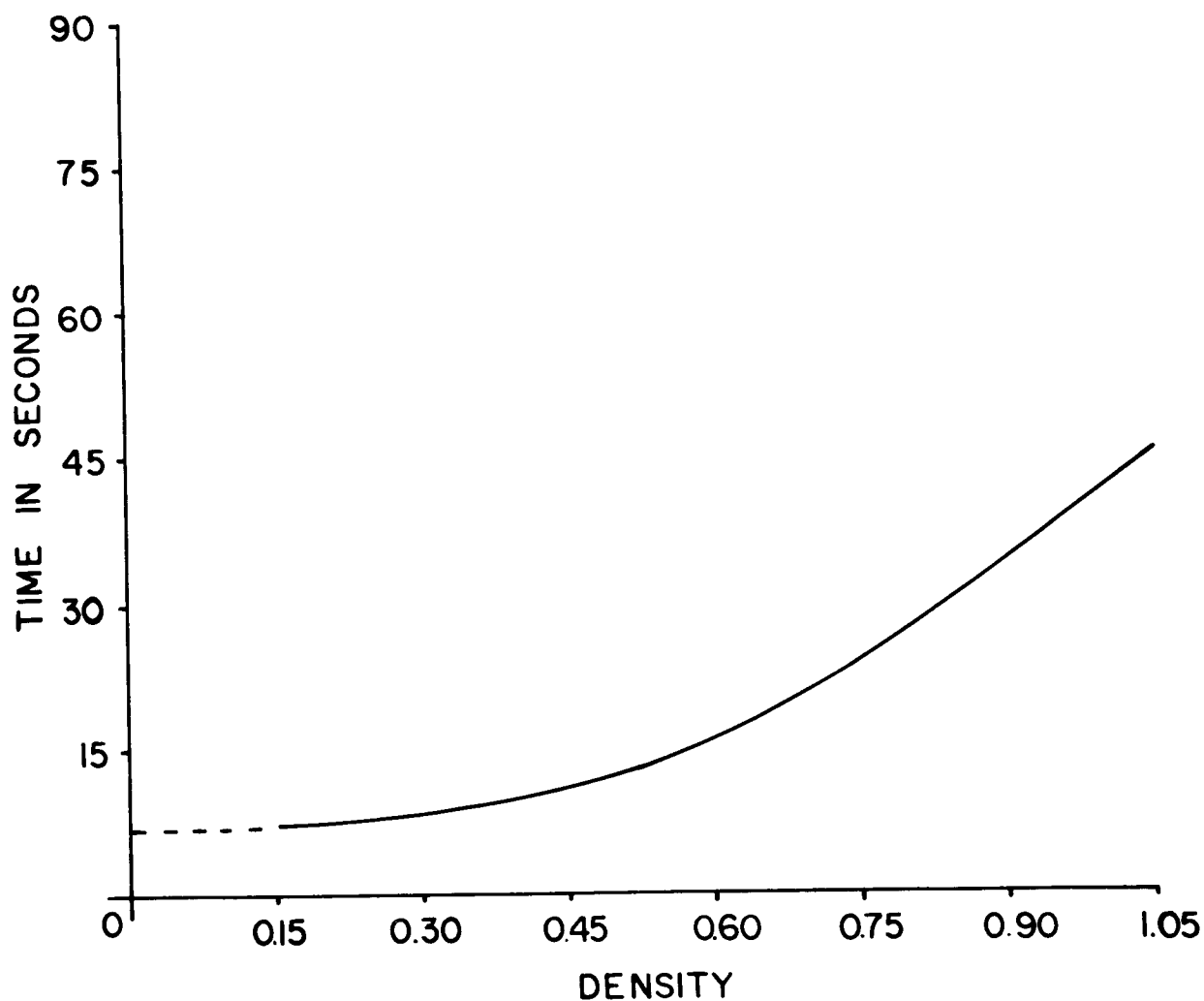
Fig. 3.--Functional relation between exposure time and density, as determined by imprinting the calibrated step wedge on Ortho Litho S film at f/16.

2. Differential limb brightness due to the + 4° phase angle departure from full moon (0° phase angle).

3. Dimensional inaccuracies in enlarging the Ortho Litho S positive from approximately 1:27,000,000 to 1:5,000,000.

4. Inaccuracies incorporated in Sytinskaya's (1953) compiled albedo measurements.

Although figure 1 shows a possible linear relationship between optical density and albedo, considerable scatter is clear when all of the data points from table 1 are plotted against density in figure 1. In addition to small instrumentation errors, these departures are due to the 4° deviation from 0° phase angle of this 1939 full-moon plate. It is therefore clear that upon division of the plate density range into five levels, albedo measurements slightly higher and lower than the stated ranges are included in each unit, and that the isopleth lines represent only the best approximation now possible.

Positional inaccuracies involved in enlargement and transferral of the boundaries are difficult to ascertain but are estimated to be approximately 15 km. No correction has been made for libration.

Traverses along the equator on plates with opposing phase angles show that differential limb brightening is less than 2 percent within the extremes of the eastern and western limits of the map area.

Photographic inconsistencies were minimized by using a constant lens setting (f/16) and varying time of exposure only. Exposure time is most critical at low levels where reproducibility was checked and found to be reasonably good. Photographic processing mixtures were measured carefully and changed with every film developed. Temperature was maintained at 68° ± 1° F.

The writers believe that the inaccuracies accumulated during the photographic process and the transferral of the isopleths are slight when compared to the small number of reliable albedo measurements available. It is clear that a high-quality albedo map depends primarily on a large number of photometrically reliable measurements and precise selenographic control.

Table 1. Selected values of albedo compiled by Sytinskaya (1953)
with corresponding locations and optical density measurements

Area	Lat.	Long.	Albedo	Density
Oceanus Procellarum	27°N	60°W	0.051	0.85
Sinus Aestuum	12°N	5°W	0.057	0.22
Mare Nubium	23°S	14°W	0.062	0.38
Mare Tranquillitatis	12°N	37°E	0.066	0.21
Mare Tranquillitatis	9°N	29°E	0.066	0.23
Mare Vaporum	10°N	8°E	0.060	1.00
Sinus Medii	4°N	5°W	0.067	0.36
Mare Imbrium	43°N	16°W	0.067	0.30
Mare Serenitatis	26°N	28°E	0.070	0.23
Oceanus Procellarum	9°S	24°W	0.071	0.27
Oceanus Procellarum	10°N	45°W	0.060	0.19
Mare Nubium	6°S	14°W	0.073	0.31
Mare Nectaris	15°S	33°E	0.080	0.44
Mare Frigoris	55°N	19°W	0.084	0.45
Archimedes	29°N	4°W	0.088	0.40
Mare Nectaris	7°S	26°E	0.089	0.65
Continent	5°S	0°	0.108	1.08
Aristoteles	50°N	17°E	0.110	1.24
Continent	3°S	8°W	0.112	0.54
Continent	28°N	12°E	0.123	1.18

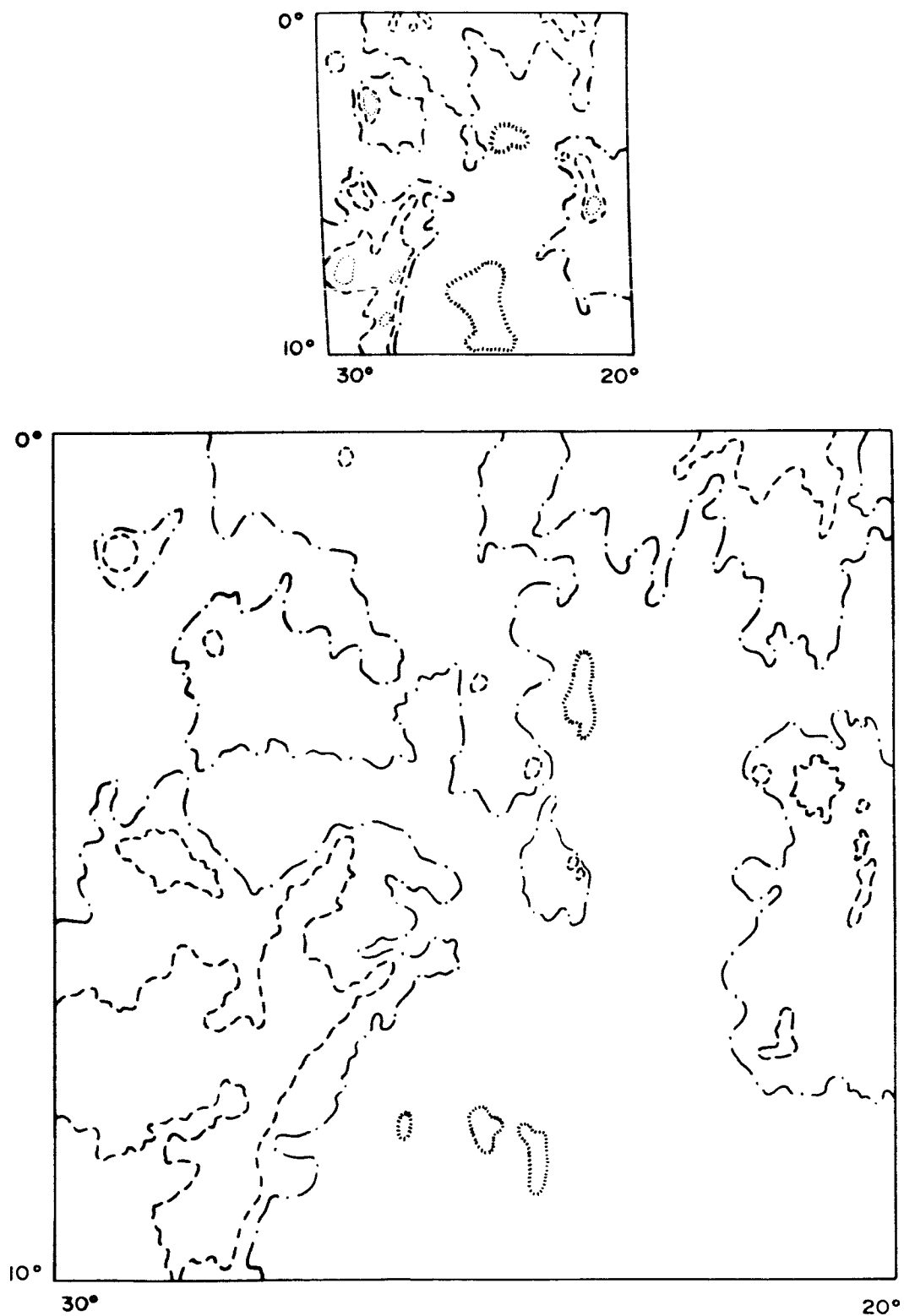Fig. 4.--Comparison of Hackman's (1962) isotonal map (lower) with the writers' map in the Riphaeus region.
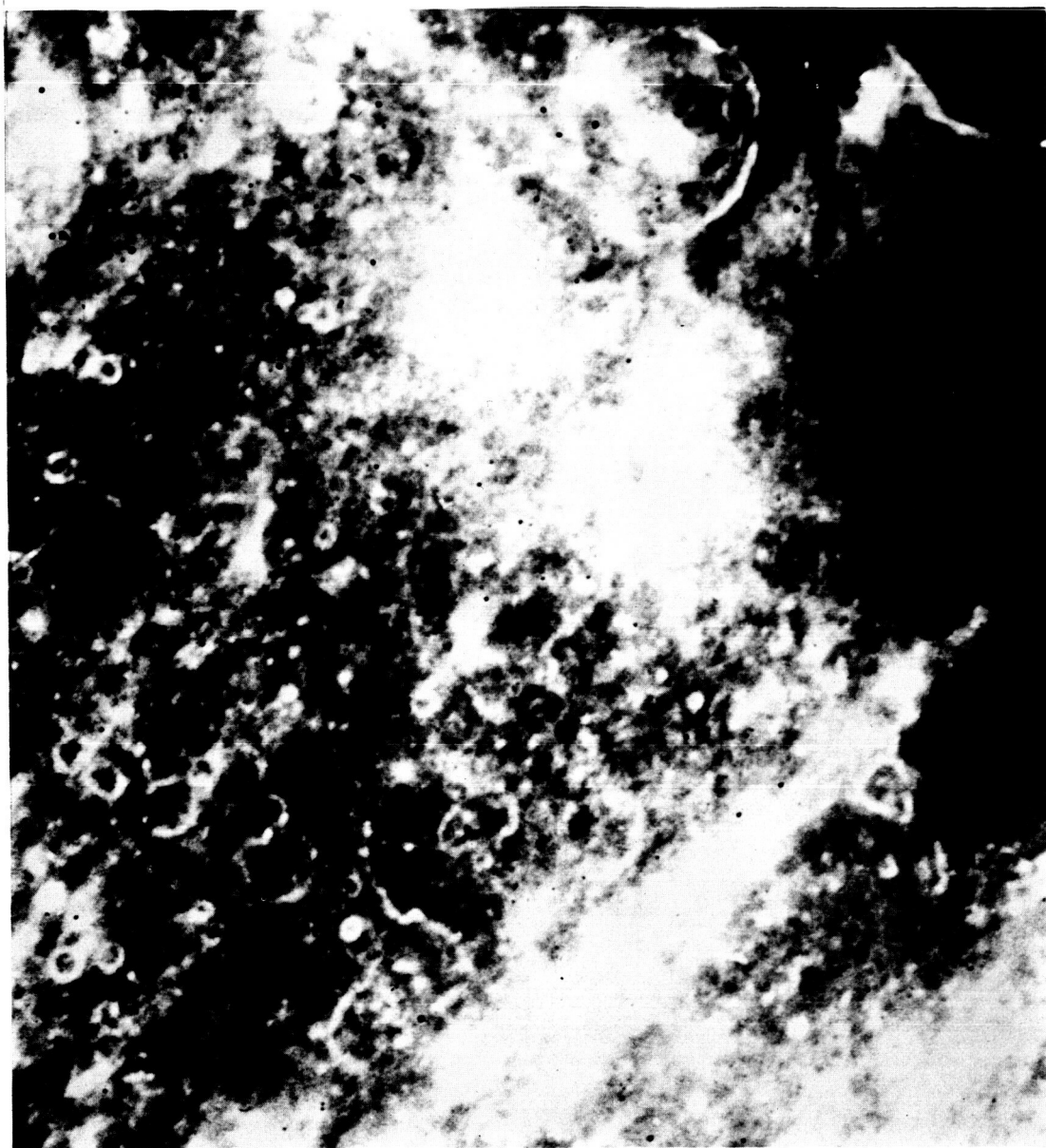
Fig. 5.--The 1939 Lick Observatory full-moon photograph for comparison with figure 6, Ortho Litho S positive copy in the Rupes Altai region (albedo > 0.115). Material of the Tycho rays and Copernican slope material (albedo > 0.115) is shown as the white area. The area in each is from approximately 16° to 32°E and 10° to 28°S.
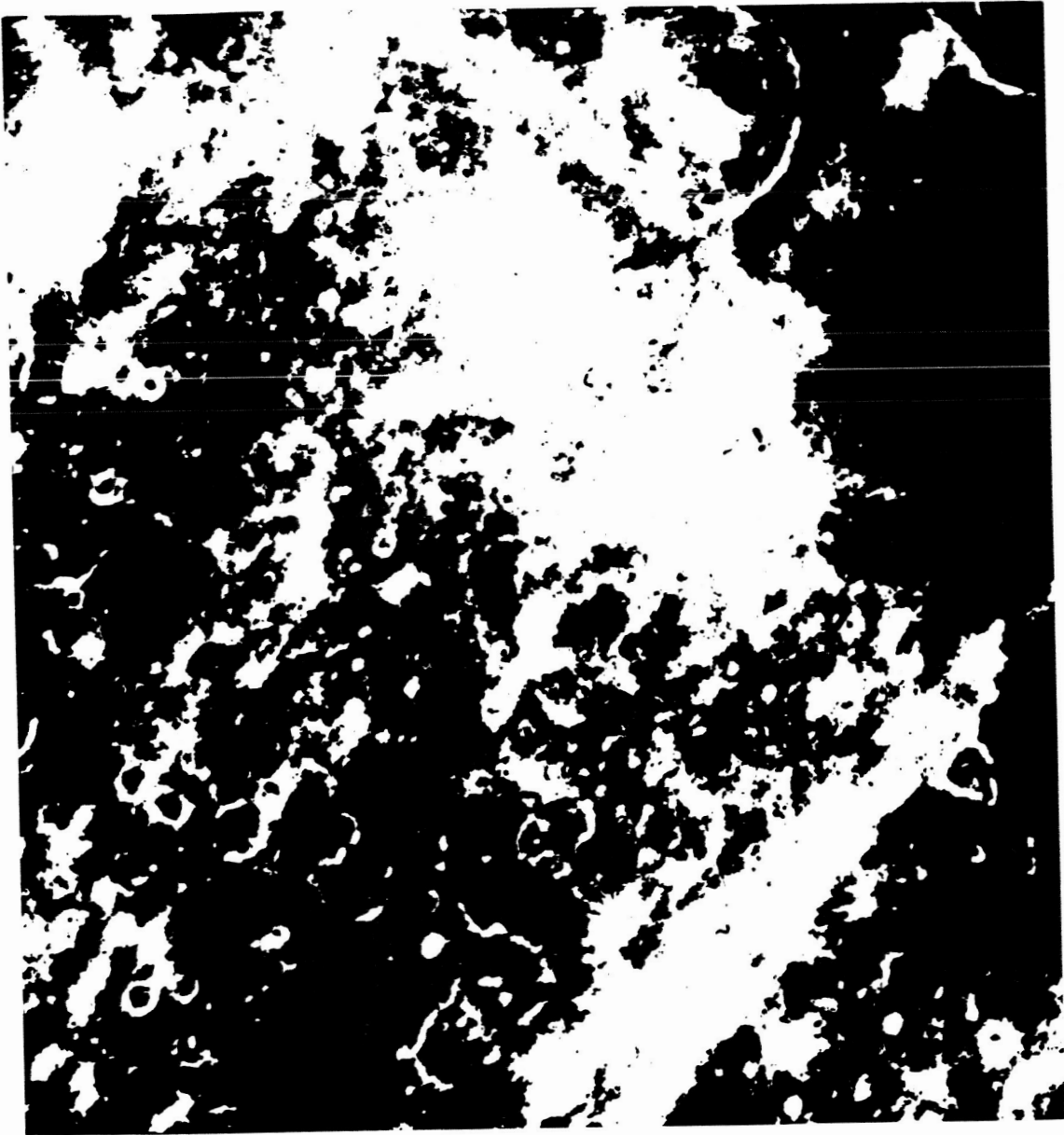
Fig. 6.--See figure 5.

Some measure of the confidence to be placed in the density-controlled boundaries of the 1:5,000,000 map is obtained by comparison of our map with Hackman's (1962) isotonal map (fig. 4). His map was prepared by traversing a full-moon plate with a MacBeth densitometer. It was necessary to delete some of his isotonal lines so that the two maps could be compared at similar degrees of detail. The writers feel that the high degree of similarity in the two maps is some confirmation of the validity of the more rapid photographic technique used.

Applications and future work

Because of its small scale, this preliminary isopleth map has its greatest application to regional mapping. We plan to construct an improved map that will incorporate a large number of full-moon photoelectric measurements. Full-moon photographs will be taken simultaneously with these photoelectric measurements. Defining the functional relations between these albedo measurements and the optical density and contouring density levels on the full-moon plate will permit a detailed isopleth map at a 1:2,000,000 scale. The Joyce-Loebl Isodensitracer provides a convenient and accurate method for obtaining the detailed density data in map form.

As previously mentioned, enlargements of the five Ortho Litho S positives are of value in lunar mapping problems at a 1:1,000,000 scale. The senior author has used these positives projected on photographs and on the geologic map of the Rupes Altai Quadrangle (map supplement to this report) to assign quantitative albedo ranges to the rock-stratigraphic units. This technique was especially useful in mapping the local extent of Tycho ray material and Copernican slope material (figs. 5 and 6). Utilization of these albedo positives in other lunar quadrangles by geologic mappers will eventually provide consistent definitions of these stratigraphic units, and the subjective albedo terminology used in the earlier geologic map explanations can be replaced. The writers believe that the forthcoming 1:2,000,000 scale isopleth map of albedo will enable workers to make critical decisions regarding the albedo of numerous stratigraphic units.

References

Hackman, R. J., 1964, A lunar isotonal map, _in_ Astrogeologic Studies Ann. Prog. Rept., August 1962 to July 1963, pt. D: U.S. Geol. Survey open-file report, p. 13-28.

Hawkins, J. K., and Munsey, C. J., 1963, Automatic photo reading: Photogramm. Eng., v. 29, no. 4, p. 632-640.

McCauley, J. F., 1964, Terrain analysis of the lunar equatorial belt-- Preliminary report: U.S. Geol. Survey open-file report, 44 p.

Miesch, A. T., and Davis, C. W., 1963, Computer analysis of areal microphotometer data from lunar photographs, _in_ Astrogeologic Studies Ann. Prog. Rept., August 1962 to July 1963, pt. D: U.S. Geol. Survey open-file report, p. 85-114.

Sytinskaya, N. N., 1953, Summary catalog of the absolute values of the visual reflecting power at full moon of 104 lunar objects: Astron. Zhur., v. 30, no. 3, p. 295-301; English translation, Los Angeles, Calif., Space Technology Laboratories, STL-TR-61-5110-24, 1961, 11 p.

THE MARIUS HILLS VOLCANIC COMPLEX

by J. F. McCauley

Location and general description

The Marius Hills volcanic complex occupies an area of some 35,000 km^2 near the middle of Oceanus Procellarum, mostly within the Hevelius quadrangle. The large, mare-filled crater Marius (42 km in diameter) is the principal named topographic feature in the area; it lies at the eastern margin of the complex but is unrelated to it. The Marius Hills volcanic complex is a broad, southward-dipping plateau consisting of extensive smooth, undulating areas and numerous closely spaced domes 3 to 10 km wide rising to heights of several hundred meters above the surface of the plateau. The northern contact with the mare material of Oceanus Procellarum is well marked by a sinuous scarp several hundred meters high; but to the south and west, the boundary with the mare is gradational.

The Marius Hills complex was studied in the course of mapping the Hevelius quadrangle (50°-70°W, 0°-16°N) at a scale of 1:1,000,000. The 30-inch reflecting telescope of the U.S. Geological Survey at Flagstaff, Arizona, was used in visual studies along with unpublished photographs from Lick and Lowell (ACIC) Observatories. The best photograph of the complex, with a recognition resolution of about 1 km, is Lick-Herbig ECD-75 taken at the 120-inch reflector (fig. 1).

Significant geologic features

The most striking features of the area are domes, approximately 130 of which have been recognized and mapped at a scale of 1:1,000,000 (fig. 2). Two distinct types are present. The first are broad, relatively low features 3 to 10 km wide with convex-upward profiles. They are similar to domes common to the maria in other parts of the Moon. The second type of dome is steeper and higher and has a concave-upward profile. The average height of this type above the surrounding
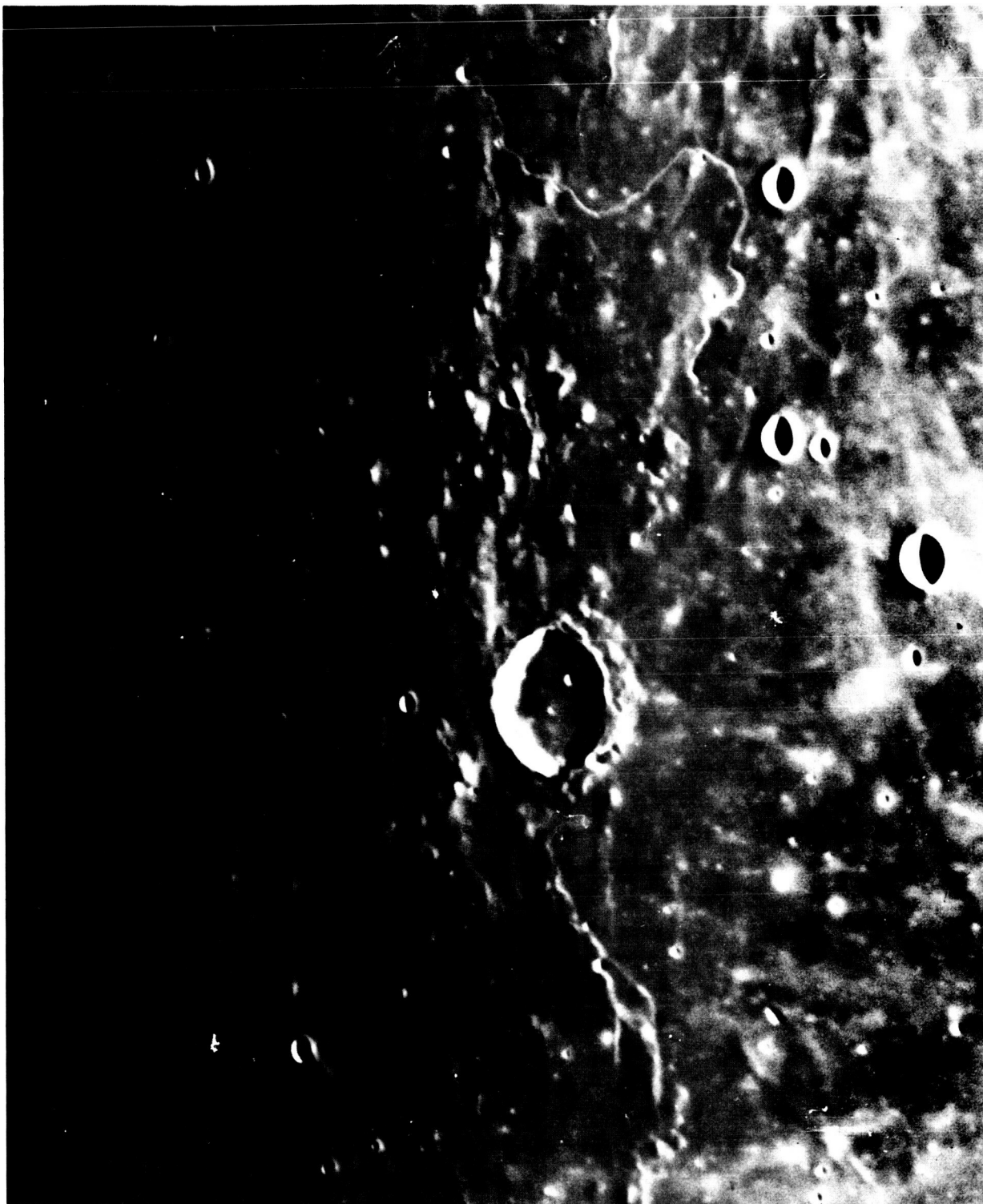
Fig. 1.--Photograph taken at the Lick Observatory 120-inch teles-
cope showing the Marius Hills volcanic complex. Marius is the large,
mare-filled crater near the center.

undulating terrain is about 300 meters, but the highest dome has about
1000 meters of local relief. Several steep domes lie near the crests of
the broad low domes. Slopes of the broader domes average 2° or 3°,
whereas the steeper domes slope from 7° to as much as 15° near their
crests. The broader domes are more common; 87 of these and 41 of the
steeper variety have been recognized. Both types are slightly asymmet-
rical in profile, with greater slopes on the east side, and are somewhat
elongated in the northeast-southwest direction.[1]

Unusually good seeing conditions over a period of an hour in
January 1965 at the U.S. Geological Survey 30-inch reflector showed
many of the domes to have small summit pits not resolved in the best
photographs. In addition, numerous fine rille-like structures were
observed on the flanks of many of the steeper domes.

The crater density of the Marius Hills complex is markedly lower
than that of the mare directly to the east in the Kepler quadrangle
(Hackman, 1961), which is the type area of the Procellarum Group of
Imbrian age. Crater size-frequency distribution curves for two areas
of comparable size (approximately 32,000 km^2)--one in the Marius Hills
complex and one in the type area of the Procellarum--are shown in
figure 3. The number of craters in the complex more than 1 km in diam-
eter is 7, whereas the number in the Procellarum is 39. The number of
craters in the complex in the 1- to 2-km range is 3, and the number
in the Procellarum is 20. The size-frequency distribution for the
sample area in the Procellarum Group is typical of the maria as a whole
(Shoemaker, 1965), so the sample taken here is probably large enough
to permit statistically significant comparison with the sample in the
Marius Hills complex.

Despite the contrast in surface morphology, the albedos of the
Marius Hills complex and of the surrounding mare of Oceanus Procellarum

---

[1] The detailed morphology of the domes has been studied by a modi-
fication of the Van Diggelen photometric technique (McCauley, 1964).
Detailed results of this study will be the subject of a separate report.

GEOLOGIC MAP OF THE MARIUS HILLS AREA

By

J. F. McCauley

1965

Fig. 2.

Ccr
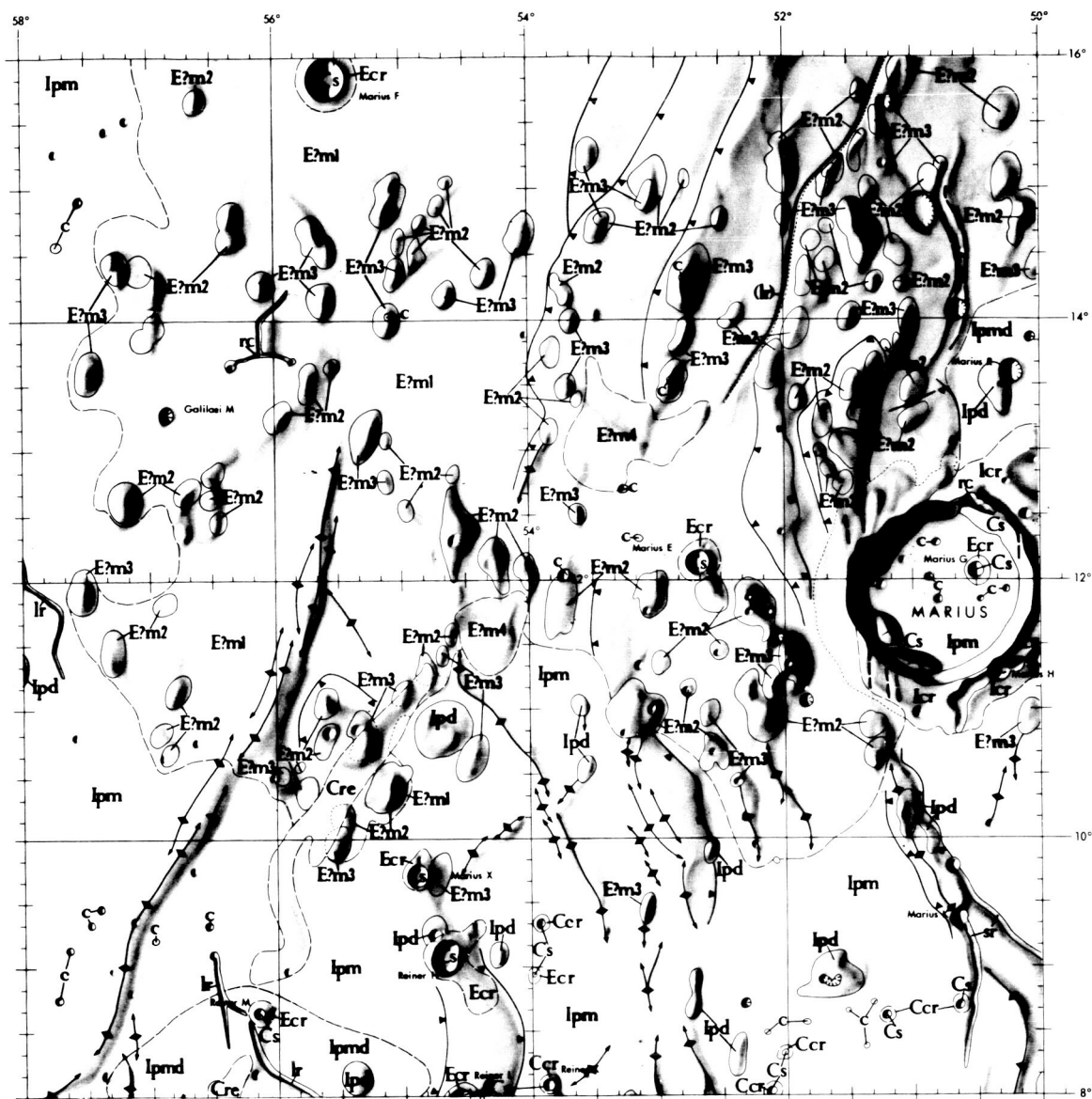
Crater rim material

Characteristics

Surrounds craters with diameters from 2 to 3 km. Albedo moderate to high. Topography around these small craters appears smooth. Rim material of some craters grades to ray material away from craters.

Interpretation

Poorly sorted crushed rock containing scattered large blocks. Greatest thickness is near the crater rim.

Cre

Reiner Gamma Formation

Characteristics

Albedo moderate. Contact at outer margin gradational; more abrupt at inner margin. Appears to be superimposed on surrounding units but has no discrete topographic expression of its own.

Interpretation

Poorly sorted crushed rock thinly blanketing the underlying units (Mare material and Marius Formation).

Cs

Slope material

Characteristics

Present mostly on interior crater walls which range in slope from 20° to 40°. Albedo high to very high; generally greater than adjacent crater floor or crater rim material.

Interpretation

Partially sorted rock fragments ranging in size from dust to large blocks. Derived principally by slumping, spalling, and mass movement or particulate materials downslope on the interior crater walls.

COPERNICAN SYSTEM

Ecr

Crater rim material

Characteristics

Albedo low to moderate with little local contrast. Topography around large craters is hummocky near the rim crest and radial on the flanks; around small craters it is apparently smooth. No bright ray material surrounds the rim deposits. Reiner H has two large lobes of rim material on its eastern side.

Interpretation

Poorly sorted crushed rock containing scattered large blocks. Greatest thickness is near the rim crest. Rim materials associated with certain craters (Reiner H) may consist of volcanic flows or pyroclastics.

Marius Formation

Ehul

Smooth undulating material

Characteristics

Extensive smooth undulating areas between domes lying several hundred meters higher than the surrounding mare. Albedo generally low and uniform. Ridges and plateaus of the type generally found on mare are present locally.

Interpretation

Complex series of volcanic flow materials intercalated with pyroclastic deposits derived from the craters and pits at the crests of many of the domes.

Ehm

Dome materials, convex form gentle slopes

Characteristics

Albedo generally low and uniform. Asymmetrical elliptical domes with typical side slopes of 2° to 3°. Many have small pits at or near the summit. In general form, these structures are similar to mare domes (Ipd).

Interpretation

Probably shield volcanoes composed mostly of basaltic lava flows with some intercalated ash.

Ehm1

Dome materials, concave form, steep slopes

Characteristics

Albedo generally low and uniform. Asymmetrical elliptical domes with typical side slopes of 6° to 7°. Many have small pits at or near the summit and fine "rille-like" structures on the flanks. These domes are generally steeper sided and higher than typical mare domes.

Interpretation

Plugs of intrusive material of intermediate to acid composition or cones composed of flows and pyroclastics.

Ehm2

Dome materials, clusters of small domes

Characteristics

Small dome fields or clusters of individual domes too small to be individually mapped. Albedo generally low and uniform. Most of the domes appear to be of the convex variety with gentle side slopes. (Ehm2)

Interpretation

Small volcanoes composed mostly of basaltic flows formed from many closely spaced vents.

ERATOSTHENIAN SYSTEM

Procellarum Group

Ipd

Dome material

Characteristics

Occur generally as symmetrical to elliptical domes from 3 to 15 km across and up to 300 meters high. Small craters are often seen on the crests or flanks. Albedo and local contrast low. Some domes exhibit a cleft along their crests with a small crater at one end.

Interpretation

Volcanic flows for the most part but also may include volcanic ash. The generally low reflectivity and low slopes along with the overall form suggest that these structures may be shield volcanoes of basaltic composition.

Ipm

Mare material

Characteristics

Albedo generally low and uniform except where superimposed craters and rays are present. Forms extensive, relatively smooth dark areas marked by elongate, broad low ridges and by numerous craters of Eratosthenian and Copernican age. Terminates abruptly against higher topographic features and earlier topography.

Interpretation

Complex overlapping series of volcanic flows covered by a relatively thin layer of fine-grained granular material. The wide extent and low relief suggest either basalt flows or ash fall deposits (ignimbrite). Ranges in thickness from a maximum near the centers of the largest older craters to a thin veneer over buried topography.

Ipmd

Mare material, dark

Characteristics

Albedo very low, considerably darker than Ipm. Generally exhibits a lower crater frequency rate and a lower incidence of superimposed ray material. Other topographic characteristics are similar to those of Ipm.

Interpretation

Similar genetically to Ipm but either younger in age or composed of material of more mafic composition.

Icr

Crater rim material

Characteristics

Albedo low to moderate and uniform. Topography hummocky near the crest. Floor generally filled and flanks partially inundated by mare material of the Procellarum Group.

Interpretation

Poorly sorted, finely crushed rock with scattered large blocks. Ranges in thickness from a meter on the flanks to several hundred meters on the rim.
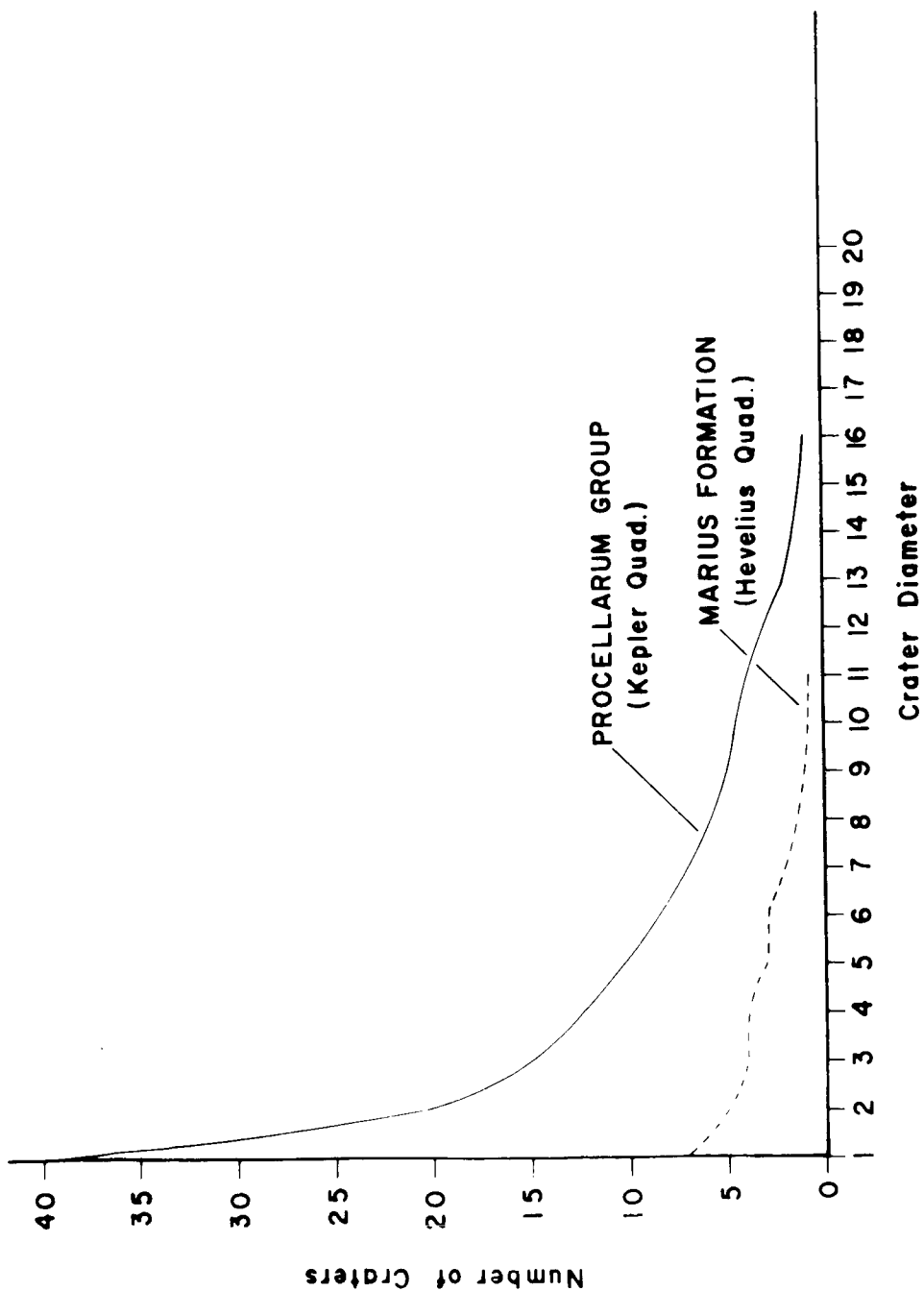
IMBRIAN SYSTEM

Fig. 3.--Crater size-frequency distribution for two areas of
3.2 x 10⁴ km² in Oceanus Procellarum.

are essentially the same, except for a small area of mare (mostly in the Kepler quadrangle) north and east of the crater Marius which has a lower albedo than the complex.

North of the crater Marius is a subdued linear depression 30 km long, near which are several roughly circular, rimless depressions. Also present is a series of north-northeast trending, east-dipping scarps parallel to this depression. Scarps and linear depression are roughly parallel to the direction of elongation of the domes and to their general alignment. Along a ridge south of Marius are large (photographically resolvable) sinuous rilles, similar to the smaller rilles seen visually on the domes. Two chains of craters are present on the rim of Marius itself, suggesting that the original rim, as well as the mare-covered floor, has been modified by later volcanic activity.

Stratigraphic relations

The Marius Hills complex, an area of domes and the smooth undulating terrain between them (fig. 2), is here designated the Marius Formation. Clear-cut superposition of the formation on the mare material of the Imbrian Procellarum Group at the northern boundary, along with a markedly lower crater density than on the type area of Procellarum, argues for post-Imbrian age. The Marius Formation is overlain by faint rays from both Kepler and Aristarchus, and is therefore older than these Copernican craters. The greater part of the surface material is therefore probably Eratosthenian, although some could be Imbrian and some Copernican, and for convenience the entire formation is tentatively designated as Eratosthenian.

A number of separate facies are mapped within the Marius Formation. The smooth, undulating areas between the domes are designated as Em1. The broad domes of the type generally found on the maria are designated as Em2. The steep-sided domes are Em3. In addition, clusters of small domes in the 1- to 2-km range, too small to be mapped individually, have been designated as Em4.

Geologic interpretation

In general, the features described--domes, summit pits, rilles, rimless depressions--are similar both in form and scale to many structures in terrestrial volcanic provinces. The different morphologic expression of the two types of domes suggests formation by magmas of different composition. The steeper domes, by analogy to terrestrial examples, as in northern California and southern Oregon (Williams, 1957), may have been formed by material more viscous and more silicic (rhyolitic or dacitic composition) than the material responsible for the lower domes that may be basaltic. The presence of steep domes near the crests of some lower domes inplies a close genetic relation between the two types; the later steep domes could be the product of local magmatic differentiation.

References

Hackman, R. J., 1961, Geological map and sections of the Kepler region of the Moon: U.S. Geol. Survey Map I-355.

McCauley, J. F., 1964, Terrain analysis of the lunar equatorial belt-- Preliminary report: U.S. Geol. Survey open-file report, 44 p.

Shoemaker, E. M., 1965, Ranger VII, Part II--Experimenters' analyses and interpretations: California Inst. Technology, Jet Propulsion Lab. Tech. Rept. no. 32-700.

Williams, Howell, 1957, A geologic map of the Bend quadrangle, Oregon, and a reconnaissance geologic map of the central portion of the high Cascade Mountains: Oregon Dept. Geology and Mineral Industries.

PHOTOELECTRICALLY DERIVED HERTER AND DRYFIELD CURVES OF

UNCALIBRATED PLATES

by H. A. Pohn and R. L. Wildey

One of the greatest difficulties in using lunar photographs to extract information on the variation of albedo over the lunar surface is that most of the original plates are uncalibrated as to their Herter and Dryfield (H and D) or density-versus-log-of-exposure (d-log E) curve. Most of the lunar plates taken between 1919 and 1940 were basically attempts at high pictorial resolution and are not of high photometric reliability. Quantitative data cannot be extracted from these essentially qualitative plates without the use of special techniques for two main reasons. The first is that the astronomers almost always neglected to expose a step wedge on the original plate, and the second is that the spectral response of the emulsion was rarely recorded. Even if the nominal emulsion characteristics had been recorded, the plate-to-plate variations would prevent any use of a standard curve.

In the past year, several promising experiments have been conducted with the aim of obtaining characteristic curves of these previously uncalibrated lunar plates. The technique is basically as follows. The Branch of Astrogeology possesses positive copies of the original negative plates taken at numerous observatories over the past 50 years. When these plates were copied, a standard calibrated step wedge was exposed on the copy plate. This enables us to determine the H and D curve of the copy plate. Photoelectric measurements are made of selected spots on the Moon at the same phase angle and near the same libration as the plate in question, and these measurements are read out in stellar magnitudes. Since stellar magnitudes of a small area of lunar surface are in essence the $\log_{2.512}$ of the brightness in watts/cm^2/sterad/A for a given spot, these readings can be converted to $\log_{10}$ exposure and plotted against the density of the corresponding lunar regions on the plate under consideration to obtain the d-log E curve of the original plate.

The curve derived in this way is always in the Johnson-Morgan V radiation bandpass in the yellow region, regardless of the bandpass of the plate. This means that the d-log E curve obtained from the copy plate is not necessarily the same as the one that would have been derived had a step wedge been exposed on the original plate, inasmuch as the original emulsion-filter combination probably possessed a different spectral sensitivity. Disagreement in bandpass can result in data dispersion only insofar as the Moon shows coloration. Recent photoelectric investigations by the authors show that the dispersion in UBV color indices for many spots on the lunar surface is below the detectability of photographic colorimetry (Wildey and Pohn, 1964). The present d-log E curves therefore contain as much information as the originals would have. They have the additional advantages that the bandpass is precisely known and the brightness can be determined in absolute units. It may therefore be reasonably supposed that the dispersion in the curves derived by the present method is, by and large, a measure of the previously unknown photometric uniformity of the original plate.

Reference

Wildey, R. L., and Pohn, H. A., 1964, Detailed photoelectric photometry of the Moon: California Inst. Technology, Div. Geol. Sciences Contr. no. 1254, 30 p.